NNT : 2013 EMSE 0701

THÈSE

présentée par

Yeonhee JUNG

pour obtenir le grade de
Docteur de l'École Nationale Supérieure des Mines de Saint-Étienne
en cotutelle avec l'Universite Nationale de Séoul

Spécialité : Mécanique et Ingénierie

Une analyse efficace du procédé RTM à l'aide de la méthode XFEM

Soutenue à Séoul en Corée, le 2 septembre 2013

Membres du jury

Président :		
Rapporteurs :	Olivier ALLIX	Professeur, ENS de Cachan, Cachan
	Dongwoo SHEEN	Professeur, Universite Nationale de Séoul, Séoul
Examinateur(s) :	Jean-Michel BERGHEAU	Professeur, ENISE, Saint-Etienne
	Ji-Hwan KIM	Professeur, Universite Nationale de Séoul, Séoul
Directeur(s) de thèse :	Woo-Suck HAN	Maître de recherche, ÉNSM-SE, Saint-Etienne
	Seung Jo KIM	Professeur, Universite Nationale de Séoul, Séoul

Spécialités doctorales :
SCIENCES ET GENIE DES MATERIAUX
MECANIQUE ET INGENIERIE
GENIE DES PROCEDES
SCIENCES DE LA TERRE
SCIENCES ET GENIE DE L'ENVIRONNEMENT
MATHEMATIQUES APPLIQUEES
INFORMATIQUE
IMAGE, VISION, SIGNAL
GENIE INDUSTRIEL
MICROELECTRONIQUE

Responsables :
K. Wolski Directeur de recherche
S. Drapier, professeur
F. Gruy, Maître de recherche
B. Guy, Directeur de recherche
D. Graillot, Directeur de recherche
O. Roustant, Maître-assistant
O. Boissier, Professeur
JC. Pinoli, Professeur
A. Dolgui, Professeur

EMSE : Enseignants-chercheurs et chercheurs autorisés à diriger des thèses de doctorat (titulaires d'un doctorat d'État ou d'une HDR)

AVRIL	Stéphane	PR2	Mécanique et ingénierie	CIS
BATTON-HUBERT	Mireille	PR2	Sciences et génie de l'environnement	FAYOL
BENABEN	Patrick	PR1	Sciences et génie des matériaux	CMP
BERNACHE-ASSOLLANT	Didier	PR0	Génie des Procédés	CIS
BIGOT	Jean Pierre	MR(DR2)	Génie des Procédés	SPIN
BILAL	Essaid	DR	Sciences de la Terre	SPIN
BOISSIER	Olivier	PR1	Informatique	FAYOL
BORBELY	Andras	MR(DR2)	Sciences et génie de l'environnement	SMS
BOUCHER	Xavier	PR2	Génie Industriel	FAYOL
BRODHAG	Christian	DR	Sciences et génie de l'environnement	FAYOL
BURLAT	Patrick	PR2	Génie Industriel	FAYOL
COURNIL	Michel	PR0	Génie des Procédés	DIR
DARRIEULAT	Michel	IGM	Sciences et génie des matériaux	SMS
DAUZERE-PERES	Stéphane	PR1	Génie Industriel	CMP
DEBAYLE	Johan	CR	Image Vision Signal	CIS
DELAFOSSE	David	PR1	Sciences et génie des matériaux	SMS
DESRAYAUD	Christophe	PR2	Mécanique et ingénierie	SMS
DOLGUI	Alexandre	PR0	Génie Industriel	FAYOL
DRAPIER	Sylvain	PR1	Mécanique et ingénierie	SMS
FEILLET	Dominique	PR2	Génie Industriel	CMP
FOREST	Bernard	PR1	Sciences et génie des matériaux	CIS
FORMISYN	Pascal	PR0	Sciences et génie de l'environnement	DIR
FRACZKIEWICZ	Anna	DR	Sciences et génie des matériaux	SMS
GARCIA	Daniel	MR(DR2)	Génie des Procédés	SPIN
GERINGER	Jean	MA(MDC)	Sciences et génie des matériaux	CIS
GIRARDOT	Jean-jacques	MR(DR2)	Informatique	FAYOL
GOEURIOT	Dominique	DR	Sciences et génie des matériaux	SMS
GRAILLOT	Didier	DR	Sciences et génie de l'environnement	SPIN
GROSSEAU	Philippe	DR	Génie des Procédés	SPIN
GRUY	Frédéric	PR1	Génie des Procédés	SPIN
GUY	Bernard	DR	Sciences de la Terre	SPIN
GUYONNET	René	DR	Génie des Procédés	SPIN
HAN	Woo-Suck	CR	Mécanique et ingénierie	SMS
HERRI	Jean Michel	PR1	Génie des Procédés	SPIN
INAL	Karim	PR2	Microélectronique	CMP
KERMOUCHE	Guillaume	PR2	Mécanique et Ingénierie	SMS
KLOCKER	Helmut	DR	Sciences et génie des matériaux	SMS
LAFOREST	Valérie	MR(DR2)	Sciences et génie de l'environnement	FAYOL
LERICHE	Rodolphe	CR	Mécanique et ingénierie	FAYOL
LI	Jean Michel		Microélectronique	CMP
MALLIARAS	Georges	PR1	Microélectronique	CMP
MOLIMARD	Jérôme	PR2	Mécanique et ingénierie	CIS
MONTHEILLET	Franck	DR	Sciences et génie des matériaux	SMS
PERIER-CAMBY	Laurent	PR2	Génie des Procédés	DFG
PIJOLAT	Christophe	PR0	Génie des Procédés	SPIN
PIJOLAT	Michèle	PR1	Génie des Procédés	SPIN
PINOLI	Jean Charles	PR0	Image Vision Signal	CIS
POURCHEZ	Jérémy	CR	Génie des Procédés	CIS
ROUSTANT	Olivier	MA(MDC)		FAYOL
STOLARZ	Jacques	CR	Sciences et génie des matériaux	SMS
SZAFNICKI	Konrad	MR(DR2)	Sciences et génie de l'environnement	CMP
TRIA	Assia		Microélectronique	CMP
VALDIVIESO	François	MA(MDC)	Sciences et génie des matériaux	SMS
VIRICELLE	Jean Paul	MR(DR2)	Génie des Procédés	SPIN
WOLSKI	Krzystof	DR	Sciences et génie des matériaux	SMS
XIE	Xiaolan	PR1	Informatique	CIS

ENISE : Enseignants-chercheurs et chercheurs autorisés à diriger des thèses de doctorat (titulaires d'un doctorat d'État ou d'une HDR)

BERGHEAU	Jean-Michel	PU	Mécanique et Ingénierie	ENISE
BERTRAND	Philippe	MCF	Génie des procédés	ENISE
DUBUJET	Philippe	PU	Mécanique et Ingénierie	ENISE
FORTUNIER	Roland	PR	Sciences et Génie des matériaux	ENISE
GUSSAROV	Andrey	Enseignant contractuel	Génie des procédés	ENISE
HAMDI	Hédi	MCF	Mécanique et Ingénierie	ENISE
LYONNET	Patrick	PU	Mécanique et Ingénierie	ENISE
RECH	Joël	MCF	Mécanique et Ingénierie	ENISE
SMUROV	Igor	PU	Mécanique et Ingénierie	ENISE
TOSCANO	Rosario	MCF	Mécanique et Ingénierie	ENISE
ZAHOUANI	Hassan	PU	Mécanique et Ingénierie	ENISE

Mise à jour : 07/04/2013

PR 0	Professeur classe exceptionnelle
PR 1	Professeur 1ère classe
PR 2	Professeur 2ème classe
PU	Professeur des Universités
MA (MDC)	Maître assistant
DR	Directeur de recherche

Ing.	Ingénieur
MCF	Maître de conférences
MR (DR2)	Maître de recherche
CR	Chargé de recherche
EC	Enseignant-chercheur
IGM	Ingénieur général des mines

SMS	Sciences des Matériaux et des Structures
SPIN	Sciences des Processus Industriels et Naturels
FAYOL	Institut Henri Fayol
CMP	Centre de Microélectronique de Provence
CIS	Centre Ingénierie et Santé

NNT : 2013 EMSE 0701

THÈSE

présentée par

Yeonhee JUNG

pour obtenir le grade de
Docteur de l'École Nationale Supérieure des Mines de Saint-Étienne
en cotutelle avec l'Universite Nationale de Séoul

Spécialité : Mécanique et Ingénierie

Une analyse efficace du procédé RTM à l'aide de la méthode XFEM

Soutenue à Séoul en Corée, le 2 septembre 2013

Membres du jury

Président :		
Rapporteurs :	Olivier ALLIX	Professeur, ENS de Cachan, Cachan
	Dongwoo SHEEN	Professeur, Universite Nationale de Séoul, Séoul
Examinateur(s) :	Jean-Michel BERGHEAU	Professeur, ENISE, Saint-Etienne
	Ji-Hwan KIM	Professeur, Universite Nationale de Séoul, Séoul
Directeur(s) de thèse :	Woo-Suck HAN	Maître de recherche, ÉNSM-SE, Saint-Etienne
	Seung Jo KIM	Professeur, Universite Nationale de Séoul, Séoul

Acknowledgement

Above all, I would like to express immeasurable gratitude to my two supervisors, Prof. Seung Jo Kim at Seoul National University and Prof. Woo-Suck HAN at Ecole Nationale Supérieure des Mines de Saint-Etienne, who gave me good advices on the research as well as showed me what the sincere attitude and enthusiasm toward the research is. And also, I'll remember forever the kind teaching and support of Prof. Alain VAUTRIN.

I express my gratitude to Prof. Olivier ALLIX and Prof. Dongwoo SHEEN who accepted to be rapporteur of my thesis and gave me helpful advice. And also, I appreciate Prof. Ji-Hwan KIM and Prof. Jean-Michel BERGHEAU who accepted to be member of the jury and gave me good comments.

The life in Saint-Etienne was very fruitful, thanks to my kind friends and colleagues. Ola Suleiman AHMAD, Dina Al AKHRASS, Yi HOU, Quyhn NGUYEN, Renata TROIAN, Lara ABOUORM, and Laura DUBIUS gave me unforgettable memories. I could concentrate on my work and overcome loneliness in the foreign country because of their friendships. And, every member of Department MPE gave me a lot of help for my research and stable school life.

My thesis was done by dual degree program between Ecole Nationale Supérieure des Mines de Saint-Etienne in France and Seoul National University in Korea. I could have a good chance to study both excellent curriculum and with both excellent researchers because of the program. I appreciate everyone giving me helps to join to the program.

Finally, I'd like to express my love and respect for my parents and my family who constantly gave me comfort and courage whenever I felt down.

An efficient analysis of resin transfer molding process using extended finite element method

Yeonhee JUNG

École Nationale Supérieure des Mines de Saint-Étienne

Abstract

Numerical simulation for Resin Transfer Molding (RTM) manufacturing process is attempted by using the eXtended Finite Element Method (XFEM) combined with the level set method. XFEM allows to obtaining a good numerical precision of the pressure near the resin flow front, where its gradient is discontinuous. The enriched shape functions of XFEM are derived by using the level set values so as to correctly describe the interpolation with the resin flow front. In addition, the level set method is used to transport the resin flow front at each time step during the mold filling. The level set values are calculated by an implicit characteristic Galerkin FEM. The multi-frontal solver of IPSAP is adopted to solve the system. This work is validated by comparing the obtained results with analytic solutions.

Moreover, a localization method of XFEM and level set method is proposed to increase the computing efficiency. The computation domain is reduced to the small region near the resin flow front. Therefore, the total computing time is strongly reduced by it. The efficiency test is made with simple channel or radial flow models.

Several application examples are analyzed to demonstrate ability of this method. A wind turbine blade is also treated as industrial application. Finally, a Graphic User Interface (GUI) tool is developed so as to make easy the pre/post-processing of the simulation.

Keywords: RTM Process, XFEM, Level Set Method, Numerical Analysis, Localization method.

Contents

Symbols III

List of Figures IV

List of Tables VII

Chapter 1. Introduction 1

1.1. Overview 1

1.2. Literature Review 5

1.3. Scope of Study 7

1.4. Summary 8

Chapter 2. Analytical Models and Numerical Methods 11

2.1. Mathematical models 12

2.2. Methods for Transport of Resin Front 16

2.3. Methods for Pressure Calculation 20

Chapter 3. Analysis of RTM Process 27

3.1. Modeling 28

3.2. Formulation 31

3.3. Computing Procedures 35

3.4. Validation 36

3.4.1. Pressure Calculation 37

3.4.2. Transport of Flow Front 39

3.4.3. Comparison with Analytic Solutions 45

Chapter 4. Efficiency of Localization Method 49

4.1. Level Set Method 50

4.2. XFEM 54

4.3. Efficiency Test 57

Chapter 5. Applications 61

5.1. Plate with Complex Edge 62

5.2. Thin and Complex Shape Structure 64

5.2.1 Race Tracking Effect 65

5.2.2 Macro Void Formation 67

5.3. Wind Turbine Blade 69

Chapter 6. Conclusions 81

Reference 83

Appendix A. Multi-frontal solver of IPSAP & Diamond/RTM

Appendix B. Key-points of cross-sections for the composite wind turbine blade model

Appendix C. Introduction to Parallel Computing

Résumé Etendu en Français

Extented Abstract in Korean

Symbols

$\boldsymbol{u}$	:	Flow velocity
p^h	:	Approximated pressure function
p_I		Nodal pressure at node I
N_I	:	Shape function at node I
N_J^e	:	Enriched shape function at enriched node J
a_J	:	Additional nodal parameter at enriched node J
n	:	Number of nodes
n_e	:	Number of enriched nodes
φ	:	Level set function
φ_J	:	Level set value at enriched node J
$sign(\ )$	:	Signed function
$d(\ \ )$	:	Distance function
Ω	:	Computational domain
Ω_r	:	Resin region
Ω_a	:	Air region
ρ	:	Density
$\mathbf{K}$	:	Permeability
μ	:	Viscosity
$p_{injection}$	:	Injection pressure
p_{air}	:	Air pressure
H	:	Heaviside function
h	:	Mesh size
ϕ	:	Porosity

List of Figures

Figure 1.1. Applications of the RTM process in the industry of transport.
Figure 1.2. Manufacturing procedures of the RTM process.
Figure 1.3. Defects of structures manufactured by the RTM process.
Figure 2.1. Permeability depending on the fiber volume fraction.
Figure 2.2. The degree of cure as a function of the time and temperature.
Figure 2.3. Interactions between resin flow, heat transfer, and curing reaction processes.
Figure 2.4. Filling factors at filled, front, or empty region (the red color means the region filled by resin).
Figure 2.5. Level set values composed by the filled region, the front, and the unfilled region
Figure 2.6. An ideal case of the level set function.
Figure 2.7. Control volume into three-node triangular elements.
Figure 2.8. Definition of enriched nodes.
Figure 2.9. Enriched shape functions of one-dimensional linear element.
Figure 2.10. Types of enrichment.
Figure 3.1. Computational domain for analysis of RTM process.
Figure 3.2. Subdivision in elements intersected by flow front.
Figure 3.3. Flow chart of the computational procedures.
Figure 3.4. A simple square plate.
Figure 3.5. Pressure contours & graphs of a simple square plate quarter-filled by resin.

Figure 3.6. Geometry and mesh information of a thin square plate for verifying level set calculation.
Figure 3.7. A model for the verification of the re-initialization procedure.
Figure 3.8. Change of level set values by the re-initialization procedure.
Figure 3.9. Thin square plate with the uniformly expanded fluid flow.
Figure 3.10. Change of level set values by the level set calculation procedure including the transport of flow front and the re-initialization.
Figure 3.11. Plate for uniform expansion flow with two fronts.
Figure 3.12. Merging of two flow fronts.
Figure 3.13. Geometry and mesh of the channel flow rectangular plate
Figure 3.14. Geometry and mesh of the radial flow model.
Figure 4.1. Computational domain for localization of the level set method.
Figure 4.2. Change of a level-set function by applying a cut-off function.
Figure 4.3. Level set contours obtained without (Top) and with (Bottom) localization of the level set method.
Figure 4.4. Pressure contour of the channel flow model.
Figure 4.5. Localized computational domain (Localization of XFEM).
Figure 4.6. Pseudo-code to make a node list on the boundary.
Figure 4.7. Pressure contours during the mold filling.
Figure 5.1. Geometry and mesh of the plate.
Figure 5.2. Comparison of results on 2D complex geometry plate(Position of flow front at every 15 sec.).
Figure 5.3. Geometry of the thin and complex shape structure.
Figure 5.4. Two different permeability regionsfor the race-tracking effect.
Figure 5.5. Results of the race tracking effect model (Position of flow front at every 5 sec.).
Figure 5.6. Formation of macro voids (Position of flow front at every 5 sec.).
Figure 5.7. Insertion of vents (Position of flow front at every 5 sec.).
Figure 5.8. AOC 15/50 wind turbine blade.
Figure 5.9. Three parts and seven sections of the composite wind turbine blade.
Figure 5.10. Injection gates & vents on the top skin.

Figure 5.11. Resin flow pattern during the mold filling of the top skin.

Figure 5.12. Injection gates & vents on the spar.

Figure 5.13. Resin flow pattern during the mold filling of the spar.

Figure 5.14. Injection gates & vents on the bottom skin.

Figure 5.15. Flow pattern during the mold filling of the bottom skin.

List of Tables

Table 4.1. Calculation time of the channel flow mode.

Table 4.2. Calculation time of the radial flow model.

Table 5.1. Permeability of the seven sections.

Chapter 1. Introduction

1.1. Overview

The Resin Transfer Molding (RTM) process is a manufacturing method of composite structures.

(a) Automotive

(b) Shipbuilding

(c) Aerospace

Figure 1.1. Applications of RTM process in the industry of transport.

It is widely used in the industry of transport (automotive, aerospace, etc.) as shown in the figure 1.1. RTM process offers relatively low cost for manufacturing structures of complex shape and medium/large size. The surface definition and appearance of the structures are good because RTM is a closed molding process.

(a) Placing the preform.

(b) Closing mold.

(c) Injection of resin.

(d) Curing.

(e) Demolding.

Figure 1.2. Manufacturing procedures of RTM process.

The manufacturing procedures of RTM process are described in the figure 1.2. RTM process uses lower and upper molds. The cavity between the molds takes the shape of structure to be produced. The fiber preform is inserted in the mold cavity and compressed by closing the molds. The preform is filled with the resin which is injected through gates from a pressured container. After completely filling the preform, the resin is allowed to cure. The mold is opened when the structure is hardened after the curing.

(a) Formation of air voids.

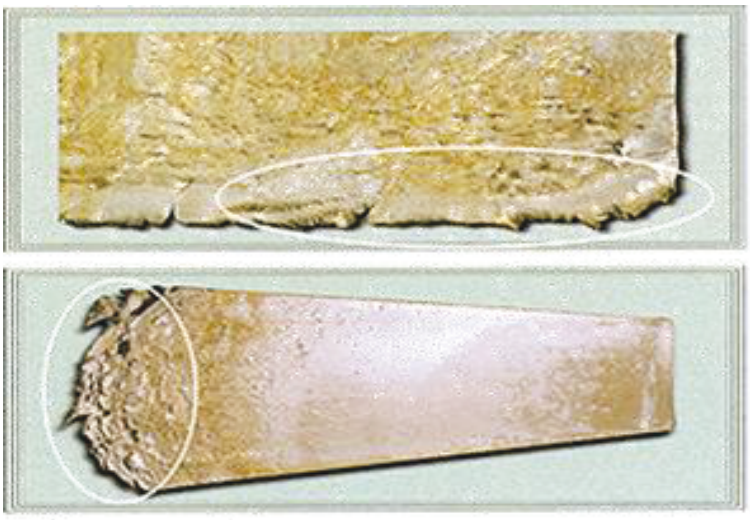

(b) Incomplete filling.

Figure 1.3. Defects of structures manufactured by RTM process.

For the manufacturing of composite structures by RTM process, it is important to predict weld lines and to avoid the formation of air voids, which could cause critical defects in the structure. The some defects by incorrect filling of the mold are shown in the figure 1.3. These defects could lead to modify the mold. That is expensive and time-consuming. Furthermore, to set up the mold filling stage during RTM process, various variables should be considered such as injection and vent pressure, injection gate and vent numbers, and their locations. The design of these variables is sometimes expensive and time-consuming since the motion of the resin flow is impossible to check in a closed mold while the mold filling. That's why the numerical simulation could be very interesting so as to save the cost and time.

During RTM process, the resin flow in the mold is affected by resin viscosity and permeability of fiber preform. The resin viscosity is changed during injection process due to the change of temperature. However, the viscosity could be assumed to be isothermal and constant during the filling process if the filling time is shorter than curing time or the change of temperature is small. Permeability is related to fabric of fiber preform. When the preform is closed fabric, the resin flow slowly moves. On the contrary, when the preform is opened fabric, the resin passes fast. On macroscopic scale, the preform could be assumed as non-deformable condition, therefore, it could be considered to be constant during the mold filling.

The resin flow in the mold represents a moving interface problem since the resin flow front moves through the preform placed in the mold during the filling process. The numerical methods for the moving interface problem could be divided into two groups: moving grid and fixed grid. The fixed grid approach has been more widely used because the moving grid approach needs relatively expensive and difficult computation [Park CH et al., 2003-2004; Kang MK et al., 2000].

In the industry, the structures manufactured by RTM process generally have complex shapes with holes and curvatures. However, the simulation results could be inaccurate when applying traditional numerical approaches for analysis of the complex shape structures. Even though it is possible to acquire appropriate results by using very fine mesh models, the computation time becomes longer. Therefore, many researchers have investigated to increase the accuracy and efficiency of RTM process simulation.

1.2. Literature Review

RTM process has become a popular method of manufacturing middle/large structures of fiber reinforced composite materials because of its capabilities including non-expensive process equipment, excellent control on mechanical properties, closed mold process, low filling pressure, and so on [Trochu F et al., 1992; Morren G et al.,2008; Lin R et al.,1991]. However, the design of mold filling equipment is quite difficult because the reinforcement consisting of several layers of fiber mats inside the closed mold should be perfectly impregnated by the resin injected through several injection gates [Rouison D et al., 2006; Danisman M et al., 2007]. Therefore, many researchers have investigated for numerical simulation of mold filling stage in RTM process [Boccard A, 1995; Jiang S, 2002]. Designers have used the simulation to predict pressure distribution, resin flow pattern, void formation, and other phenomena during mold filling [CH Park et al., 2003-2004]. Nevertheless, the simulation has been restrictedly utilized because the simulation could not give an accurate prediction of the mold filling stage for manufacturing complex shape structures. Actually, early researches had analyzed a simple shape structures due to the difficulty to analyze the moving resin fronts [Bruschke MV et al., 1990; Kang MK et al., 1999]. Still now, many researchers have investigated to develop more proper methods for the analysis of complex shape structures [Liu XL, 2000; Shojaei A et al., 2002].

The Volume of Fluid (VOF) method was popularly used to track the resin flow front for RTM process simulation [Trouchu F et al., 2006; Young WB et al., 1991]. The VOF method is one of the representative methods to track moving interfaces [Hirt CW et al., 1981]. However, because the moving interface is defined by the fractional fluid volume in the element or control volume according to the used method, it could be inaccurate for the cases to track complex movements of the resin front [Kim MS et al., 2003; Lin CL, 2005]. The level set method is the representative of methods to capture moving interfaces [Malladi R et al., 1995; Peter DM et al., 2005]. The level set method is often used for RTM process simulations since it predicts intuitively the flow front's position and is very efficient for multiple flow fronts occurred by complex shapes of the mold or by multiple injection gates [Gantois R, 2010; Soukane S and Trochu F, 2006].

In RTM process simulation, the most frequently used numerical methods during the last two decades are the Control Volume Finite Element Method (CVFEM) and the nonconforming FEM [Dong C, 2008; Jiang S et al., 2007]. CVFEM was the most frequently developed numerical method for RTM process simulation until the beginning of the years 2000, because CVFEM could efficiently satisfy the mass conservation of the resin between two adjacent elements, with regard to the standard finite element approach [Estacio KC et al.,2007; Feerick R, 1997]. However, the construction of control volumes in the whole computational domain could make the computation complex [Shojaei A et al., 2003]. Trochu et al. proposed to apply nonconforming FEM to RTM process simulation. Since the nonconforming FEM calculates the pressure at the inter-elements boundaries, the flow rate at the element boundaries can be obtained without any additional treatment, from which the filling factor is derived. However, the filling factor is not the nodal value but the element one [Trochu F, 1993]. That is why these methods could not properly approximate the pressure field in the elements intersected by the resin flow front because of the discontinuity of the pressure gradient field near the flow front. This point is very important in the case of industrial problems having complex shapes.

The eXtended Finite Element Method (XFEM) is widely used to treat various discontinuity problems such as crack or interface problems [Belytschko T et al., 2009; Sukumar N et al., 2000-2001]. The early works about XFEM were focused on the simulation of fracture and went towards the development of XFEM for fracture mechanics [Moes N and Belytschko T, 2002]. Furthermore, in the field of contact mechanics, XFEM techniques for powder compaction problems are presented by Khoei et al. [2006]. Moes et al. [2003] used XFEM to solve scales with complex geometry in multiscale analysis of components. Chessa et al. [2002] presented XFEM for the multi-dimensional Stefan problems. And, Chessa et al. [2003] applied XFEM to two-phase immiscible flow problems having a discontinuity of the pressure gradient at the interface between two fluids.

1.3. Scope of Study

One of the important points to simulate the resin flow in the mold is to provide accurate approximation of the moving resin flow front during the mold filling process. Moreover, it is necessary to increase the computational efficiency so as to be able to treat industrial problems within an acceptable computing time.

This study suggests to apply eXtended Finite Element Method (XFEM) combined with level set method to analyze the mold filling stage during RTM process. The main advantage of this approach is more accurate approximation of the pressure distribution in the mold and resin flow front location at each time step. And, this study attempts the formulation compels the coefficient matrix to be symmetric and positive definite in order to apply a more efficient linear solver. In addition, this study proposes to apply some techniques, such as localization of XFEM and level set method and usage of an effective solver, for increasing the computational efficiency.

The enriched shape functions of XFEM describing the pressure field are defined by the level set values. The pressure field is divided into two regions: normal and enriched. The enriched region is defined only near the resin flow front; therefore, the size of the linear system slightly increases. Since XFEM formulation done by this study makes the coefficient matrix to be symmetric and positive definite, the multi frontal solver proposed by IPSAP [Kim JH, 2005; Chung SW, 2003], an effective approach for solving the equilibrium systems, is used in order to reduce the computing time.

The level set method is composed of two procedures. The first one is to transport the flow front, and the second is the reinitialization to keep the level set function close to the signed distance function. An implicit characteristic Galerkin Finite Element Method (FEM) is used to stabilize numerical oscillations caused by the convective term in the governing equations. This formulation also makes the coefficient matrix to be symmetric and positive definite.

This study is validated through several examples in comparison with analytical or experimental results found in the literature. Additionally, complex shaped plate examples are used to simulate race-tracking effect and the formation of macro voids. The wind turbine blade example is also simulated. The exclusive program for RTM process simulation (Diamond/RTM) is implanted in Diamond program, a general finite element program having a Graphic User Interface (GUI).

1.4. Summary

This thesis is organized as follows.

Chapter 2 explains about analytical models and numerical methods in order to give the basic knowledge about the analysis of RTM process. At first, the process models and parameters for mathematical modeling are introduced. After that,

there is explanation about the numerical methods traditionally used for RTM process simulation and applied in this study.

Chapter 3 presents in detail the advanced numerical analysis proposed by this work. At first, it is explained about mathematical modeling of RTM process. Next, the numerical formulations by XFEM and level set method are presented. This section is divided by two parts: the formulations for the pressure calculation (XFEM) and the transport of resin flow front (level set method). Furthermore, the whole computational procedures are minutely depicted. Finally, this study is validated by using some examples. Especially, the analysis result by this study is compared with an analytical result.

Chapter 4 goes on to trace the computing efficiency. At first, localization of XFEM and level set method are explained in this chapter. Furthermore, the computational efficiency by the localization is investigated.

Chapter 5 shows the applications. The plate with complex edge is analyzed to show. In addition, the race tracking effect and the macro void formation in the mold are analyzed by the thin and complex shaped structure. The analysis for manufacture of the wind turbine blade is presented. Finally, the pre and post processors of Diamond/RTM are described.

In Chapter 6, the conclusions of this research are summarized with suggestion for future work.

Chapter 2. Analytical Models and Numerical Methods

In this chapter, the analytical models and numerical methods of RTM process simulation are described. First of all, in the section 2.1, the process models and process parameters are introduced for the manufacturing operation of RTM process. In the section 2.2, VOF method and Level set method are presented for tacking the resin flow front. And, in the section 2.3, CVFEM and XFEM are described. These methods are used to calculate the pressure distribution in the mold during the mold filling.

2.1. Mathematical models

In the analysis of RTM process, the mathematical models are derived from the physical laws of fluid flow. When considering fluid flow with velocity, $\boldsymbol{u}$, and density, ρ, the conservation of mass in fluid mechanics is written as:

$$\frac{\partial \rho}{\partial t} + \nabla \cdot (\rho \boldsymbol{u}) = 0, \tag{2.1}$$

where t is time. In RTM process, because the resin is assumed as an incompressible fluid, the density, ρ, is constant. Therefore, the equation (2.1) becomes:

$$\nabla \cdot \boldsymbol{u} = 0. \tag{2.2}$$

The equation of momentum conservation is written as:

$$\rho \frac{D\boldsymbol{u}}{Dt} = -\nabla p + \nabla \cdot \boldsymbol{\tau} + \mathbf{F}_B, \tag{2.3}$$

where p, $\boldsymbol{\tau}$, and $\mathbf{F}_B$ are the pressure, viscous stress and body force, respectively. The inertia term, the left hand side term of the equation (2.3), is important if the velocity is high and the viscosity is low. It's why this inertia term is in general neglected for RTM process. The term $\mathbf{F}_B$ of the equation (2.3) means the body forces due to the gravity and might be negligible when the gravity effect is insignificant. The term $\nabla \cdot \boldsymbol{\tau}$ means the damping forces due to the viscosity. In the model for fluid flow through the porous medium, this term can be expressed by fluid viscosity, fluid velocity, and permeability of porous media as:

$$\nabla \cdot \boldsymbol{\tau} = -\frac{\mu}{\boldsymbol{K}} \boldsymbol{u}, \tag{2.4}$$

where μ and $\boldsymbol{K}$ are the viscosity and permeability. The fluid flow in RTM process can be described as fluid flow through the porous medium. Therefore, for RTM process, the equation (2.3) can be simplified as:

$$0 = -\nabla p - \frac{\mu}{\boldsymbol{K}} \boldsymbol{u} + \mathbf{F}_B. \tag{2.5}$$

When the gravity is insignificant, Darcy's equation is derived from the equation (2.5) as:

$$\mathbf{u} = -\left(\frac{\mathbf{K}}{\mu}\right)\nabla p, \tag{2.6}$$

By substituting the equation (2.6) in the mass conservation equation (2.2), the model of the resin flow could be derived as:

$$\nabla \cdot \left(\frac{\mathbf{K}}{\mu}\nabla p\right) = 0. \tag{2.7}$$

Generally, this model is widely used to simulate the resin flow in RTM process when engineers and researchers are interested in the overall relationship between the process parameters. As we can see in this model, the velocity is related to the viscosity and permeability.

In general, the viscosity depends on the temperature and degree of cure and can be modeled as:

$$\mu = \mu_0\left(\frac{c_1}{T} + c_2\alpha\right), \tag{2.8}$$

where μ_0, c_1, and c_2 are constants and determined experimentally. The viscosity could be treated as a constant value with the assumptions that the mold filling is finished before the curing reaction and the temperature is constant during the mold filling [Advani SG, 2003].

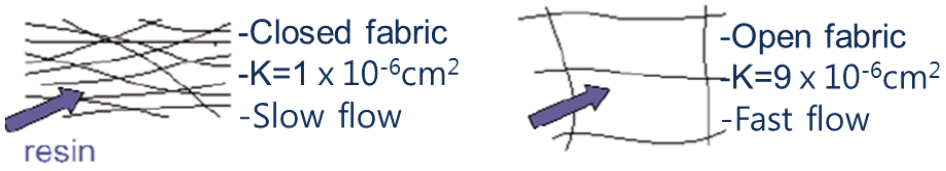

Figure 2.1. Permeability depending on the fiber volume fraction.

In RTM process, the value of permeability is necessary to predict the flow behavior of the resin and determined by the fiber architecture. For instance, the

permeability is small in closed fabric conditions and the resin flows slowly with small permeability as shown in the figure 2.1. The permeability has been developed by a function of the fiber volume fraction. Carman-Kozeny equation is one of the most representative models:

$$\boldsymbol{K} = \mathrm{A}\frac{(1-V_f)^3}{V_f^2}, \tag{2.9}$$

where V_f , $\boldsymbol{K}$, and A are the fiber preform, permeability, and Kozeny constant (empirical value), respectively. For RTM process simulation, the permeability could be putted as a constant value with the assumption that the fiber arrangement is non-deformable during the mold filling.

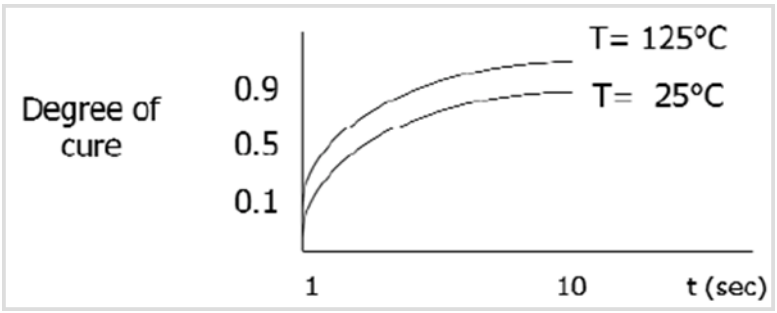

Figure 2.2. The degree of cure as a function of the time and temperature.

The degree of cure influences the resin viscosity and the time of resin gelation. The degree of cure is defined as a function of the time and temperature as shown in the figure 2.2. The degree of cure has been generally obtained by an empirical model of curing reaction as:

$$\frac{\mathrm{d}\alpha}{\mathrm{d}t} = C_1 \exp(-\frac{E}{RT})(1-\alpha)^n, \tag{2.10}$$

where α, t, and R are the degree of cure, time, and universal gas constant, respectively. And, C_1, E, and n are constants to be determined experimentally [Advani SG et al., 2003]. As mentioned earlier, the degree of cure could be

neglected if the analysis target is the mold filling stage and the mold filling is completed before the curing reaction.

The temperature influences the viscosity and degree of cure. The temperature of the resin and the fiber mixture are generally governed by a heat transfer model, such as:

$$\rho c \frac{\partial T}{\partial t} + \rho_r c_r (\boldsymbol{u} \cdot \nabla T) = k \nabla^2 T + \phi \Delta H \dot{G}, \qquad (2.11)$$

where ρ, c and k are the density, specific heat, and thermal conductivity of the resin and fiber mixture, respectively. The subscript *r* denotes the resin. And, ϕ, ΔH, $\dot{G}$ are the porosity, heat of reaction, and reaction rate, respectively [Advani SG et al., 2003]. According to the analysis target, this model could be negligible with the assumption that the process is under the isothermal condition.

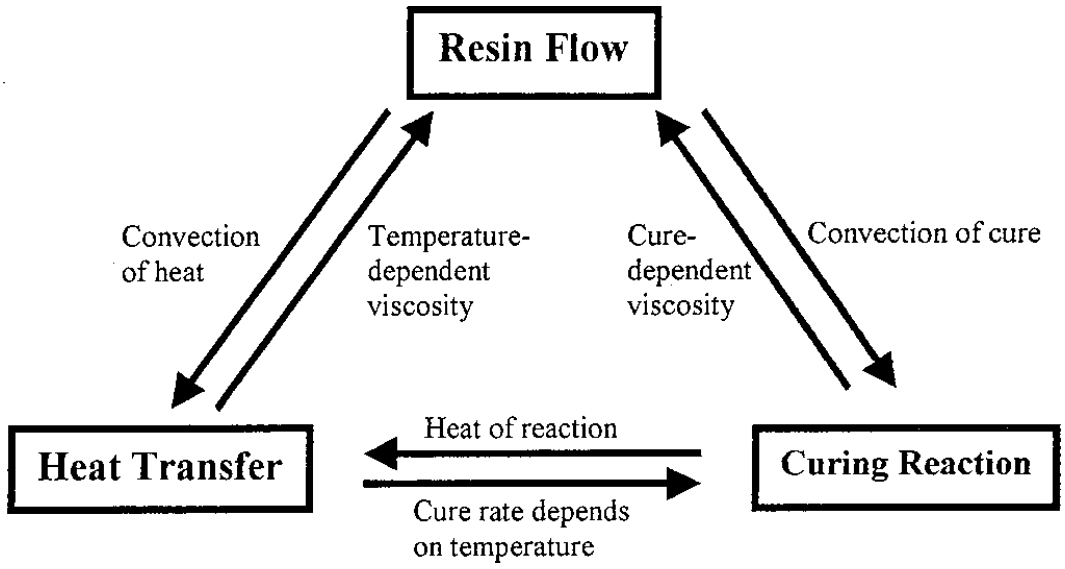

Figure 2.3. Interactions between resin flow, heat transfer, and curing reaction processes.

After all, the interactions between resin flow, heat transfer, and curing reaction processes is described in the figure 2.3. The resin flow is affected by the change of viscosity which is dependent on the temperature and degree of cure. And, the heat

is convected through the resin flow and generated during the curing reaction. The cure is convected through movement of the resin and affected by heat transfer because the temperature changes the degree of cure. However, these models is often modified or simplified according to the study targets. For example, when the target is focused on its quick computation on the structure with complex geometry, the resin flow motion could be assumed under isothermal and no-curing reaction conditions. And, the resin flow model could be used with constant viscosity and permeability for numerical simulation.

2.2. Methods for Transport of Resin Front

A. VOF (Volume of Fraction) Method

VOF method has been frequently used to solve moving boundary problems in a fixed mesh. And, it is the representative of the boundary tracking method. For the numerical simulation of RTM process, the resin flow front position in the mold is obtained by VOF method [Hirt CW et al., 1981].

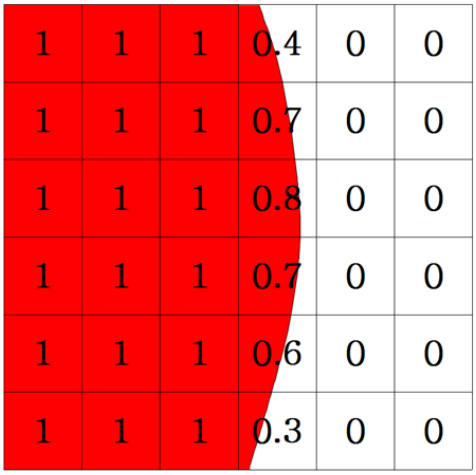

Figure 2.4. Filling factors in the filled, front, or empty region
(the red color means the region filled by resin).

In VOF method, the filled or empty region is divided by using a filling factor, which is the volume of fraction in each volume. The figure 2.4 shows filling factors in the filled, front, and empty regions. The number marked in the volumes is the filling factor. By the filling factor, it is possible to assume the filled condition of each volume. When the filling factor of a volume is equal to 1, the volume is perfectly filled by resin. And, the filling factor of an empty volume is equal to 0. At the resin flow front, the filling factor is between 0 and 1.

For the analysis of RTM process, the VOF method is applied to transport the resin front when the resin flow is solved under quasi-steady state condition. To be specific, the flow front position is determined by calculating the filling factor of VOF method. After that, the resin flow equation (2.7) is solved to calculate the pressure in the mold filled by resin.

B. Level Set Method

The level set method is a representative method to capture the moving interface, boundary, or flow front. In this study, the motion of the resin flow front is described by the level set method. Thus, the level set method is explained in detail to help better understanding of readers. The level set values are used to determine the flow front position/interface as the role of filling factors in the VOF method.

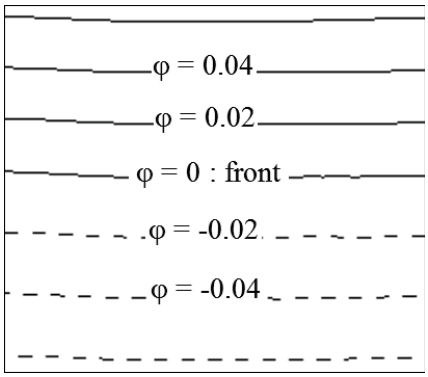

Figure 2.5. Level set values composed by the filled region, the front, and the unfilled region.

The level set means the signed distance from the flow front as shown in the figure 2.5. The dashed lines are in the unfilled region, therefore, the level set values are negative signed distance from the front. The level set values at the flow front are equal to zero. In the filled region, marked by solid lines, the level set values are positive signed distance from the front.

The transport of the resin flow is established by solving a motion equation of the level set. The topological change in the flow front is naturally handled by the motion equation of the level set. The motion equation is derived from the initial value formulation of J. A. Sethian [1999]. The level set value of a particle on the front with path ***x(t)*** is equal to zero and the total derivative of the level set function becomes zero as:

$$\varphi(\boldsymbol{x}(t), t) = 0, \qquad \frac{D\varphi}{Dt} = 0. \tag{2.12}$$

By the chain rule, the differential equation (2.13) is derived as

$$\frac{\partial \varphi}{\partial t} + \mathbf{u} \cdot \nabla \varphi = 0. \tag{2.13}$$

Even though the velocity **u** varies rapidly, the motion of flow front can be naturally described by the equation (2.13).

However, the equation (2.13) can correctly transport just the flow front and cannot correctly change the level set values of the regions except the flow front. It is why, a re-initialization procedure is necessary after solving the equation (2.13). The re-initialization procedure is to modify the level set values of the regions except the flow front to the exact distance values. The level set function should satisfy the condition as:

$$|\nabla \varphi| = 1. \tag{2.14}$$

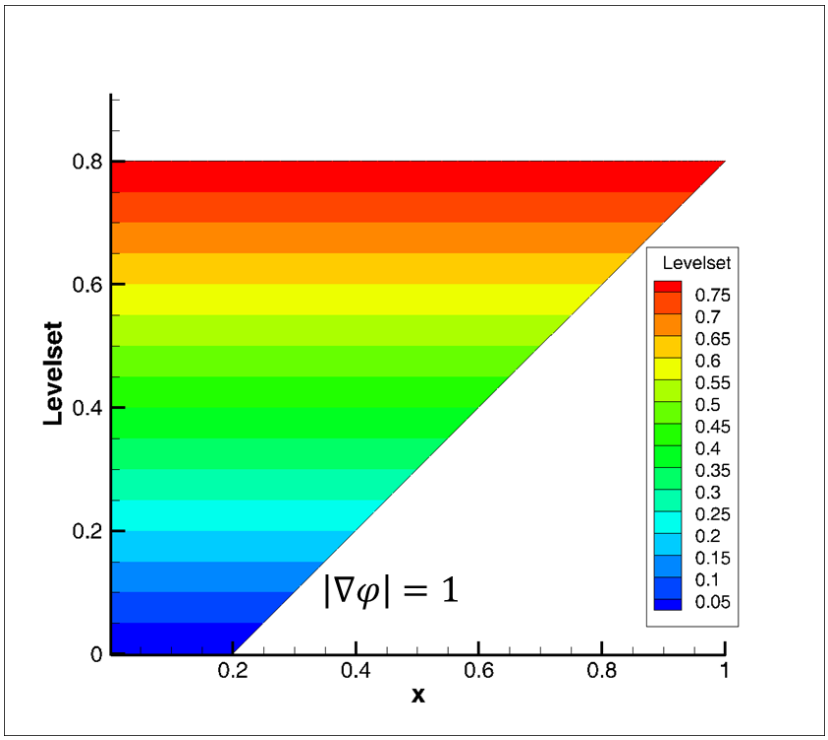

Figure 2.6. An ideal case of the level set function.

The figure 2.6 schematically shows the meaning of the equation (2.14). That is to say, the gradient value of the level set function is equal to 1.

Following the methodology proposed by [Peng D et al., 1999], the differential equation for re-initialization of the level set values is defined as:

$$\frac{\partial d}{\partial \tau} + sign(d_0)(|\nabla \mathrm{d}| - 1) = 0, \qquad (2.15)$$

where d is the signed distance function from the front, τ the imaginary time within the re-initialization procedure, and $sign(d_0)$ the sign function of the initial value d_0.

Additionally, the $sign(d)$ function is defined as

$$sign(d) = \frac{d}{\sqrt{d^2 + h^2}}, \qquad (2.16)$$

where h is the mesh size [Peng D et al., 1999].

The initial value of d is defined as:

$$d(\boldsymbol{x}, 0) = d_0(\boldsymbol{x}) = \varphi(\boldsymbol{x}, t). \tag{2.17}$$

After the calculation, the level set function φ is re-initialized as

$$\varphi(\boldsymbol{x}, t) = d(\boldsymbol{x}, \tau). \tag{2.18}$$

The re-initialization procedure is repeated for several times at each time step of the equation (2.13).

2.3. Methods for Pressure Calculation

A. CVFEM

CVFEM is one of the representative methods for RTM process simulation. To be more concrete, CVFEM is used for the discretization of the differential equation to calculate the pressure in the mold. And, this method is often combined with VOF method to calculate the flow front position.

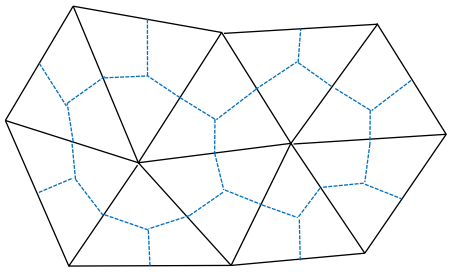

Figure 2.7. Control volumes of three-node triangular elements.

For applying CVFEM, control volumes are determined in elements so as to make the nodal value to the control volume value. An example of the control volume is illustrated in the figure 2.7. The control volume of three-node triangular elements is discretized as a polygonal surrounded by dotted lines. The polygonal is made by connection of the centroids of elements and the midpoints of element sides.

Generally, CVFEM is used with VOF method for RTM process simulation. After transporting the resin front by VOF method, the pressure in the mold is calculated by CVFEM. As mentioned before, the filling factors are the values of volumes. If the pressure in the mold is calculated by FEM, it is difficult to satisfy the conservation of mass in the boundaries between elements because the filling factors can be defined as the values of elements. In CVFEM, the filling factors can be defined as the values of control volumes (nodes). And, the integral formulation by using CVFEM is obtained by applying the conservation principle for pressures in the control volume [Baliga BR et al., 1980]. Therefore, CVFEM can naturally satisfy the mass conservation in the boundaries between elements.

However, CVFEM cannot reflect the discontinuity of pressure gradient on the interface/flow front. Hence, the pressure distribution on the interface/flow front is bluntly expressed, and, this phenomenon could make the simulation results inaccurately. To overcome this week point of CVFEM, we applied XFEM.

B. Extended Finite Element Method (XFEM)

XFEM has been developed to treat problems which have discontinuous field. The early usage of XFEM was limited to the problems of crack propagation [Sukumar N et al., 2000]. However, these days, the usage of XFEM is widely expanded to various problems such as the fluid-structure interaction and multiphase flows [Belyschko et al., 2009]. The reason why many researchers use XFEM might be that XFEM is easy to apply and more accurately approximates the discontinuity by just adding a few enrichment terms in the general FEM term. In this section,

XFEM is specifically explained because this method is applied to calculate the pressure in our study.

During mold filling in RTM process simulations, the gradient of the pressure (flow velocity) is discontinuous at the resin flow front. The traditional fixed grid methods such as CVFEM and FEM could not reflect this discontinuity. Despite the high computational efficiency of these fixed grid approaches, the approximation not to reflect the discontinuity causes a low accuracy of the simulation results. XFEM is adopted so as to reflect the discontinuity of the pressure gradient field near the flow front. XFEM makes it possible to include the discontinuity in the interpolation function or its derivative. Therefore, XFEM approximation is more precise than traditional methods to calculate the pressure in RTM process simulation.

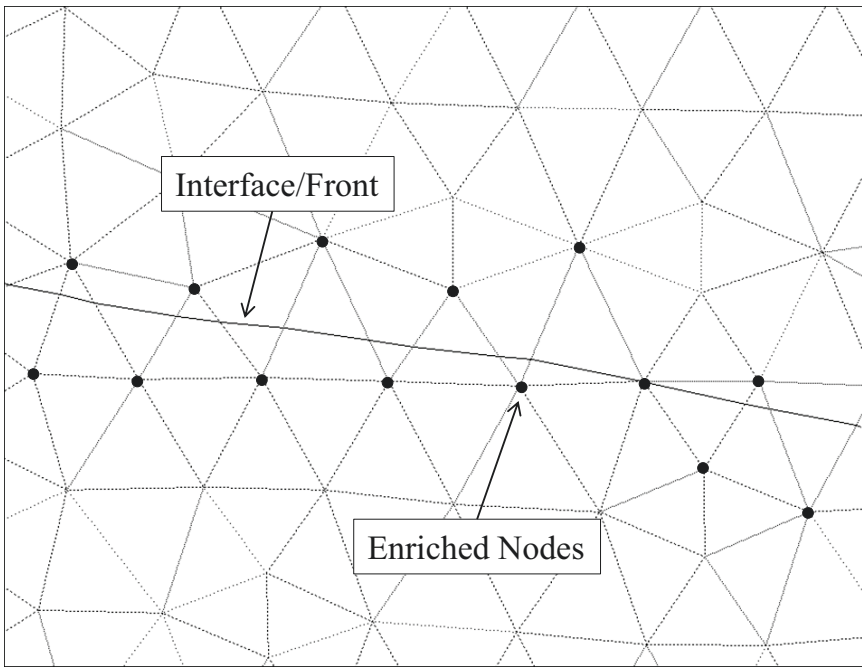

Figure 2.8. Definition of enriched nodes.

XFEM approximation is established by enrichment of the interface/front region. The enriched region is defined as shown in the figure 2.8, where enriched nodes are marked by dots. And, they are composed by the nodes of elements intersected by the interface/front.

The enrichment means that supplementary degrees of freedom (DOF) are added in a classical finite element. The approximation of the pressure function for the enrichment is defined as:

$$p^h = \sum_{I \in n} N_I p_I + \sum_{J \in n_e} N_J^e a_J, \tag{2.19}$$

where p^h is the pressure function, p_I the pressure value of the node I, a_J the additional nodal parameter at the enriched nodes J, N_I the shape function, N_J^e the enriched shape function, n the number of nodes, and n_e the number of enriched nodes [Chessa J et al., 2003]. The enriched shape function is built as:

$$N_J^e = N_J\left(|\varphi| - |\varphi_J|\right), \tag{2.20}$$

where φ_J is a level set value of the enriched node J [Chessa J et al., 2003].

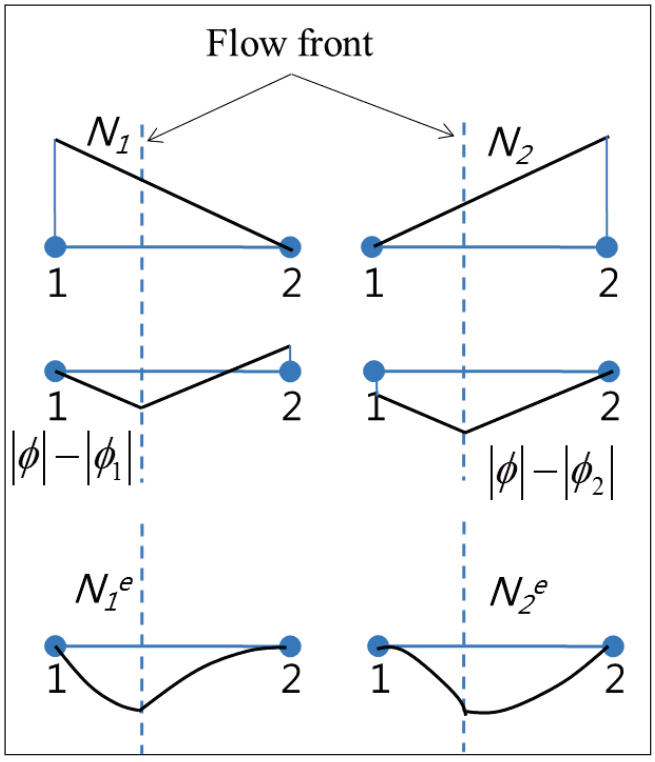

Figure 2.9. Enriched shape functions of one-dimensional linear element.

The discontinuity at the flow front can be reflected by the functions consisting of the level set functions and values. For example, the enriched shape functions of a

one-dimensional two-node element are plotted in the figure 2.9. The N_1 and N_2 are general shape functions of two-node elements. And, the second column shows the functions constructed by level set values of the nodes and level set function of the element. The enriched functions N_1^e and N_2^e are derived by multiplying the general shape functions and the functions of level set values and function as shown in the third column of the figure 2.9. The significant character of the enriched shape functions is that the position of the flow front is reflected in the enriched shape functions. It is noted that the values of the enriched shape functions should be zero at the nodal points.

The pressure gradient at the flow front should be calculated carefully. The gradient of the approximated pressure function on the enriched region is obtained as [Chessa J et al., 2003]:

$$\nabla p^h = \sum_{I \in n} p_I \nabla N_I + \sum_{J \in n_e} a_J \left[\nabla N_J \left(|\varphi| - |\varphi_J| \right) + N_J sign(\varphi) \nabla \varphi \right]. \quad (2.21)$$

The jump in the approximated pressure function across the resin front is given as [Chessa J et al., 2003]:

$$[\![\nabla p^h]\!] = 2 \sum_{J \in n_e} N_J a_J \nabla \varphi \quad \text{on the resin front.} \quad (2.22)$$

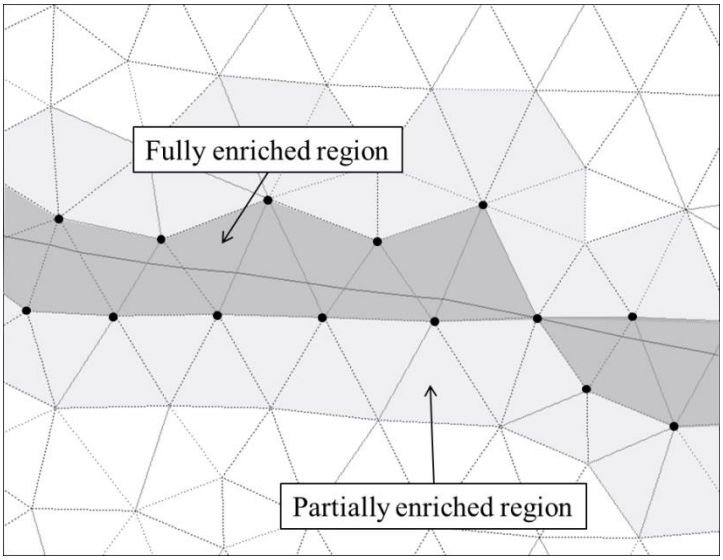

Figure 2.10. Types of enrichment.

There are two types of enrichment as shown in the figure 2.10: full enrichment and partial one. The full enrichment concerns the elements having only enriched nodes. On the other hand, the partial enrichment concerns the elements having both enriched and normal nodes. The partial enrichment is necessary to continuously keep the pressure between the fully enriched and normal regions.

Chapter 3.

Analysis of RTM Process

This chapter delineates our work on the analysis of RTM process using XFEM and level set method in detail. At first, the resin flow during mold filling is mathematically modeled. Here, there are explanations about our assumption for modeling and the mathematical models divided into two parts: the transport of resin flow front and the pressure calculation in mold. In the section 3.2, the numerical formulations of the two parts are explained in detail. After that, a flow chart of global computational procedures is shown in the section 3.3. Finally, our methods are validated through some simple examples.

3.1. Modeling

A. Assumptions

For the analysis of mold filling stage, the resin flow in the mold is simplified with the following assumptions. The resin is assumed as an incompressible fluid. And, the mold filling could be carried on under an isothermal condition if the mold filling is finished before the curing reaction. With these assumptions, the resin viscosity could be considered as constant during the mold filling. The permeability of the fiber preform in the mold could be constant with the assumption that the fiber preform is considered as uniform and non-deformable during the mold filling.

These assumptions have been used by many researchers so as to simplify the resin flow motion in the mold as a quasi-steady state problem [Young WB et al., 1991; Feerick R et al., 1997; Jiang S et al., 2007]. When the resin slowly moves, the inertia effect could be negligible and the resin flow could be assumed as a succession of a steady state flow. After obtaining the pressure field at the instance t, the flow velocity is calculated and the resin flow front is transported by the velocity. In other words, the mold filling stage is mathematically modeled into two governing equations: transport of resin flow front and pressure calculation in the mold.

B. Mathematical Models

The figure 3.1 shows a domain for analysis of RTM process. The domain (Ω) indicates that the dry preform is impregnated by the resin entered through injection gates.

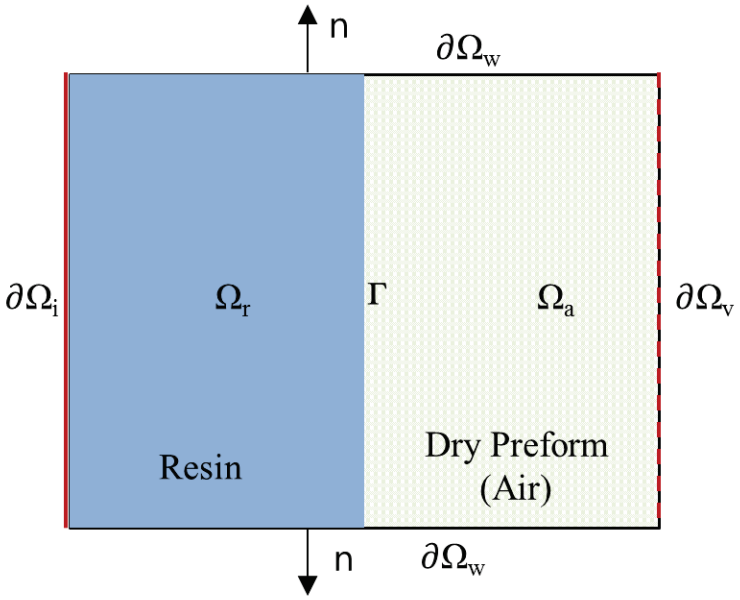

Figure 3.1. Computational domain for analysis of RTM process.

In the figure 3.1, Ω_r is the wet region by resin, Ω_a the dry region filled by air. Γ is the resin flow front, which is the interface between the resin and the air. $\partial\Omega_i$, $\partial\Omega_v$, and $\partial\Omega_w$ are the injection port, vent and mold wall, respectively.

During the mold filling, the resin and air in the mold are considered as incompressible and isothermal condition. Therefore, the mass conservation equation is given as:

$$\nabla \cdot \mathbf{u} = 0 \quad \text{in } \Omega. \tag{3.1}$$

And, the Darcy's equation is given as:

$$\mathbf{u} = -(\mathbf{K}/\mu)\nabla p \quad \text{in } \Omega, \tag{3.2}$$

where p is the pressure, **K** the permeability tensor, and μ the viscosity. The permeability tensor (**K**) and fluid viscosity (μ) are constant during the mold filling. By substituting the equation (3.2) into the equation (3.1), the governing equation for the pressure field becomes as:

$$\nabla \cdot (-(\mathbf{K}/\mu)\nabla p) = 0 \quad \text{in } \Omega. \tag{3.3}$$

The boundary conditions are defined as the below equation (3.4). At injection gates, resin is injected by constant pressure or flow rate in the mold. Thus, the boundary conditions are set to injection pressure at injection gates as:

$$p = p_{injection} \qquad \text{in } \partial\Omega_{\text{in}}. \tag{3.4 – a}$$

In addition, the pressure at vents is same with the air pressure as:

$$p = p_{air} \qquad \text{in } \partial\Omega_{\text{v}}. \tag{3.4 – b}$$

At mold walls, the resin flow cannot pass through mold walls; therefore, the partial derivative of pressure with respect to the normal direction of mold walls is equal to zero as:

$$\frac{\partial p}{\partial n} = 0 \qquad \text{in } \partial\Omega_{\text{w}}. \tag{3.4 – c}$$

Then, the pressure field and fluid velocity in the mold are solved at each time as steady-state problem, the resin flow front is transported for the next time step.

The resin flow front is transported by solving the following equation:

$$\partial\varphi/\partial t + \mathbf{u}\cdot\nabla\varphi = 0 \quad \text{in } \Omega, \tag{3.5}$$

where t is the time, φ the level set function, and **u** the fluid velocity [Sethin JA, 1999]. By solving the equation (3.5), the level set values are updated at each time step. The details to derive the equation (3.5) are explained in the section 2.2. To correctly transport the flow front, re-initialization of level set values should be performed after solving the equation (3.5). The details for the re-initialization are also presented in the section 2.2.

3.2. Formulation

A. Transport of Flow Front

The differential equations for transport of flow front are solved by the implicit characteristic Galerkin FEM [Lin CL et al., 2005]. The implicit characteristic Galerkin FEM is employed to stabilize the non-self adjoint term. The time derivative term is discretized by the implicit characteristic method as [Zienkiewicz OC et al., 2000]:

$$\varphi^{n+1} - \varphi^{n} = -\Delta t[\mathbf{u} \cdot \nabla\varphi]_{n} + \frac{\Delta t^{2}}{2}\left[\nabla \cdot \left((\mathbf{u}\otimes\mathbf{u}) \cdot \nabla\varphi\right)\right]_{n+1}, \tag{3.6}$$

where Δt is the size of the time step. For the discretization of the spatial differential terms in the equation (3.6), the standard Galerkin FEM is applied as:

$$\int_{\Omega}(\varphi^{n+1} - \varphi^{n})w dV = -\Delta t\int_{\Omega}(\mathbf{u} \cdot \nabla\varphi^{n})w dV - \frac{\Delta t^{2}}{2}\int_{\Omega}\left((\mathbf{u}\otimes\mathbf{u}) \cdot \nabla\varphi^{n+1}\right) \cdot \nabla w dV, \tag{3.7}$$

where w is the weight function and Ω is the whole space in the mold. The velocity $\mathbf{u}$ for transport of the front is calculated by the equation (3.3).

The re-initialization equation is also discretized by the procedures of the equation (3.6) and (3.7) as:

$$\int_{\Omega}(d^{n+1}-d^{n})wdV = \\ -\Delta\tau\int_{\Omega} sign(d_0)|\nabla d^{n}|wdV \\ -\frac{\Delta\tau^{2}}{2}\int_{\Omega}\nabla d^{n+1}\cdot\nabla wdV \\ +\Delta\tau\int_{\Omega} sign(d_0)\mathrm{wdV}, \tag{3.8}$$

where $\Delta\tau$ is the size of the time step in the re-initialization procedure.

In the equation (3.8), the second term of the right-hand side could be derived by the next procedure:

$$sign(d_0)|\nabla d| = sign(d_0)\frac{\nabla d}{|\nabla d|}\cdot\nabla d\,, \\ \left(sign(d_0)\frac{\nabla d}{|\nabla d|}\right) sign(d_0)|\nabla d| = \nabla d. \tag{3.9}$$

The coefficient matrices of systems obtained by the formulations are symmetric and positive definite; therefore, the multi-frontal solver of IPSAP [Kim JH, 2005] can be applied.

B. Pressure Calculation

The differential equation for the pressure calculation is solved by using XFEM. XFEM formulation is similar with the general FEM. The weak form of the equation (3.3) is obtained as:

$$\int_{\Omega}(\nabla\cdot\left(-\frac{\mathbf{K}}{\mu}\nabla p\right))wdV=0, \tag{3.10}$$

where w is the weight function. Applying the Green-Gauss theorem, the equation (3.10) is transformed as:

$$\int_{\Omega}\nabla \mathrm{w}\cdot\left(-\frac{\mathbf{K}}{\mu}\nabla p\right)dV-\int_{\partial\Omega}\mathrm{w}\left(-\frac{\mathbf{K}}{\mu}\nabla p\right)\cdot\mathbf{n}dS=0, \tag{3.11}$$

where **n** is the outward normal vector. By XFEM, the pressure and weight functions are discretized as the equation (2.19). In other words, the approximation of the solution is done by adding the additional terms for the enrichment in the terms of the standard Galerkin FEM.

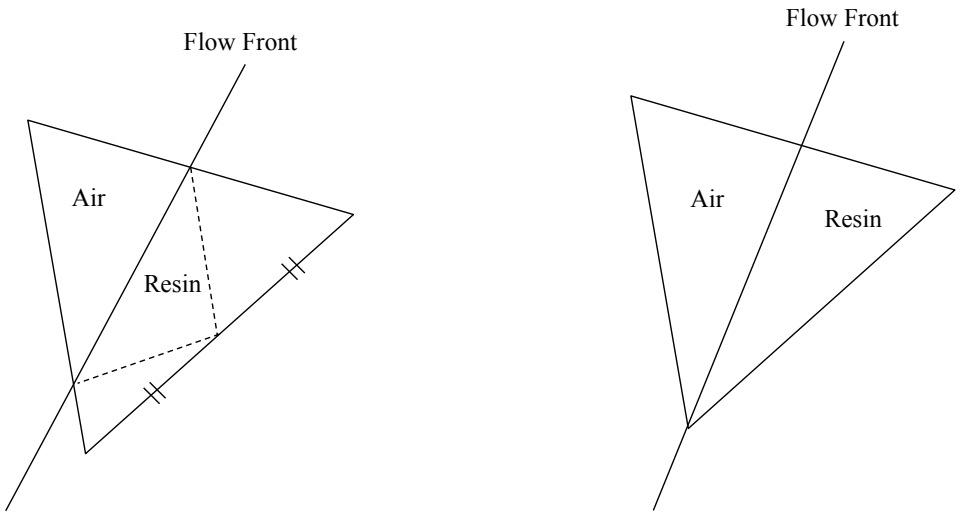

(a) Case 1 (b) Case 2

Figure 3.2. Subdivision in elements intersected by flow front.

The integral of the equation (3.11) is calculated by the Gauss quadrature method. The elements intersected by the flow front are divided into two parts: filled and unfilled regions. These two regions are separately integrated because the

derivative of the pressure function is weakly discontinuous at the flow front. At the normal region, the integration performed by the Gauss quadrature method in general FEM without any special treatment. However, for the integral on the fully enriched region, the elements intersected by the flow front are divided into several parts. As shown in the figure 3.2, four or two sub-domains are constructed. When the flow front passes through two sides of a triangle, the element is divided by four sub-domains as shown in the figure 3.2 (a). In addition, when the flow front passes through one point and one side of a triangle, the element is divided by two sub-domains as shown in the figure 3.2 (b). The integral of each sub-domain is individually calculated by the Gauss quadrature rule.

The permeability **K** of fiber preform is considered as constant in the whole domain. However, the viscosity μ of resin is different at each region. At the filled region by resin, the resin viscosity is applied. And, the empty region has air viscosity. The viscosity of the region intersected by resin flow front should have an averaged value of resin and air. Therefore, the fluid viscosity is defined as:

$$\mu = H(\varphi)\mu_r + (1 - H(\varphi))\mu_a, \qquad (3.12)$$

where μ_γ is the resin viscosity; μ_α the air viscosity, and φ the level set value. Here, $H(\varphi)$ is defined as

$$H(\varphi) = \begin{cases} 1 & if \ \ \varphi < -h \\ \frac{1}{2}\left(1 - \frac{\varphi}{h}\right) & if \ \ |\varphi| \le h \\ 0 & if \ \ \varphi > h \end{cases}, \qquad (3.13)$$

where h is the mesh size.

3.3. Computing Procedures

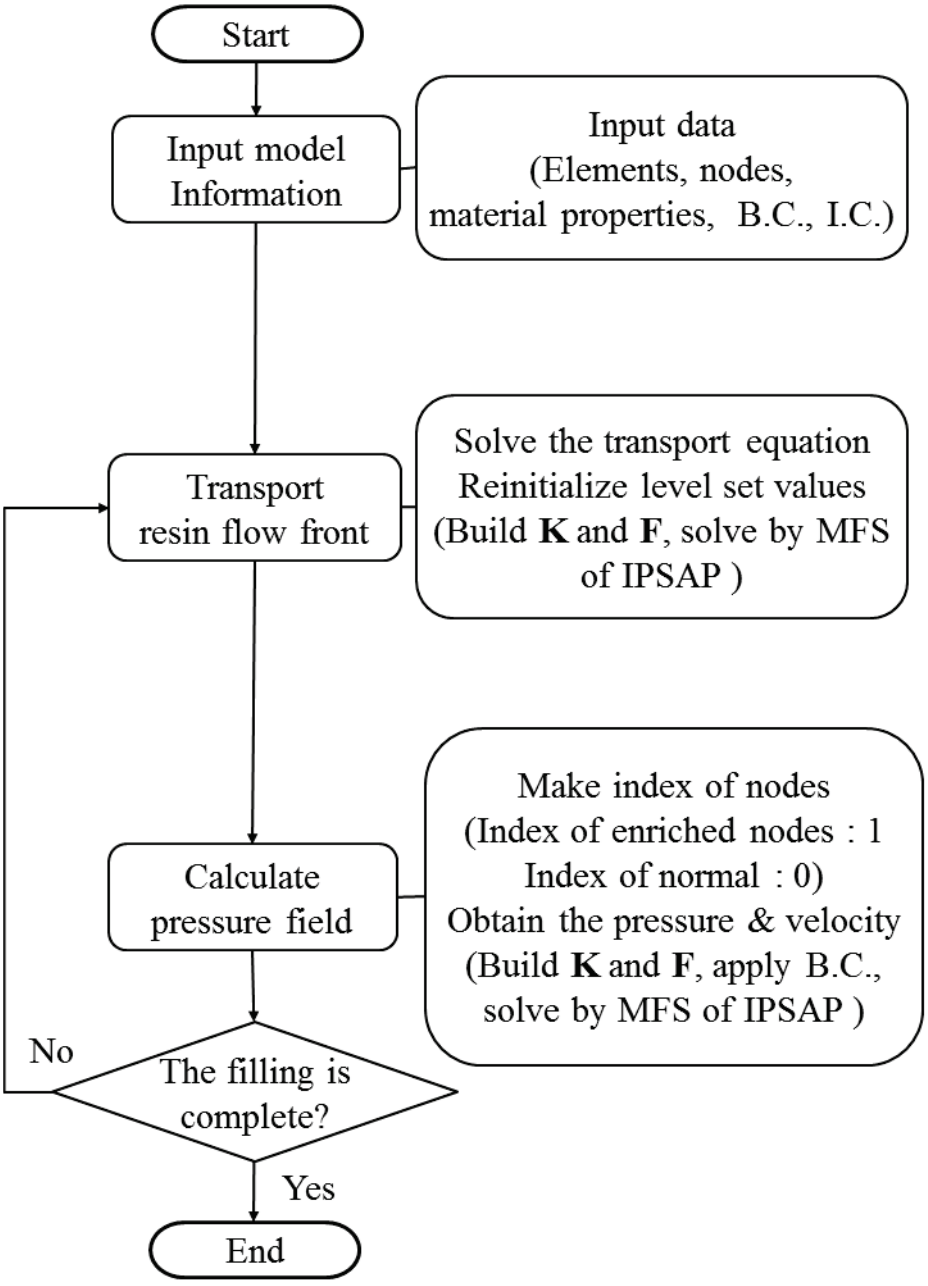

Figure 3.3. Flow chart of the computational procedures.

The whole computation scheme is shown in the figure 3.3. The details are explained as follows. The first step is to read the input data, such as the mesh information, material properties, and boundary conditions, and to initialize the pressure field and level set values. At the second step, the fluid velocity is calculated from the pressure field by using the Darcy's equation, explained in the section 3.1. The level set values are calculated in order to transport the resin front. The re-initialization of the level set values is performed at each time step. Then, the index of the nodes is set by the level set distribution: enriched nodes by 1 and normal nodes by 0 to denote the corresponding shape functions. The second and third steps are continued until the mold filling is complete. The multi-frontal solver of IPSAP [Kim JK et al., 2005] was applied to solve the discretized equilibrium systems. The multi-frontal solver of IPSAP is presented in Appendix A. This method and a GUI (Graphic User Interface) are implemented in DIAMOND program for analysis of RTM process. DIAMOND program, developed by Aerospace Structures Laboratory in Seoul National University, is presented in Appendix C [Kim SJ, 2010].

3.4. Validation

Our methods implemented in C++ are verified in this section. At first, the pressure calculation part is tested on a simple square plate quarter-filled with resin. Its object is to check whether XFEM can correctly calculate the pressure field, in particular, near the flow front. After, the level set method is tested with a square plate with an injection gate at the center of the plate. At the end, the numerical results obtained by our methods on plates are compared with the analytical results for simple channel and radial flows.

3.4.1. Pressure Calculation

The pressure calculation by XFEM is verified by using a simple square plate as shown in the figure 3.4. At the instance when this plate is quarter-filled with resin, the pressure is calculated by XFEM so as to examine that the pressure near the resin flow front is sufficiently linear when elements are intersected by the front and to compare it with FEM in order to show the effect of enrichment by XFEM.

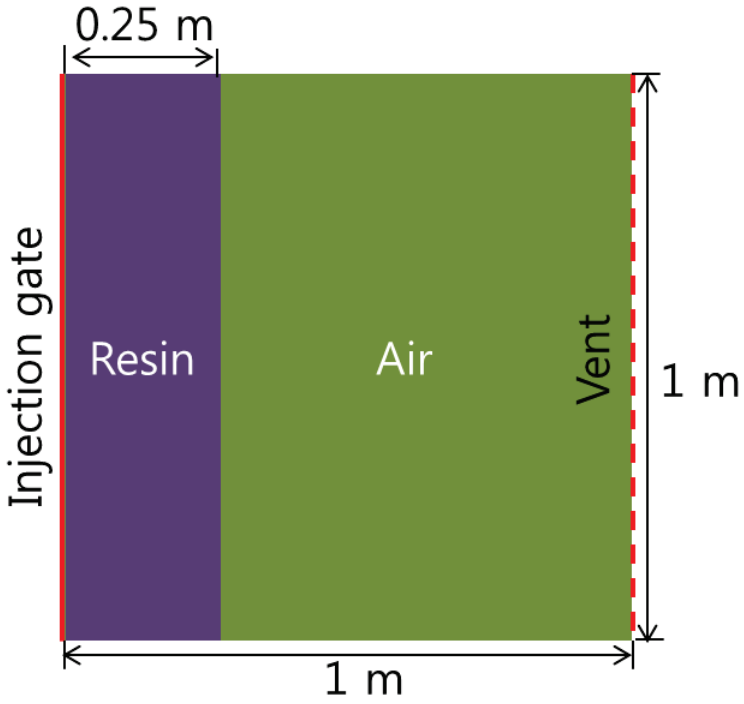

Figure 3.4. A simple square plate.

The mesh condition of the model is shown in the figure 3.5. The red line is placed on the flow front position. As shown in this figure, the elements, placed between 0.2 m and 0.3 m in the x-direction, are intersected by the red line (resin front). The numbers of nodes and elements are 121 and 200, respectively. The viscosity values of resin and air are set to 0.1 Pa·s and 0.00001 Pa·s, respectively. For the boundary conditions, the injection and vent pressure are set to 100 MPa and 10 MPa, respectively.

The computation results are plotted in the figure 3.5. As shown in the contour obtained by XFEM (Figure 3.5 (a)), the pressure distribution near the flow front looks linear along the y-axis, not zigzagged, even though the elements are intersected by the flow fronts. Therefore, XFEM might reasonably describe the pressure near the front.

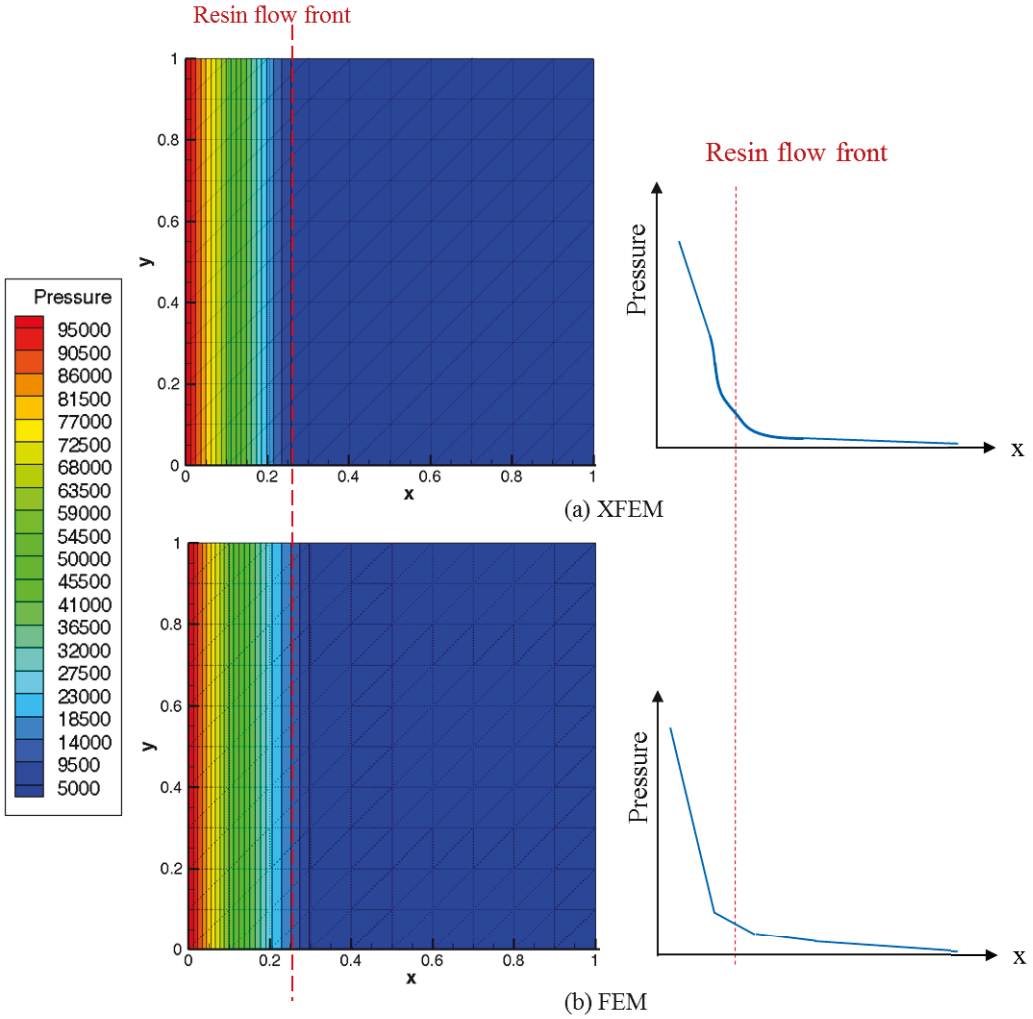

Figure 3.5. Pressure contours and graphs of a simple square plate quarter-filled by resin.

Furthermore, the contours obtained by XFEM and FEM are dissimilar, especially in the elements near the resin flow front. The pressure obtained by XFEM (Figure 3.5(a)) is more steeply decreased in the elements near the flow front, compared to the one by FEM (Figure 3.5(b)). And also, the pressure gradient obtained by

XFEM is changed near the front, contrary to the one by FEM. Therefore, it is possible to conclude that the enrichment by XFEM is well-working in this computation.

3.4.2. Transport of Flow Front

The transport of flow front is verified through simple models. The geometry and mesh information of the models is shown in the figure 3.6. The model is a thin square plate which has the width and height of 0.1 m. And the thickness is 1 mm. The type of element is three-node triangle. The number of elements and nodes are 2048 and 1089, respectively. The mesh condition is a little fine in order to well show the round shape.

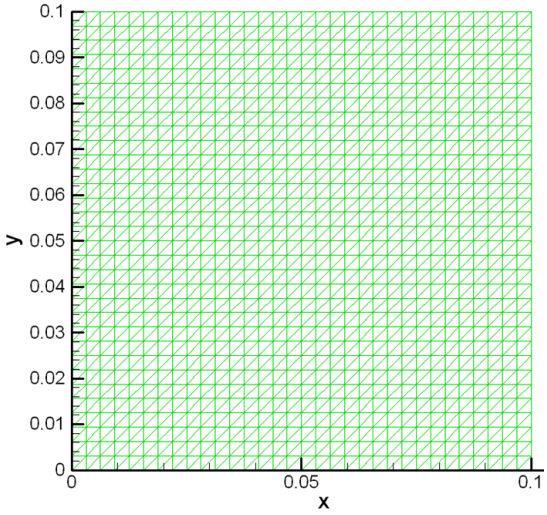

Figure 3.6. Geometry and mesh information of a thin square plate for verifying level set calculation.

At first, the verification of re-initialization procedure is performed by using the model described in the figure 3.7. The model is filled with resin until the circle region which is 0.025 meters in radius. The circle region is placed at the middle of the square. The region except the one surrounded by the circle is filled with air.

In order to set the initial level set values into incorrect values, the initial condition of level set is given as:

$$|\nabla\varphi| = |\nabla d_0| = 2. \qquad (3.14)$$

This condition means the gradient of level set values is 2. After the re-initialization computation, the level set values should be changed from the condition of the equation (3.14) to the correct condition: $|\nabla\varphi| = 1$.

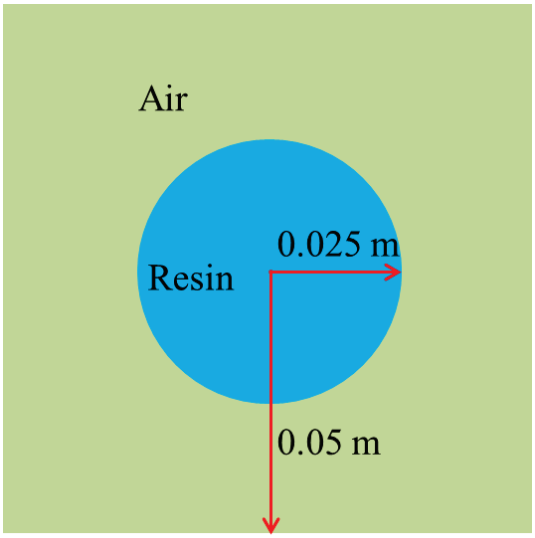

Figure 3.7. A model for the verification of the re-initialization procedure.

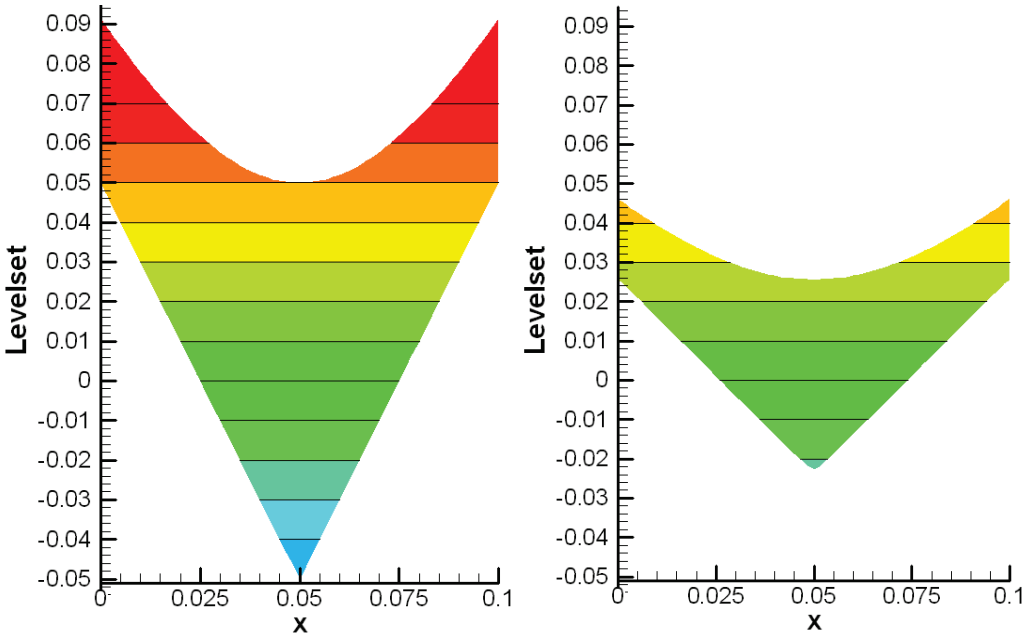

(a) Initial step (b) 70th step

Figure 3.8. Change of level set values by the re-initialization procedure.

The change of level set by re-initialization procedure is shown in the figure 3.8. As shown in the figure 3.8 (a), at the initial step, the gradient of level set function is equal to 2. After seventieth time step, the gradient of level set function becomes 1 as shown in the figure 3.8 (b).

The total level set calculation procedure including the transport of flow front and the re-initialization is verified by a uniform expansion flow model. The model is shown in the figure 3.9. At the initial condition, the resin front is placed at the region of 0.02 meters in radius from the center. The velocity of fluid flow is uniform and the flow is expanded to the normal direction of flow front.

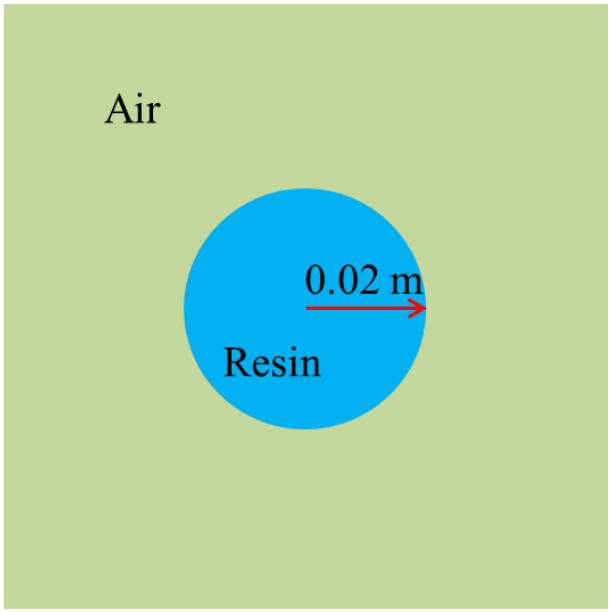

Figure 3.9. Thin square plate with the uniformly expanded fluid flow.

The figure 3.10 shows the change of level set values after the calculation. At the initial step, the flow front is placed on the 0.02 m in radius from the center. After twentieth steps, the flow front is uniformly expanded until 0.025 m in radius.

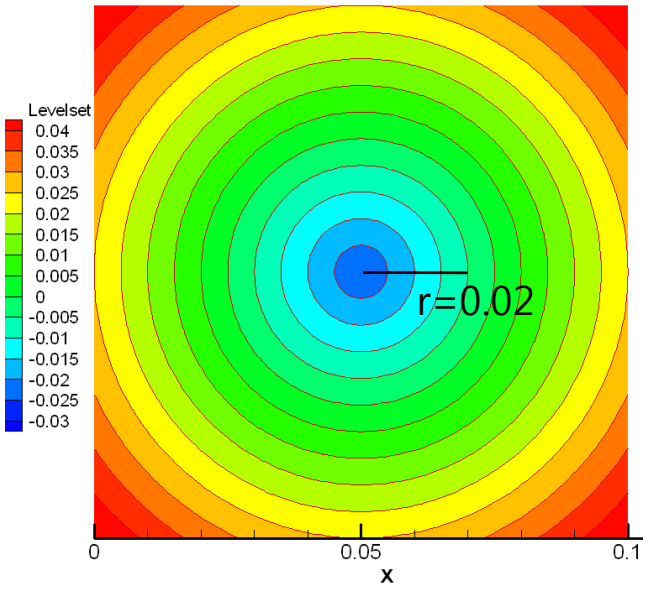

(a) Initial step

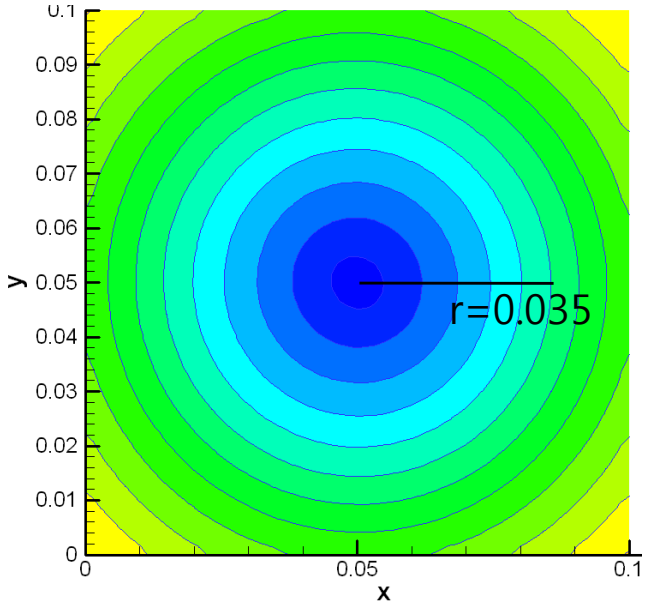

(b) 20th step

Figure 3.10. Change of level set values by the level set calculation procedure including the transport of flow front and the re-initialization.

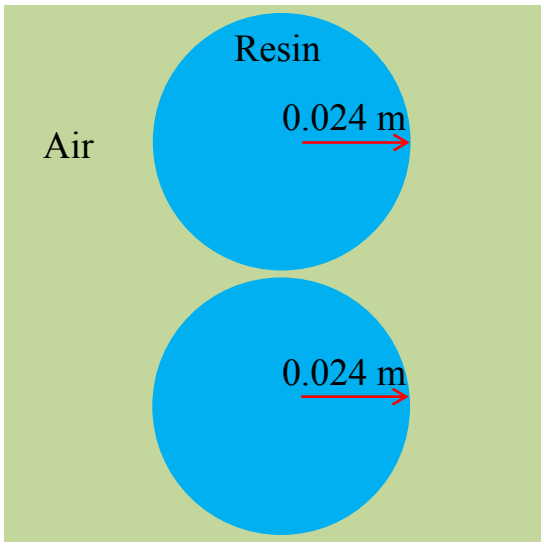

Figure 3.11. Plate for uniform expansion flow with two fronts.

For testing the merging of flow fronts, thin square plate with uniformly expanded fluid flow at two flow fronts is used. Two resin fronts are placed on the two points as shown in the figure 3.11. The fluid flow also has constantly expanded velocity field.

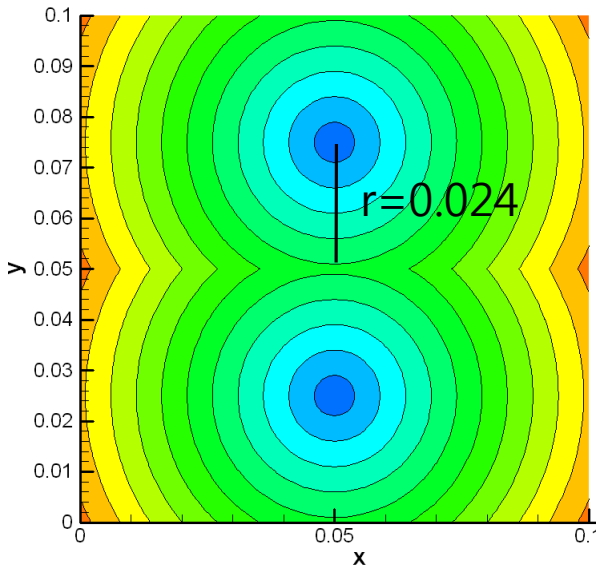

(a) Initial step

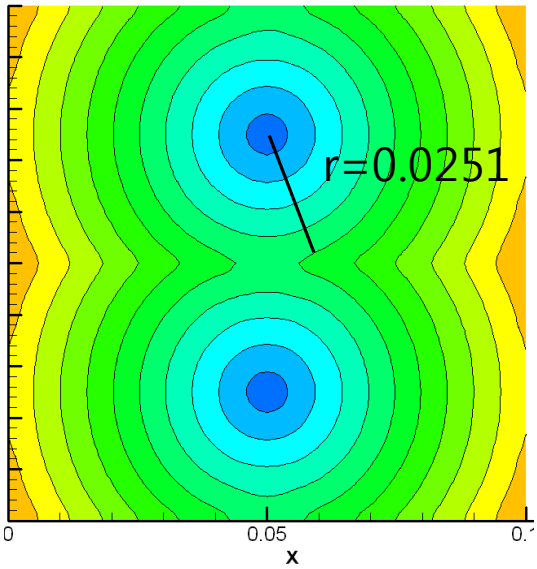

(b) 1st step

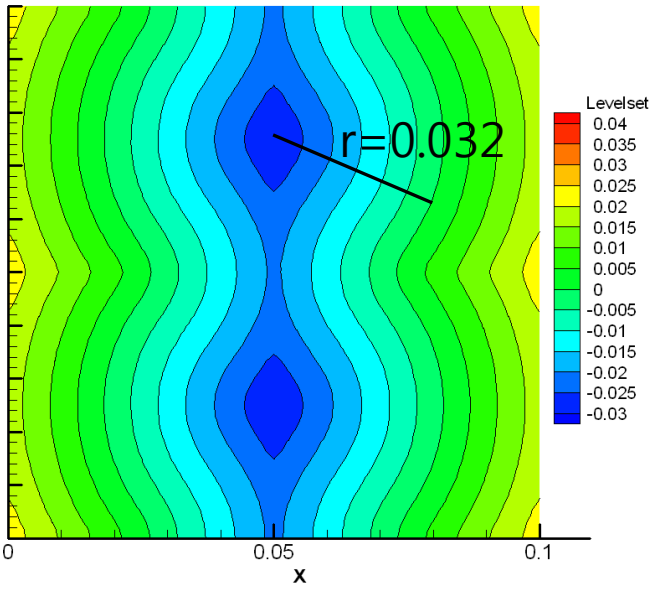

(c) 10th step

Figure 3.12. Merging of two flow fronts.

The results are shown in the figure 3.12. At initial step, the two fronts do not touch each other. The two fronts touch each other from the first step. After tenth step, the two fronts are perfectly merged.

3.4.3. Comparison with Analytic Solutions

Simple channel or radial flow examples are treated to validate the present methods in comparison with analytical solutions. The total filling time obtained in this study is compared with the analytical one proposed by Cai Z [1992]. A three node triangular element is used in this analysis

A. 2D Channel Flow in a Rectangular Plate

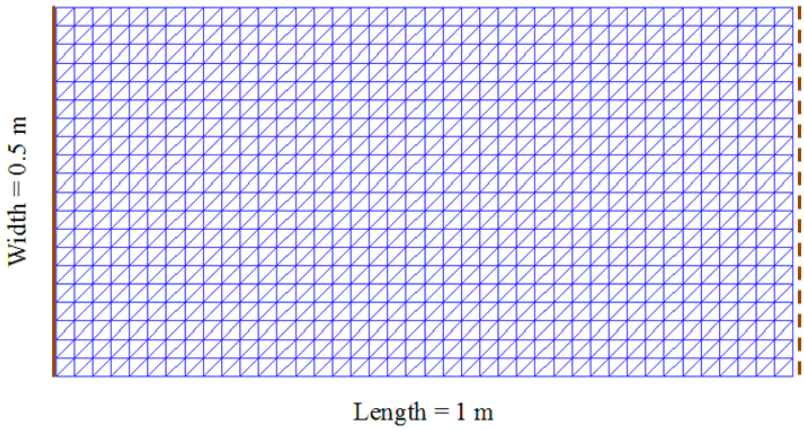

Figure 3.13. Geometry and mesh of the channel flow rectangular plate

The figure 3.13 shows a 2D channel flow of rectangular plate with a constant width. Its length, width and thickness are equal to 1 m, 0.5 m and 1 mm, respectively. The resin is injected at the whole left side of the plate, as marked by the solid line. And the resin goes out from the mold through the whole right side of the plate (dashed line). The numbers of total nodes and elements are 861 and 1600, respectively. Material properties and boundary conditions of the model are set as follows: resin viscosity = 0.1 Pa·s, preform permeability (isotropic and constant) = 10^{-9} m^2, porosity = 0.5, injection pressure = 20 KPa, vent pressure = 0.

The analytic mold filling time for the channel flow, when the injection pressure is identical to the width direction, is given as:

$$t_{filling} = \frac{L^2 \mu \phi}{2KP}, \tag{3.15}$$

where L means the position of the flow front in the length direction. And, μ, ϕ, K, and P are the viscosity, porosity, permeability, and pressure, respectively.

The analytical total filling time by the equation (3.15) is equal to 1250 seconds. The numerical total filling time obtained in this study is equal to 1268.42 seconds. The difference between the analytical and numerical results is less than 1.5%. In comparison with the numerical solution (difference of 3%) proposed by S. soukane and F. Trochu [2006], which treated the same example, our program is more accurate.

B. 2D Radial Flow Example in a Circular Plate

The figure 3.14 shows the radial flow model with a thin circular disk. Because of its axisymmetric conditions, a quarter of the disk is modeled. The radius of the disk is 1 m. And the thickness is equal to 1 mm. The resin is injected through a hole located at the center, of which the radius is equal to 0.2 m. The numbers of nodes and elements are 2082 and 3987, respectively. The dashed line at the outer side of the plate means the vent location. The value of resin viscosity, preform permeability, porosity, and injection pressure are the same as in the previous example (2D channel flow example).

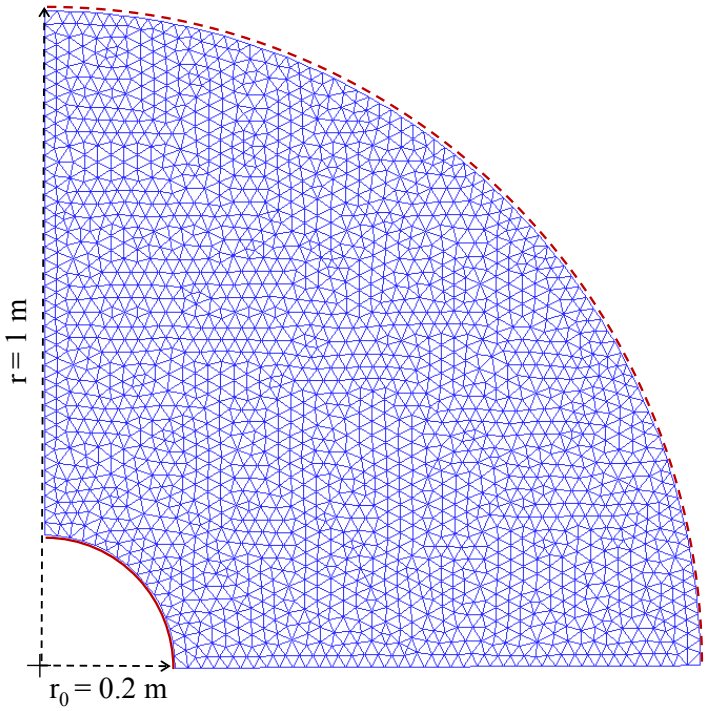

Figure 3.14. Geometry and mesh of the radial flow model.

The analytic mold filling time of the channel flow model is obtained by the following equation:

$$t_{filling} = \frac{\mu\phi r_0^2}{4KP}\left(\frac{r}{r_0}\right)^2\left(2\ln\frac{r}{r_0} + \frac{r_0^2}{r^2} - 1\right), \qquad (3.16)$$

where r is the radius of the plate and r_0 the radius of the hole. The analytical filling time of the radial flow example is equal to 1411 seconds. The numerical filling time obtained in this study is 1436 seconds. The difference between the two results is 1.8 %. Our program is more accurate in comparison with Mark Lin et al. [1998] which give 4% of difference with the analytical solution.

Chapter 4. Efficiency of Localization Method

This study presents a localization method of level-set method and XFEM so as to improve computational efficiency. The localization means to minimize the whole computational amounts through reallocating the computational domain to a small area at every time step. For the analysis of mold filling, the important data is the level set values in the region near the flow front and the pressure/velocity values in the resin region. If it is possible to calculate the data of only the small region, the computational time could be dramatically decreased. However, the localization is quite difficult to apply because the level set values easily oscillate at the boundaries of the local domain. And also, when calculating the pressure values, the boundary location is changed every time step. Therefore, the key points in the localization method are how to prevent the oscillation and detect the boundary location at the every time step. In the section 4.1, the method to prevent the oscillation is introduced as well as the method to reallocate the local domain for calculating the level set values. And, the section 4.2 is focused on how to detect the boundary location with the method to reallocate the local domain for the pressure calculation. The efficiency of the localization method is explained in the section 4.3.

4.1. Level Set Method

In the analysis of RTM process, only the level set values near the flow fronts are used to calculate the pressure values. Therefore, the localization of level set method is attempted to obtain only the necessary level set values without any influence about the analysis results. Generally, the most time-consuming procedure is the solving part of the linear system. If the system size (DOF number) becomes much smaller, the total computation time could be certainly reduced. Even though another computation is included for reallocation of the domain, the total computation time might be appreciably decreased because the time for the allocation is relatively very less.

The algorithm, used for localization of the level set method, is based on the PDE-based fast local level set method algorithm proposed by Peng et al [Peng D et al., 1999] and modified to apply to the implicit characteristic Galerkin FEM.

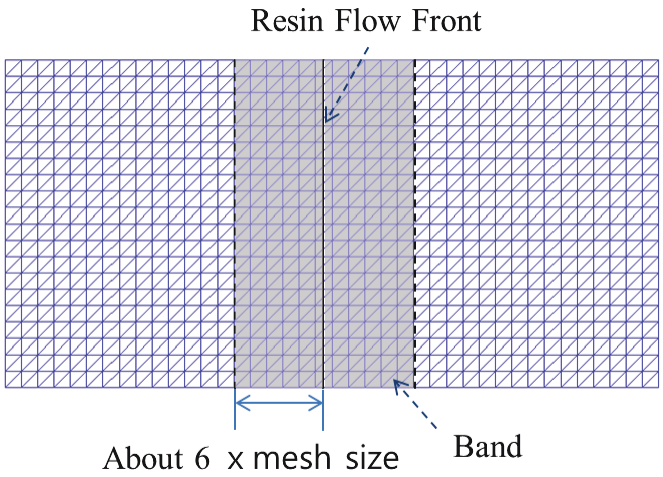

Figure 4.1. Computational domain for localization of the level set method.

A region near the flow front is allocated for the localization of level set method as shown in the figure 4.1. The band marked by grey is the allocated region. The band is newly defined at each time step because the position of the flow fronts moves. A distance from the resin flow front to the band boundary is equal or

inferior to six times as long as the mesh size in both directions. The distance includes the zones to buffer the oscillation of the boundary. And also, the distance could be changed by the order chosen by the special derivative terms [Peng D et al., 1999]. The level set values of nodes are updated only in the band at each time step. Therefore, the computational amounts become small.

Peng et al. [Peng D et al., 1999] proposed the band formation algorithm to apply to the FDM. In this study, their algorithm is modified so as to properly adapt the algorithm to the FEM. The differences with their algorithm are change of the procedure to define the list of nodes for reinitialization and addition of the procedure to define the list of elements in the band.

To explain the procedure of the level set localization, at first, the band size is chosen. Next, the level set values of every node are scanned to judge whether the node is in the band or outside of the band. By comparing the level set values of the nodes with the band size, the nodes are indexed by the number 0, 1, or 2, and classified into the three lists. The index of nodes is used while the elements are assorted. The code makes the lists of elements through scanning the index of the nodes of each element. The first list is for the element in the band. And, the second is for the elements in the band and its boundary. Only the elements included in the two lists are called when constructing the equilibrium system to calculate the level set values at each time step.

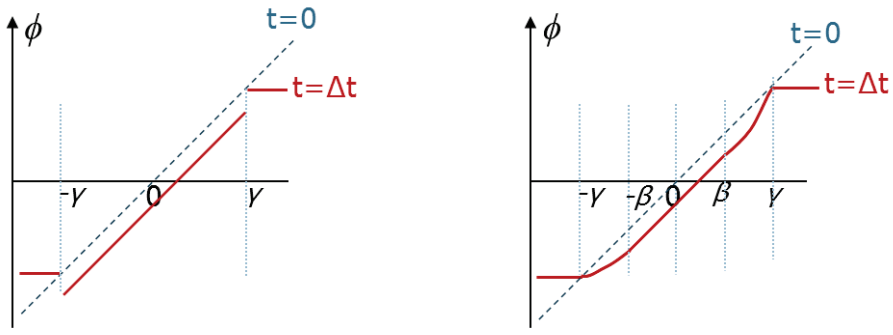

(a) Before applying a cut-off function (b) After applying a cut-off function

Figure 4.2. Change of a level-set function by applying a cut-off function.

For the localization of level set method, a cut-off function is necessary to prevent numerical oscillations at the band boundary. The role of a cut-off function is described in the figure 4.2. As shown in the figure (a), the level set function, marked by red, ought to be strongly discontinuous when it is transported only in the local domain. Therefore, a cut-off function is applied to make the level set function continuous as shown in the figure (b). The cut-off function is defined as [Peng D et al., 1999]:

$$c(\varphi) = \begin{cases} 1 & if\ |\varphi| \le \beta \\ (|\varphi| - \gamma)^2(2|\varphi| + \gamma - 3\beta)/(\gamma - \beta)^3 & if\ \beta < |\varphi| \le \gamma\ , \\ 0 & if\ |\varphi| > \gamma \end{cases} \qquad (4.1)$$

where φ is the level set value, γ six times of the mesh size, β three times of the mesh size. By applying the cut-off function in the differential equation (3.6) to calculate the level set values, the governing equation is modified as:

$$\frac{\partial \varphi}{\partial t} + c(\varphi)\mathbf{u} \cdot \nabla\varphi = 0. \qquad (4.2)$$

The level set values, obtained by the equation (4.2), are correct in the space within β range from the resin flow front. In the space between γ and β from the front, the values are modified by the cut-off function. Outside of the band of γ range from the resin flow front, the level set values are not updated.

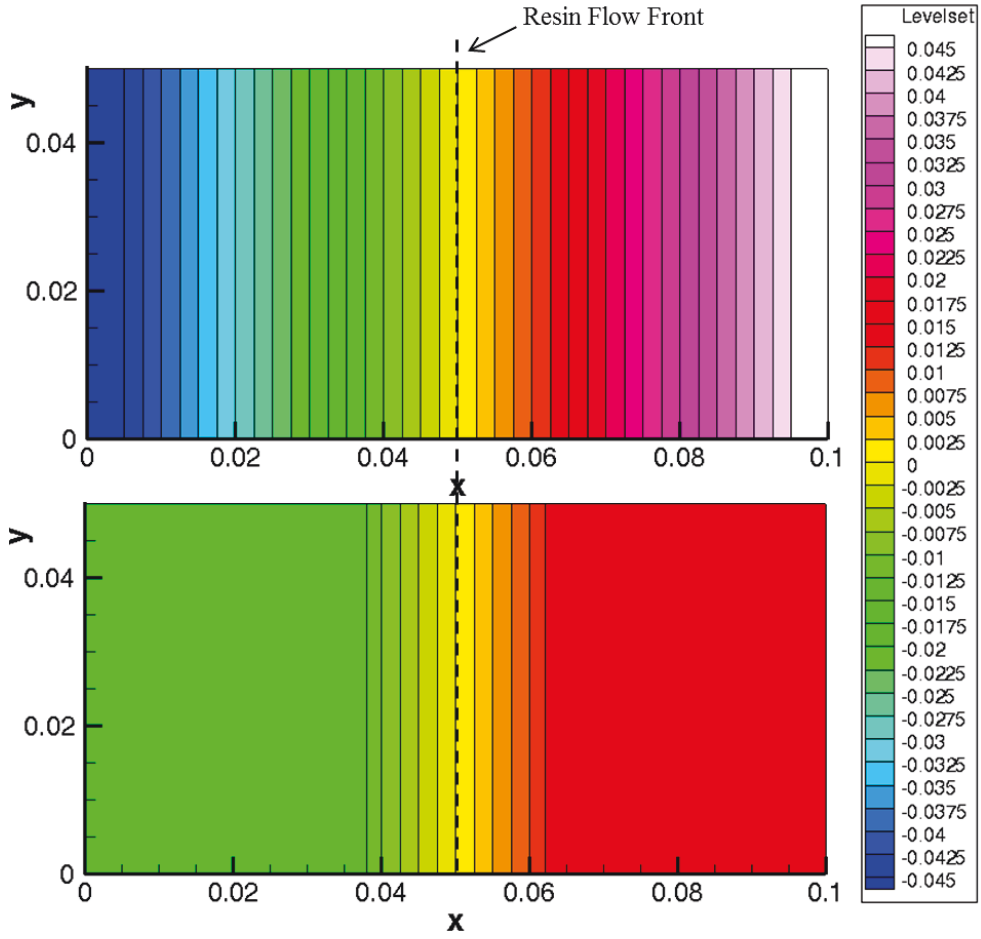

Figure 4.3. Level set contours obtained without (Top) and with (Bottom) localization of the level set method.

A channel flow example is used to show the difference of the two calculations without and with the localization of the level set method. The example information for modeling is explained in Section 3.4.3. A. The figure 4.3 shows the contour of level set values at the early stage of the mold filling. As shown in the top contour of the figure 4.3, the change of values is indicated at the whole domain because they are obtained by calculation without the localization. However, the bottom contour shows the change only in the band. At the region out of the band, the values are set to 0.15 or -0.15 which is the distance of the band boundary from the front. The total filling times obtained by the computation with the localization and without localization are totally same (1268.4 sec.).

4.2. XFEM

The localization of XFEM is proposed to reduce the computational effort of the pressure calculation. As aforementioned, the pressure in the mold is used to calculate the flow velocity. By the same way as the localization of level set method, the pressure outside of the local computation domain is not used taken into account. This study makes the local computation domain for obtaining the pressure so as to avoid unnecessary computations.

The key point of the localization of XFEM is how to apply the boundary conditions. As the initial conditions are used with the level set method, the pressure is calculated with the boundary conditions. If we take into account only the filled region by the resin and a narrow band after the flow front, the boundaries change at each time step. Therefore, the boundaries changed at each time step might be considered with the localization of XFEM.

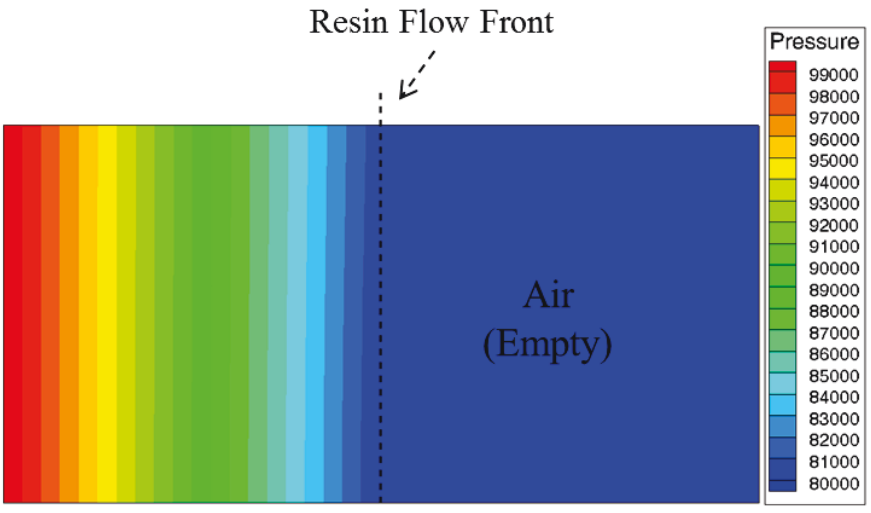

Figure 4.4. Pressure contour of the channel flow model.

The figure 4.4 shows pressure contours in the mold obtained by XFEM without localization. As shown in the figure 4.4, the air pressure in the mold remains almost constant. The pressure of the air region in a narrow band near the front flow is necessary to obtain the flow velocity. Therefore, we calculate the pressure only on the filled region and this narrow band.

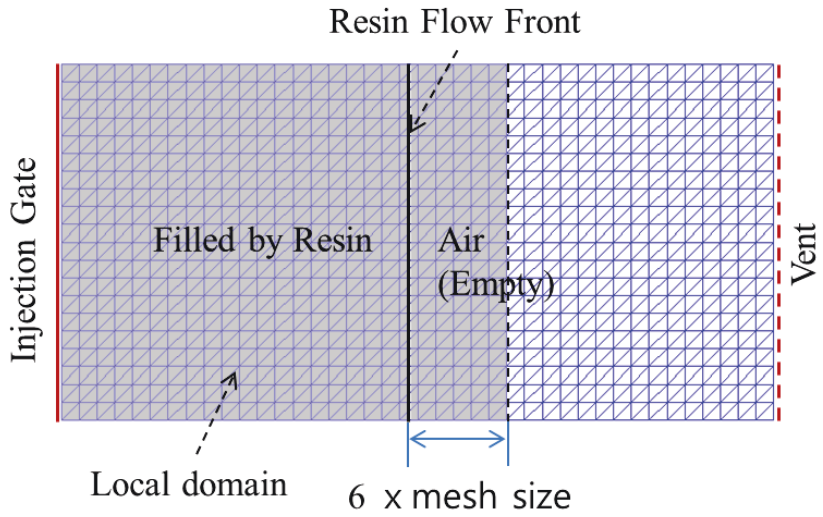

Figure 4.5. Localized computational domain (Localization of XFEM).

The local domain for the pressure calculation is defined as shown in the figure 4.5 including the filled region and the narrow band of the air region. The bandwidth is defined by six times of the mesh size as the localization of Level set method .

The boundary of empty side in the local domain is set to the vent pressure because the change of the pressure in the air region is very less. The boundary conditions at the mold wall, injection gates, and vents are same with the equation (3.4).

At first, the local domain should be allocated to apply the localization of XFEM. The every node is scanned to distinguish whether the node is in the local domain or outside. When the level set value of the node is smaller than six times the mesh size, the node is indexed to 1 and included in a list for localization. The elements in the local domain are distinguished by checking the number of nodes indexed to

1 among the nodes composing each element. The elements are included in a list of the local domain when the number of nodes indexed to 1 is equal to the number of nodes composing each element.

```
boundary=5*size_mesh;
for(i=0;i<num_node;i++){
    if(levelset[i]>boundary&&levelset[i]<gamma){
        duplication=0;
        for(j=0;j<num_vent;j++){
            if(list_vent[j]==i){
                duplication=1;
                break;
            }
        }
        if(duplication==0){
            air_bc_list[num_air_bc]=i;
            num_air_bc++;
        }
    }
}
for(i=0;i<num_vent;i++){
    if(mask[list_vent[i]]==1){
        air_bc_list[num_air_bc]=list_vent[i];
        num_air_bc++;

    }
}
```

Figure 4.6. Pseudo-code to make a node list on the boundary.

The figure 4.6 is the algorithm to make a list of the boundary. The list is used to put the boundary condition to the vent pressure. As scanning the level set value of each node, the nodes placed on the boundary of the local domain is identified. In order to prevent existence of duplicate nodes in the list, the code checks whether the node is in a list of nodes on the vent. And, when the nodes on the vents are in the local domain, the nodes are included in the list of the boundary.

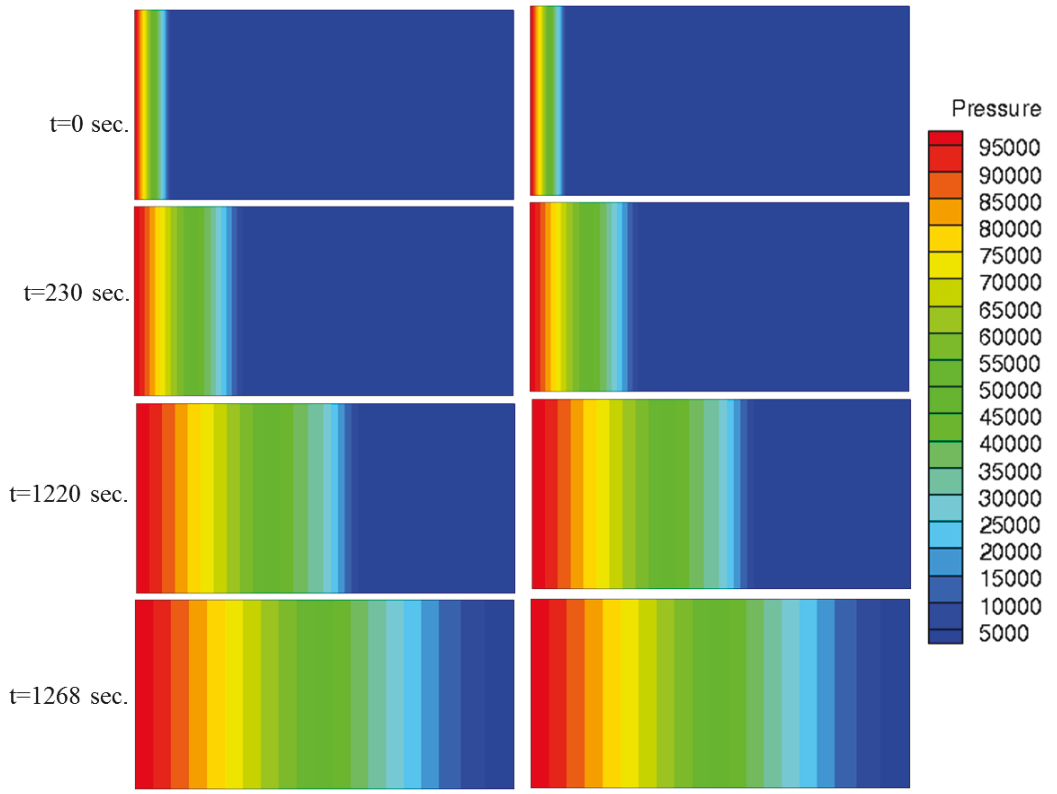

(a) With localization of XFEM. (b) Without localization of XFEM.

Figure 4.7. Pressure contours during the mold filling.

In the figure 4.7, the pressure contours are obtained from the computation with localization and without localization of XFEM. The contours mean the pressure distribution at each filling time. The left size contours are almost similar with the right size contours. Therefore, the localization method of XFEM does not affect the computation results.

4.3. Efficiency Test

The efficiency of the localization algorithm is shown by using simple examples: channel and radial flow models. The models have different mesh size in order to check the effect by the increase of the DOF size. The modeling information and

the calculation results are explained in Section 3.4.3, therefore, this section discusses only about the computation time. The used computer is Intel (R) Core(TM) i7 CPU 950 (3.07 GHz, Quad-core). Its operation system is Windows 7 Professional K for 64-bit.

Every examples used in this test are computed three times, without localization, with localization of level set method, and without localization of level set method and XFEM. The three times computation is performed to evaluate the reduction rate of the computing time by the each localization method because the computing amount of Level set method is greater than that of XFEM for pressure calculation.

The first example is the channel flow model shown in the figure 3.14. The comparison of computing times versus the number of nodes is shown in the below table.

Table 4.1. Comparison of computing times (A channel flow model).

No. of Node	Computing Time			Reduction
	Without Localization (a)	With Localization (b)		
861	37.5 sec.	Level-Set	29.0 sec.	22.7 %
		XFEM + Level-Set	24.1 sec.	35.7 %
2556	211.4 sec.	Level-Set	154.0 sec.	27.2 %
		XFEM + Level-Set	118.0 sec.	44.2 %
7381	1236.8 sec.	Level-Set	742.5 sec.	40.0 %
		XFEM + Level-Set	561.1 sec.	54.6 %

The first column indicates the number of node (DOF). The data of the second column is the computing time by the original code which does not apply the localization algorithm. The third column is the time with the localization. The calculation time by applying the localization of level set method is the upper data. And, the below date is the time with localization of XFEM and level set method.

The forth column is the percentage of the reduced time, as compared with the computation without the localization.

The reduction percentages of the three cases by localization of level set method are about 23%, 27%, and 40%, respectively. Furthermore, their reductions by localization of XFEM are about 36%, 44%, and 55%. The results show the computation time is obviously decreased by applying the localization methods.

Table 4.2. Comparison of computing times (A radial flow model).

No. of Node	Computation Time			Reduction
	Without Localization(a)	With Localization (b)		
2082	185.2 sec.	Level-Set	139.8 sec.	24.5 %
		XFEM + Level-Set	117.0 sec.	36.8 %
7295	1349.5 sec.	Level-Set	943.4 sec.	30.1 %
		XFEM + Level-Set	782.8 sec.	42.0 %
12480	3122.6 sec.	Level-Set	1965.9 sec.	37.0 %
		XFEM + Level-Set	1665.2 sec.	46.7 %

The second example is the radial flow model shown in the figure 3.15. The table 2 shows the comparison of computing times. The numbers of nodes for three cases are 2082, 7295, and 8040 nodes, respectively. The reductions of the computing times with localization of level set method are approximately 25%, 30%, and 37%, respectively. The reduction rates with localization of XFEM and level set method are 37%, 42%, and 40%, respectively.

The reduction tendency of the computing time looks similar in the channel flow and the radial flow cases. It means that we could save more computing time as the problem size becomes bigger. It might be very interesting when we treat industrial problems or optimization ones which could be very time consuming by iterations.

Efficiency of localization method

From the efficiency test, we could know that the effect by localization of Level set method is bigger than that by the localization of XFEM. The reaon might be that the computing amount of Level set method is greater than that of XFEM for pressure calculation. Nevertheless, the use of both localizations of Level set method and XFEM minimizes the computing time.

Chapter 5. Applications

Three examples are treated in this chapter to illustrate industrial applications. The first one is to analyze the filling motion of a complex edge mold with a hole. This application is used to show that our methods are well-fitted to complex shape structures. The numerical result on the filling time is compared with the experimental one. The second one shows a race tracking effect and macro void formation, which are practical phenomena frequently occurred during manufacturing. The last one concerns the numerical simulation of a composite wind turbine blade made by RTM process. This is a real industrial example with real material properties and could be used for benchmarking.

5.1. Plate with Complex Edge

A plate having complex shaped edges and a hole is chosen, and the numerical result is compared with the experimental. Since the flow pattern is affected by the structure geometry during mold filling, it is important to determine the flow front position every time in complex geometry. The experimental result and the modeling information are acquired from the research of Akbar Shojaei et al. [2003].

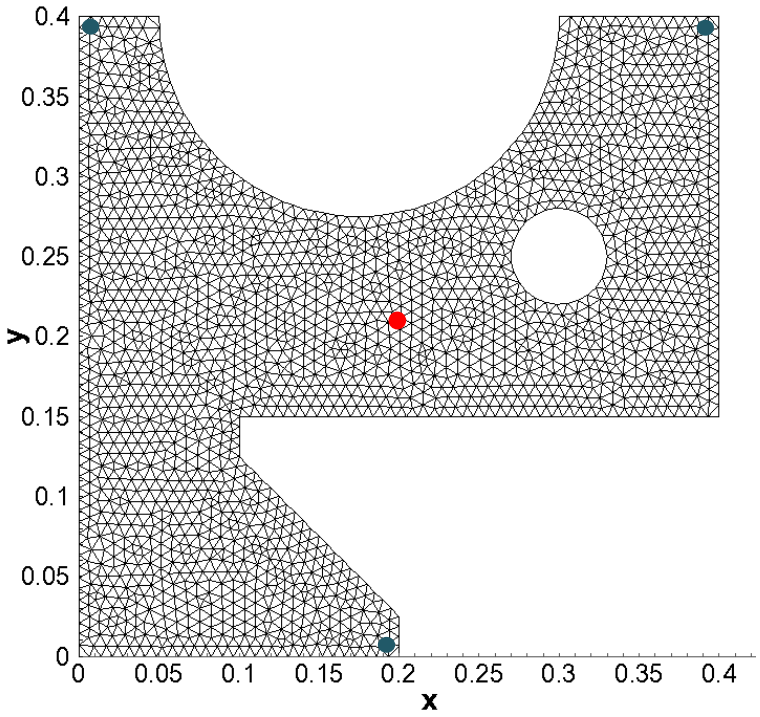

Figure 5.1. Geometry and mesh of the plate.

The geometry and mesh is shown in the figure 5.1. The width and height are equal to 0.4 m, and its thickness of the plate is equal to 6.5 mm. The injection gate is located at the center as shown by the red point. The diameter of the injection gate is 4 mm. The vents are placed at the edges as marked by three blue points. All the edges of the mold are sealed by silicone to prevent the edge effect.

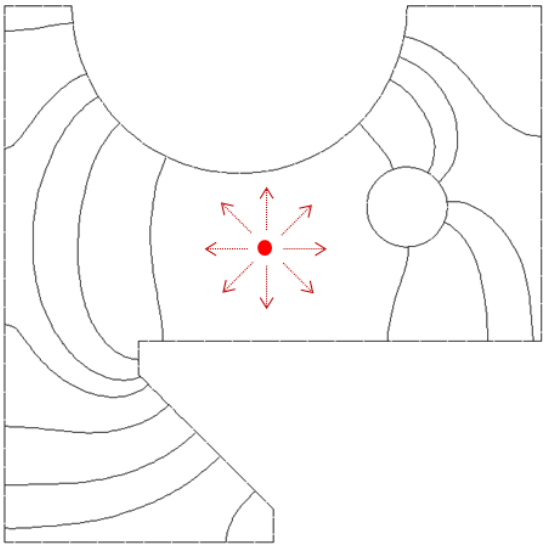

(a) Obtained by methods.

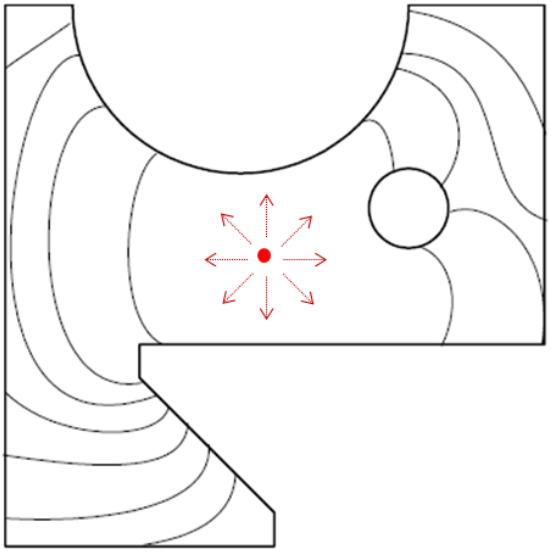

(b) Given by experiment.

Figure 5.2. Comparison of results on 2D complex geometry plate (Position of flow front at every 15 sec.).

The meshed plate has 2204 nodes and 4111 triangular elements. SAE 40 motor oil is used as resin. Its viscosity is equal to 0.3 Pa·s at room temperature (25 ℃). The permeability and porosity of the fiber preform are 6.83×10^{-9} m^2 and 0.81,

respectively. The injection pressure is set to 35 KPa. And, the vent pressure and initial pressure in the mold are set to zero.

The total filling time obtained in this study is equal to 123 sec. The experimental and numerical total filling times obtained by Akbar Shojaei et al. [2003] are equal to 117 sec. and 126 sec., respectively. The difference between the experimental result and the numerical one obtained in this study is equal to 4.3 %. In comparison with the numerical solution proposed by Akbar Shojaei et al. [2003], whose difference is equal to 7.7 %, the result of this study is closer to the experimental one. In the figure 5.2 (a) shows the location of the flow front during the filling process obtained in this work, in comparison with the experimental ones given by Akbar Shojaei et al. [2003] (Figure 5.2 (b)). The flow front locations are plotted at every 15 seconds. The computation time is 370.2 sec. when the localization method is applied and is down 37.7%, compared with the computation without localization.

5.2. Thin and Complex Shape Structure

A thin and complex shaped structure is used to analyze the race-tracking effect and macro void formation in the mold. The numerical simulations of the race-tracking effect and macro void formation in the mold could be useful to correctly design process variables, such as the injection/vent locations and their numbers. If there is no special treatment, the race-tracking effect appears in the actual injection procedure due to small space between the mold and the fiber preform edges. Macro void formation in the mold can occur due to the incorrect design of the variables such as the injection/vent positions and their numbers.

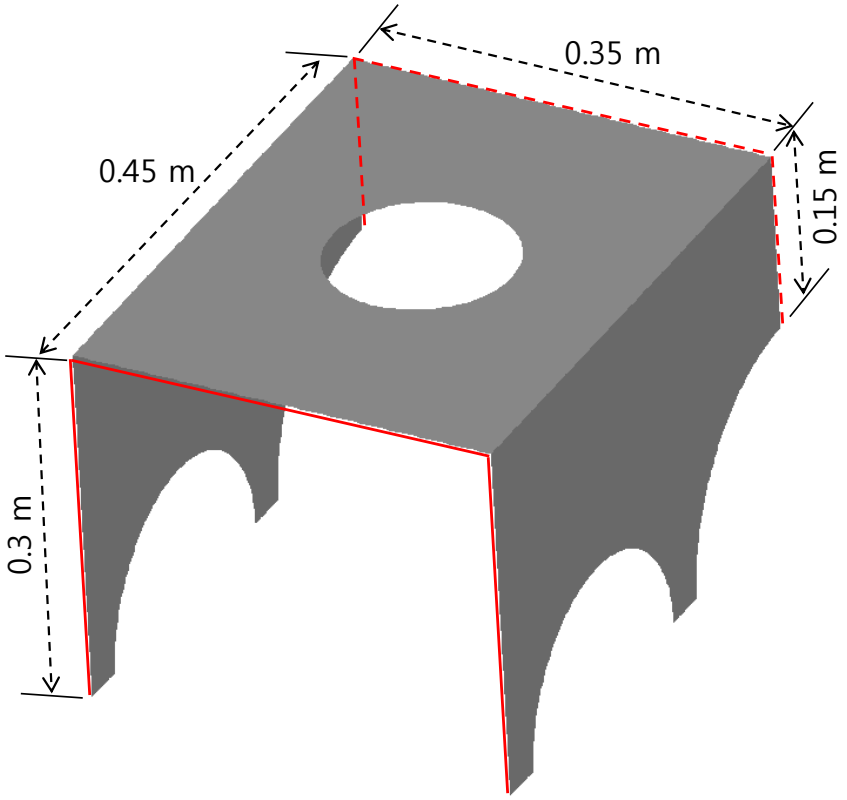

Figure 5.3. Geometry of the thin and complex shape structure.

The geometry is shown in the figure 5.3. The diameter of the hole in the example is 0.11 m. The solid line and the dashed line represent the position of the injection gates and the vents, respectively. The material properties and boundary conditions are: resin viscosity = 0.03 Pa·s, preform permeability (isotropy and constancy) = 6.21 x 10^{-11} m^2, porosity = 0.4, injection pressure = 0.3 MPa, vent pressure = 0. The type of elements used in this analysis is 3-nodes triangle.

5.2.1 Race Tracking Effect

As shown in the figure 5.4, to produce the race-tracking effect, a narrow band at the edge, of which the width is constant and equal to 10 mm, has a high

permeability, equal to 6.21×10^{-10} m^2. The meshed model has 3684 nodes and 7027 elements.

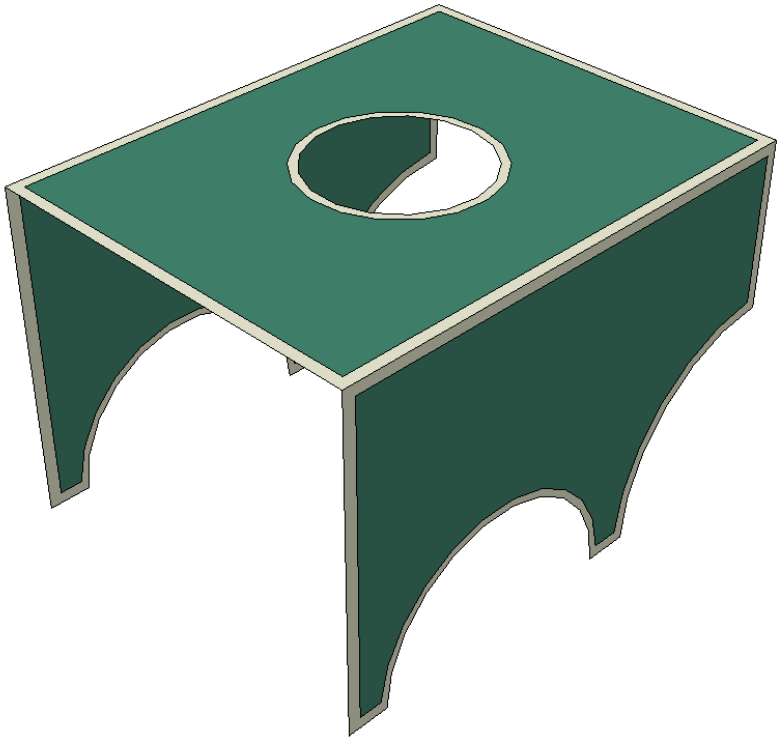

Figure 5.4. Two different permeability regions
for the race-tracking effect.

The figure 5.5 shows the resin flow front obtained in this study. The solid line represents the positions of the resin fronts at every 5 sec. during the mold filling. It shows that the resin flow fronts near the edge have curvature due to the race-tracking effect. In addition, the dividing and merging of the resin fronts are well-simulated. The computation time with localization is 707.3 sec. and down 30.3%, compared with the time without the localization.

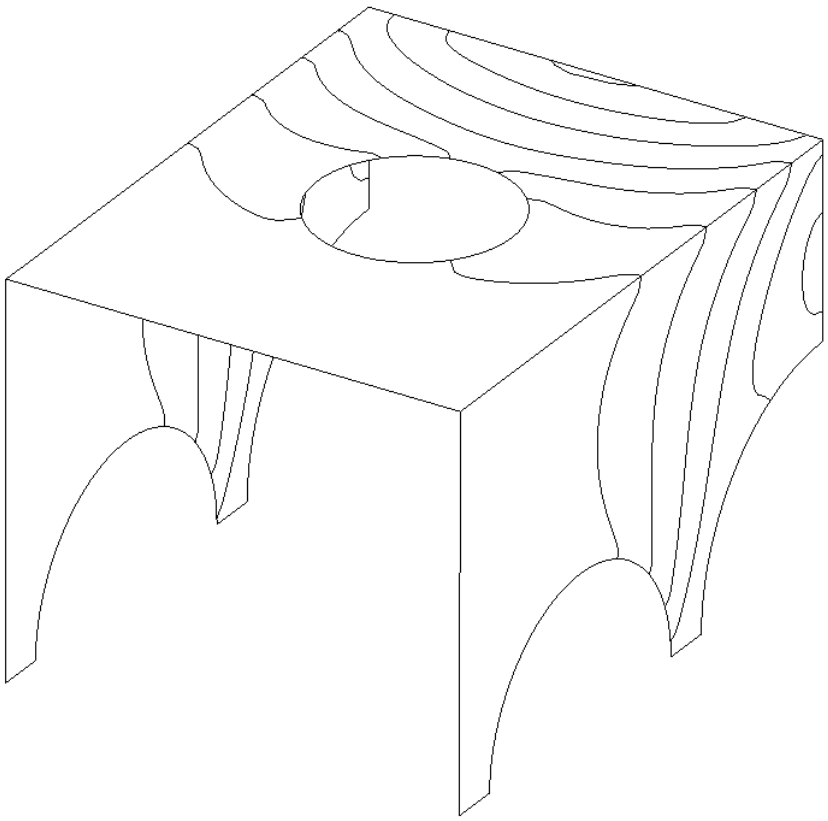

Figure 5.5. Results of the race tracking effect model
(Position of flow front at every 5 sec.).

5.2.2 Macro Void Formation

To show the formation of macro voids during the mold filling, the hole is removed at the upper side. And without the race-tracking effect, the permeability of the narrow band at the edges is as same as the value in the inside of the mold. The other geometry and injection/vent gates are same with the figure 5.3. This model has 3812 nodes and 7328 3-node elements.

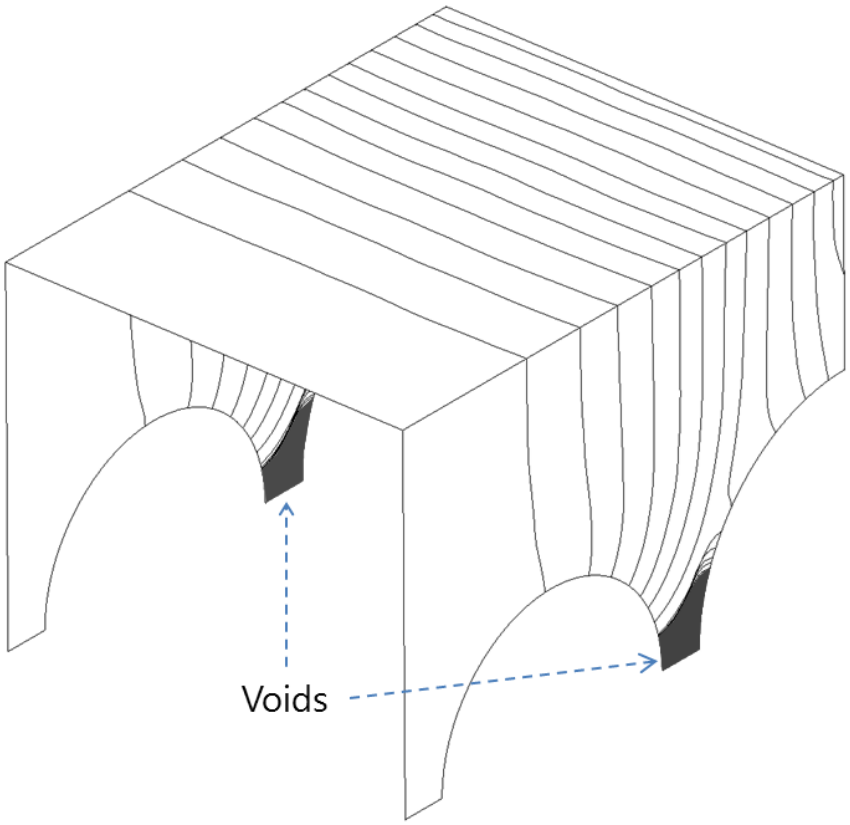

Figure 5.6. Formation of macro voids
(Position of flow front at every 5 sec.).

The computation result is plotted in the figure 5.6. It shows the position of the resin fronts every 5 sec. during filling. The macro voids were trapped at the corners marked by the dark color in the figure 5.6. The results show that our program could well catch the formation of macro voids.

The formation of macro voids can be prevented by installing vents. As shown in the figure 5.7, additional vents, marked by the red lines, is installed at the region of the trapped macro voids. The flow fronts are plotted at every 5 sec. in the figure 5.7. Because of the added vents, the macro voids at the corners are not captured at all. This analysis shows an important role of numerical simulation for the process design. The computation time with localization is 725.7 sec. and down 32.3%, compared with the time without the localization.

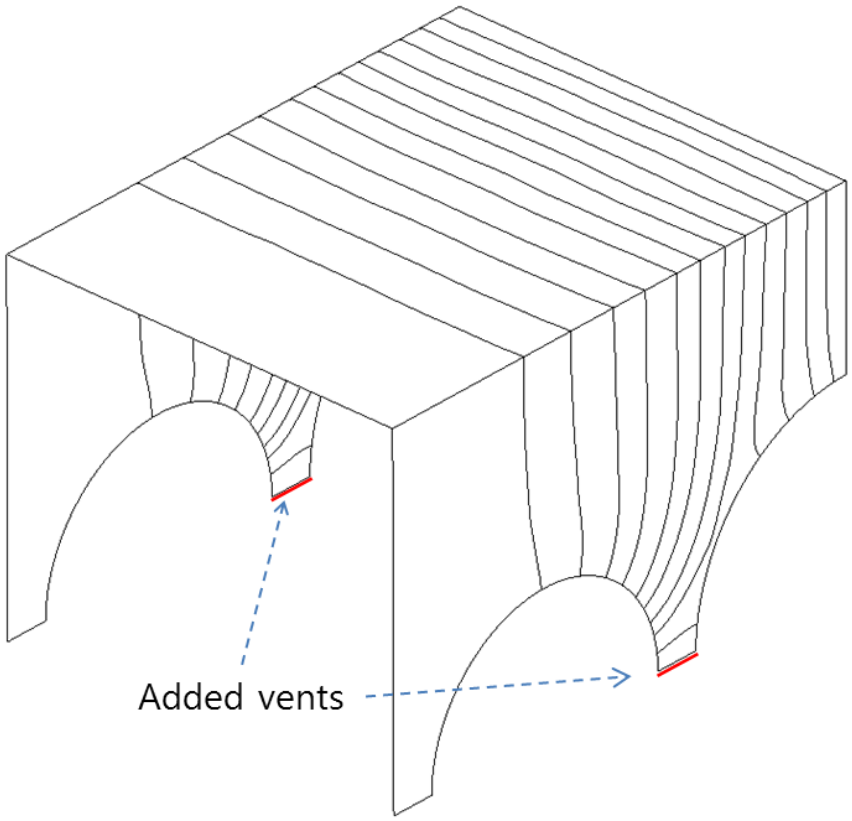

Figure 5.7. Insertion of vents
(Position of flow front at every 5 sec.).

5.3. Wind Turbine Blade

As real industrial example, a composite wind turbine blade is treated in this section. Manufacturing of composite wind turbine blades by RTM process offers less labor cost and higher fiber volume fraction than the hand lay-up process. If the size of blades is bigger, it might be essential to predict the resin flow in the mold during the filling so as to avoid problems due to large scale. For example, an engineer will simulate the resin flow in the mold when he or she wants to quickly complete the injection before curing reaction of the resin by adding more injection gates and vent. However, it might be difficult to get reasonable results by using the traditional numerical methods because the resin flow is quite complex due to the resin

injected from multiple gates and the various permeability values by mixed fabric lay-ups. Thus, the analysis methods applied in this study could help to fulfill more accurate analysis of this example. The purpose of this section is to offer a good reference, an industrial example of RTM process analysis. For that, the modeling information is minutely delineated in this section.
The computations are performed with the localization method in order to reduce the computation time.

A. Geometry and Material Properties

A composite blade for the Atlantic Orient Corporation (AOC) 15/50 wind turbine [Cairns DS et al., 1999; MCKittrick LR, 2001] is treated to simulate the resin flow during RTM process. The modeling data such as the geometry and material properties are obtained from the report of Cairns and Rossell [2004].

The geometry of the composite blade is shown in the figure 5.8. The length of the composite blade is about 5.76 m. The node coordinates to draw the blade model are in Appendix B. The blade is composed of five components: web, spar cap, flange, leading edge and trailing edge. The each component has different fiber permeability because the lay-up is different.

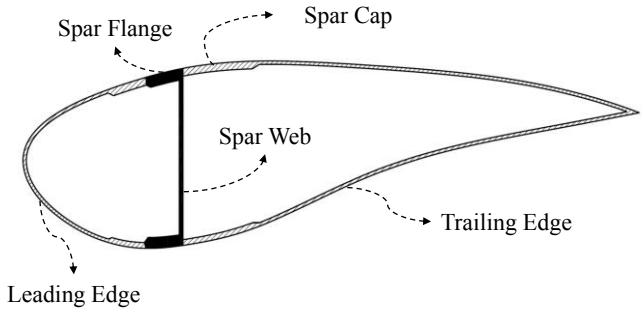

(a) Cross section.

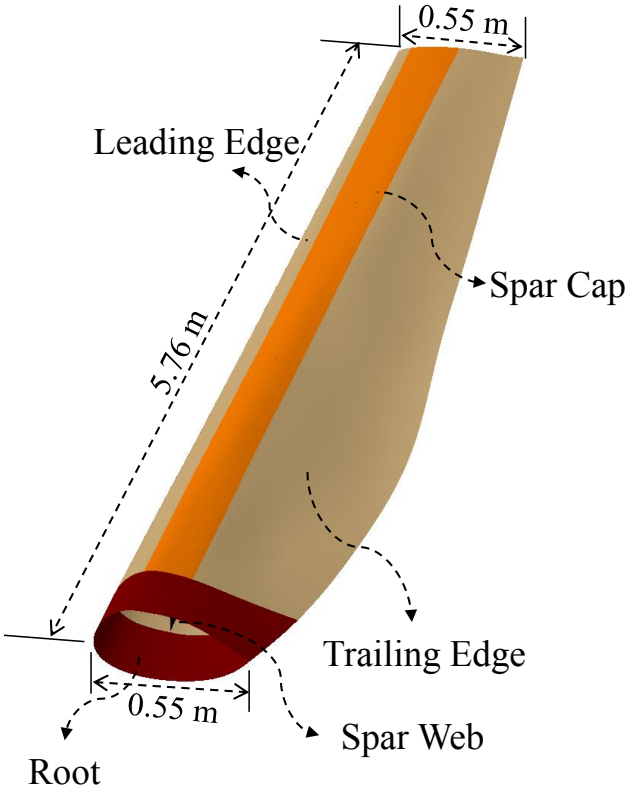

(b) Whole structure.

Figure 5.8. AOC 15/50 wind turbine blade.

When manufacturing the blade by RTM process, it is impossible to manufacture the whole structure at a once. That is to say, the mold for the fully integrated structure is impractical to manufacture because the end of blade is closed and the curvature of trailing edges changes along the length direction. Therefore, we suggest dividing the blade by three parts: top skin, spar, and bottom skin, as shown in the figure 5.9. After each part is individually manufactured by RTM process, the blade is made by assembling the three parts. The thickness of the blade is very thin (0.006~0.01 m), comparing with its length. Hence, the structure is modeled as shell elements.

There are seven sections masked by different colors in the figure 5.9. The sections have different permeability values. The values are acquired from the study of

Cairns and Rossell [2004]. Their permeability is anisotropic as shown in the table 3. The resin viscosity for the three models is 0.195 Pa·s.

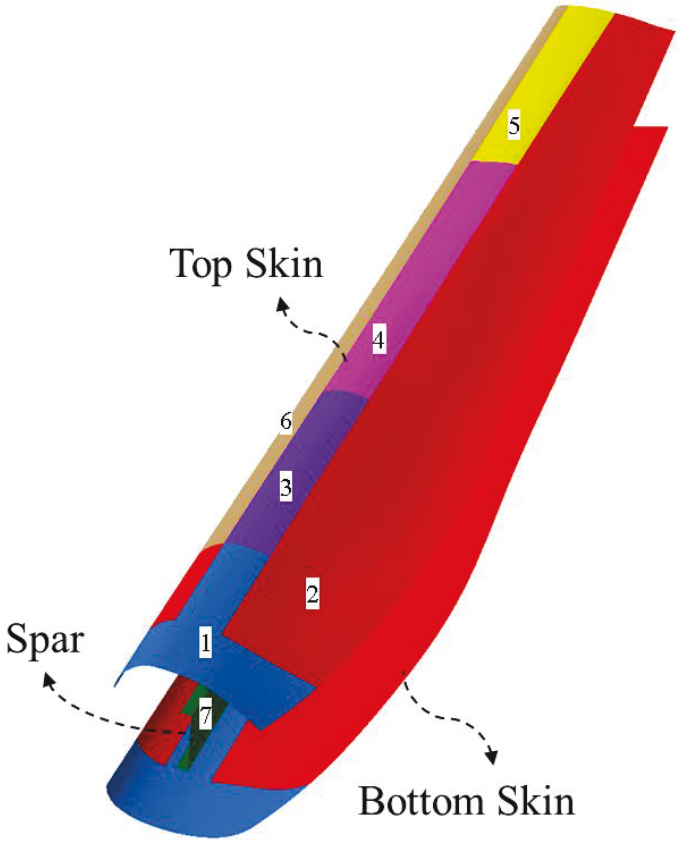

Figure 5.9. Three parts and seven sections of the composite wind turbine blade.

Table 5.1. Permeability of the seven sections

Section No.	Section Name	Permeability (m^2)	
		K_X	K_Y
1	Root + Spar Cap	2.32×10^{-10}	7.05×10^{-11}
2	Trailing Edge + Leading Edge	1.78×10^{-10}	7.06×10^{-11}
3	Spar Cap	1.97×10^{-10}	6.64×10^{-11}
4	Spar Cap	1.52×10^{-10}	5.90×10^{-11}
5	Spar Cap	9.31×10^{-11}	4.46×10^{-11}
6	Leading Edge	1.28×10^{-10}	6.13×10^{-11}
7	Spar	2.02×10^{-10}	7.79×10^{-11}

B. Top Skin

At first, the top skin is simulated. The top skin is shown in the figure 5.10. The mesh of this model is composed by 6848 nodes and 13054 elements. The type of elements is 3-nodes triangle. As shown in this figure, the injection gates are located at the three red points. The diameter of each injection gate is 0.02 m. The injection pressure is 800kPa and constant during the mold filling.

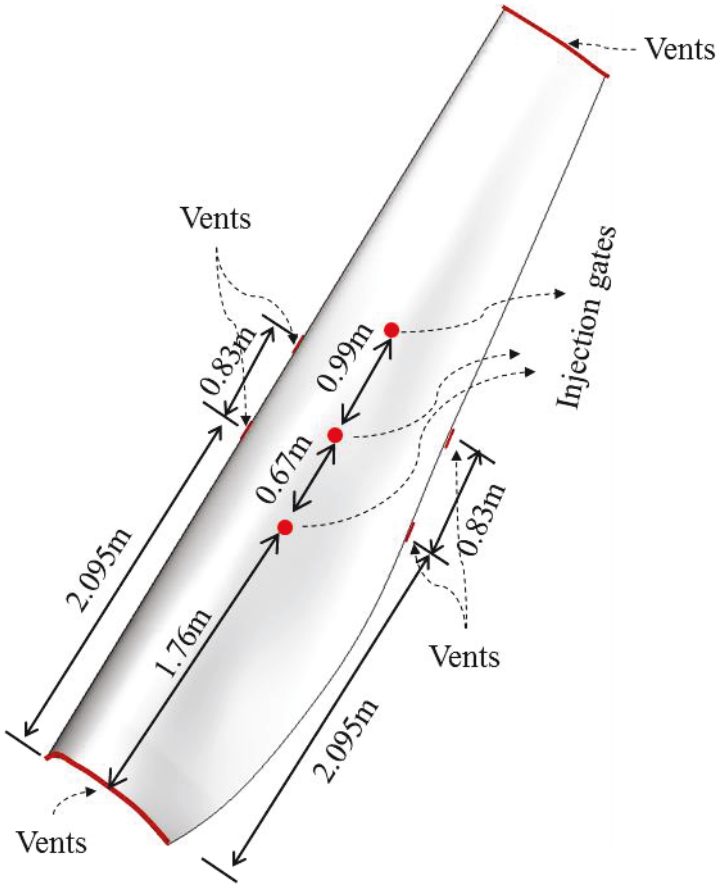

Figure 5.10. Injection gates & vents on the top skin.

The vents, marked by the red line, are placed at the ends of the structure. And, additional vents are installed at the edge, marked by red lines, in order to prevent the capture of the air voids. The length of each additional vent is 0.035 m. The vent pressure is set to 0.

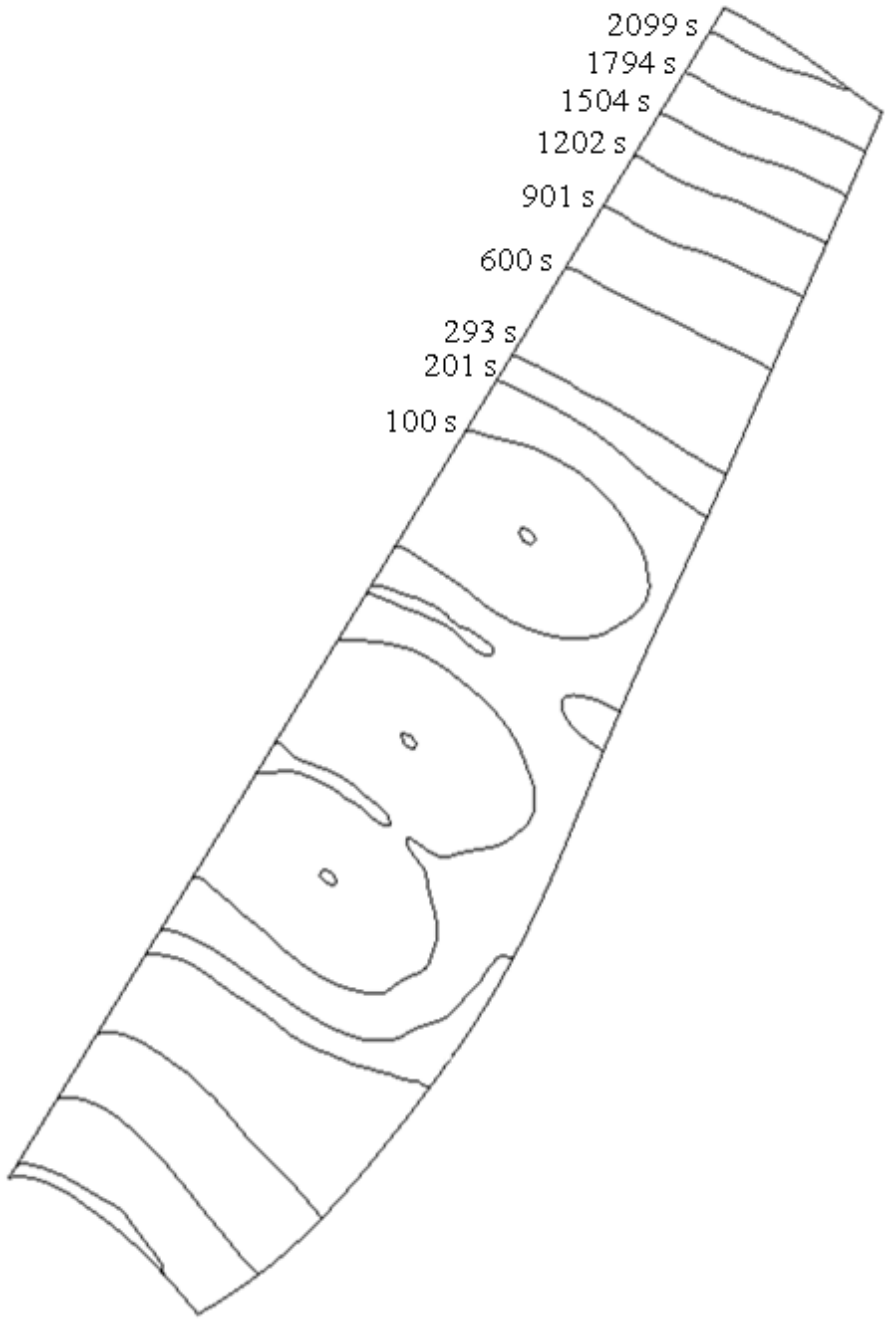

Figure 5.11. Resin flow pattern during the mold filling of the top skin.

The flow pattern obtained by numerical simulation is shown in the figure 5.11. The total filling time is 2306.4 sec. The lines on the blade mean the position of the flow fronts at each interval time marked in this figure. The fronts expanded from neighbor injection gates are merged at about 100 sec. and 200 sec., respectively.

The fronts at the trailing edge are reached earlier at the both ends because the permeability (especially, K_y) of trailing edge is larger than leading edge and spar cap. Therefore, the pattern of resin flow fronts seems to be reasonable.

C. Spar

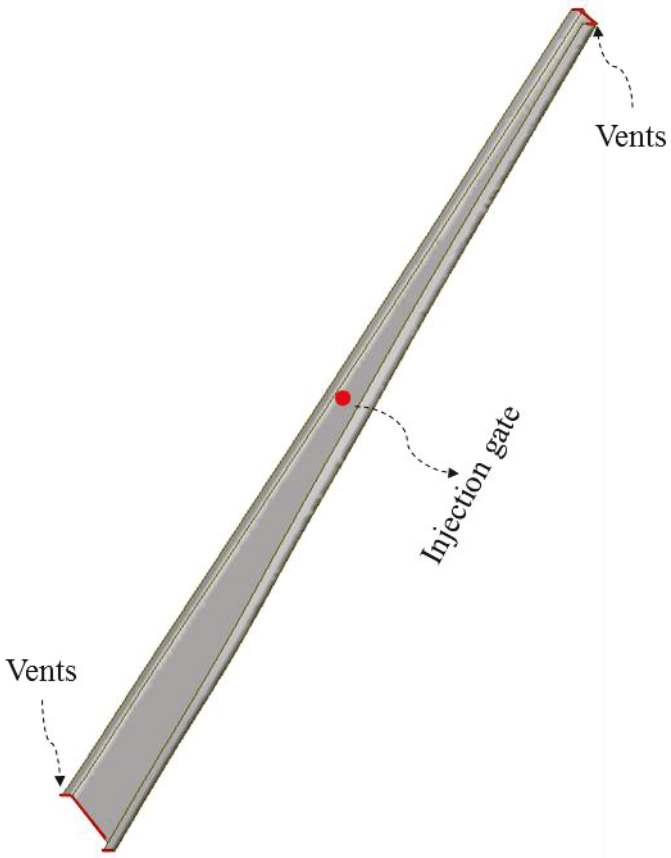

Figure 5.12. Injection gates & vents on the spar.

The second part is a spar of the blade as shown in the figure 5.12. The mesh is composed by 2447 nodes and 4442 elements. The type of elements is 3-nodes triangle. The injection gate is located at the middle point of the structure, and, its diameter is 0.02 m. The vents, marked by the red line, are place at both ends of the spar. The pressures of injection gate and vents are 800 MPa and 0, respectively, and constant during the mold filling.

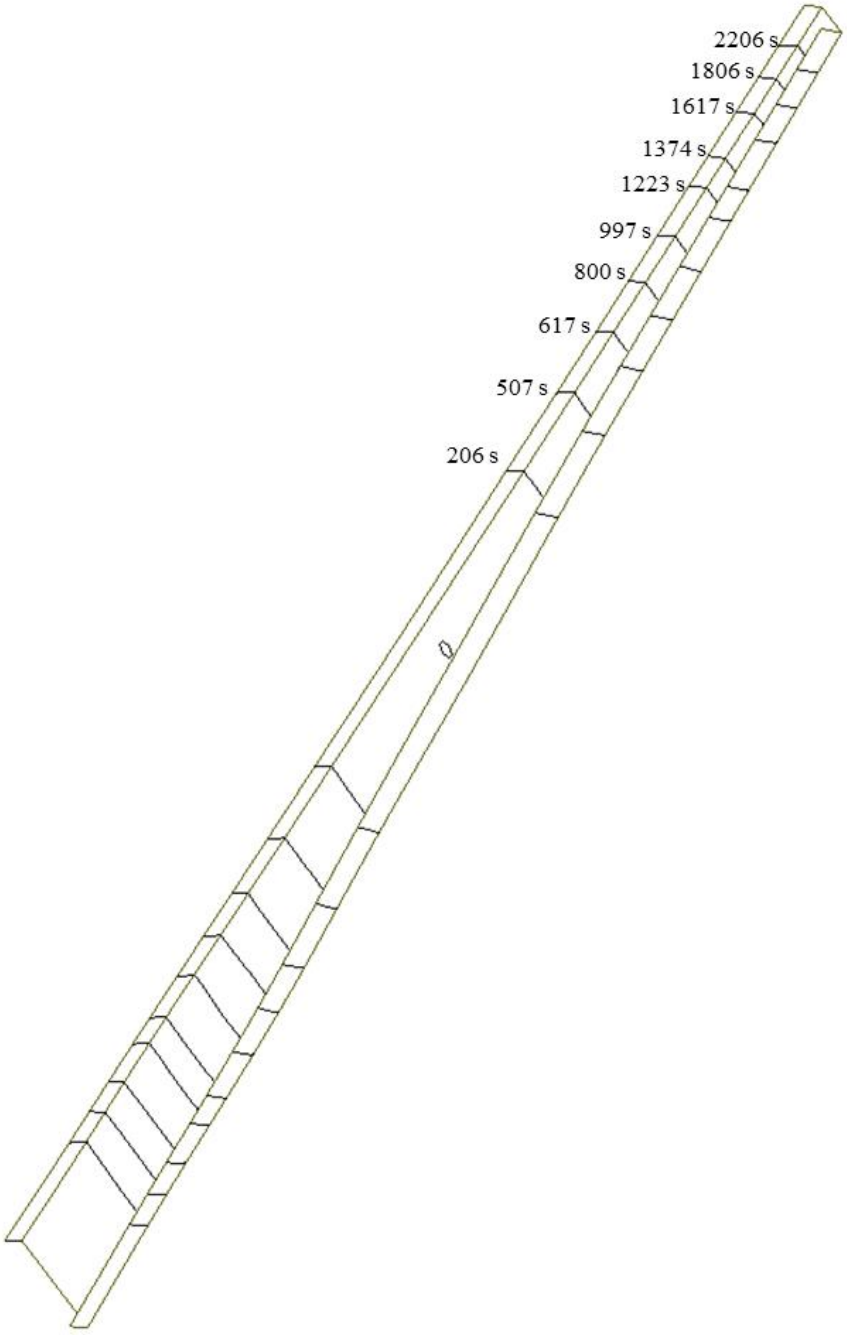

Figure 5.13. Resin flow pattern during the mold filling of the spar.

To show the computation result of the spar model, the resin flow front is plotted at each interval of 100 seconds in the figure 5.13. The flow fronts are regularly expanded from the middle injection gate because the spar has a uniform

permeability and the resin is injected from one spot with constant pressure. Therefore, the flow pattern of the spar model looks reasonable. The total filling time of the spar model is about 45 minutes.

D. Bottom Skin

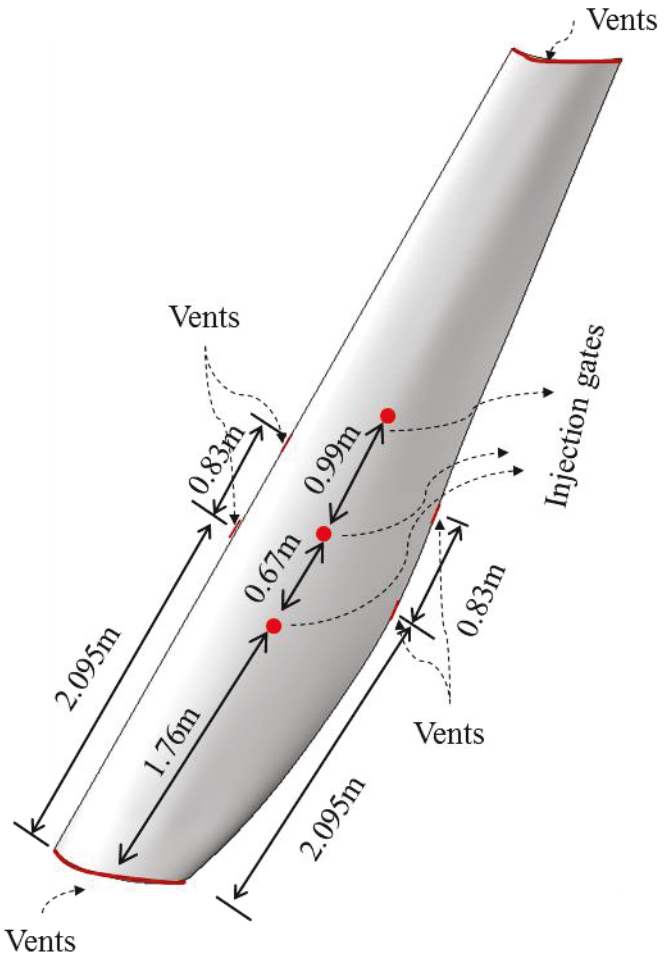

Figure 5.14. Injection gates & vents on the bottom skin.

Finally, the bottom skin of the blade is treated. The figure 5.14 shows the bottom skin model and the location of injection gates and vents. The total number of nodes and elements are 7043 and 13436, respectively. The type of elements is 3-nodes triangle. The location and size of injection gates and vents are same with

that of the top skin model. The pressures of injection gate and vents are 800 MPa and 0, respectively. As shown and explained in the figure 5.9 and table 1, the model is composed by six kinds of permeability.

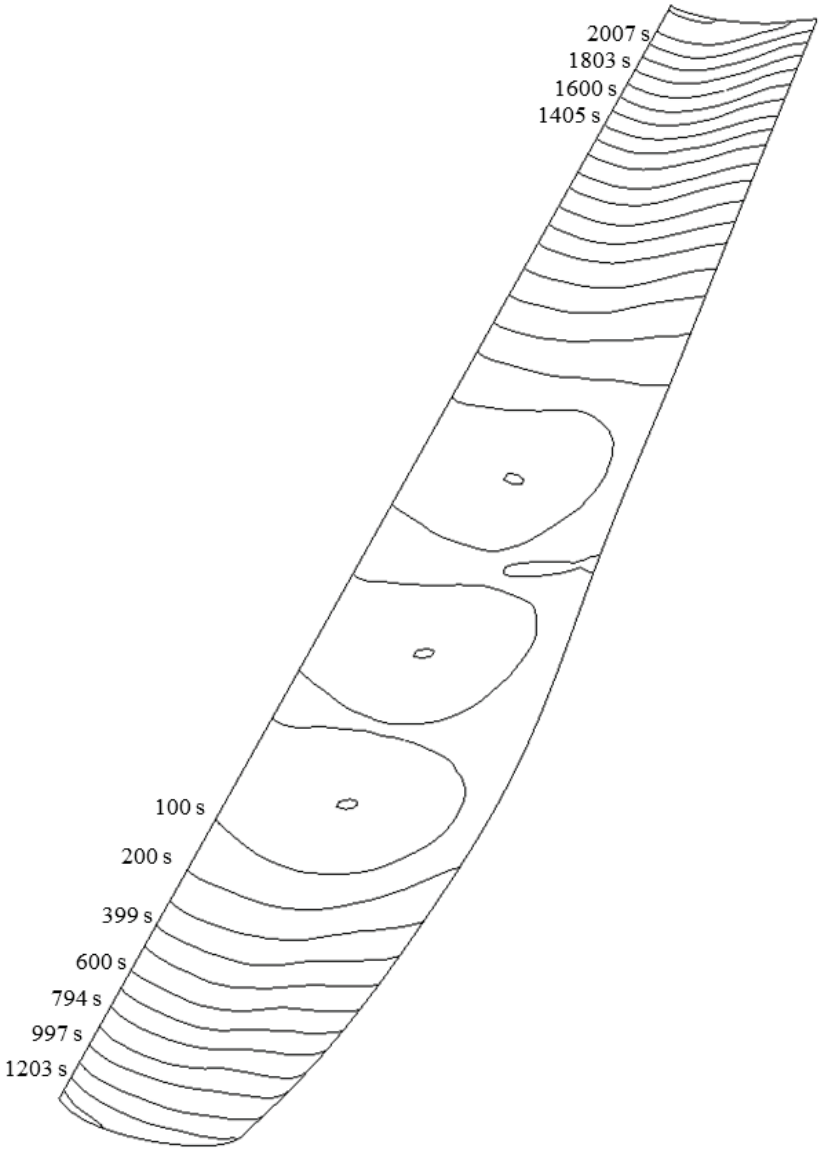

Figure 5.15. Flow pattern during the mold filling of the bottom skin.

The computation result of the bottom skin model is shown in the figure 5.15. The total filling time is 2208.6 sec. The flow fronts are plotted in the figure 5.15. The resin flow front pattern is assembled with the one of the top skin model because both of them have similar permeability and boundary conditions. The resin flow

of the trailing edge section is faster than the one of the leading edge part. And, the merged motion of flow fronts is well simulated. The slight difference of the flow front patterns and filling time between both models comes from their little different shape of the structures (especially, trailing edges). In general, the resin front pattern of this example is reasonably represented by the numerical simulation.

Chapter 6. Conclusions

In this study, the analysis of RTM process was established using XFEM combined with the level set method, so as to track more accurately the resin flow front during the mold filling. The most important advantage of this approach is the possibility to describe the discontinuity of the pressure gradient at the resin flow fronts. The enriched shape functions of XFEM were defined by the level set function and reflect the pressure distribution according to the flow front's position. Furthermore, the number of DOF was slightly increased because the enrichment was just applied to near the flow front. The position of the resin front was determined by solving the transport equation written with the level set function. The transport equation of flow front and reinitialization of the level set value were solved by an implicit characteristic Galerkin FEM. A parallel MFS solver was used to solve the equilibrium systems to reduce the computing time. Moreover, a GUI was developed and implanted to link this RTM process simulation with Diamond program (Diamond/RTM). This method was validated through several simple examples in comparison with analytical solutions found in the literature. The difference between the obtained results and the analytical solutions was very small.

Furthermore, a localization method was used to XFEM and level set method so as to increase computing efficiency. The localization of XFEM was newly proposed in this study for RTM process simulation. In particular, smaller is the flow front, the efficiency of this method becomes higher.

Through several examples having complex geometry, the separating and merging of the resin flow front were illustrated with the present method. Moreover, our method could well simulate race tracking effects and macro void formation. For the industrial application, the composite wind turbine blade was treated to simulate the mold filling stage during RTM process.

Through this study, we proved that XFEM combined with the level set method is very efficient to simulate the resin flow motion in the mold during the mold filling. In the future, these methods could be adapted to an optimization of the RTM process parameters, injection pressure, number and position of injection and vent gates, etc., because they could make the process simulation faster with a good accuracy.

This study is limited to the problem finished the filling before the curing reaction. If an engineer wants to simulate a large scale structure with a single injection gate, the gel time of resin should be considered. Therefore, if the analysis for heat transfer and curing reaction is included, it will be possible to enlarge the application examples of this study.

In this study, XFEM was used for the analysis of RTM Process. XFEM is still an efficient numerical method for other physical problems. But, the numerical integration might be carried on very carefully on the fully and partially enriched regions so as to maximize the efficiency of the method. For example, XFEM might be a good method for the analysis of inter-tow flows to capture micro-voids, and for various moving interface problems such as the explosion of fuel tank as well as the car crash.

Reference

Advani SG and Sozer EM, Process modeling in composites manufacturing, 2nd edition, Cambridge University Press (2003)

Baliga BR and Patankar SV, A new finite element formulation for convetcion-diffusion problems, Numerical Heat Transfer, Vol. 3, No. 4, P. 393-409 (1980)

Belytschko T, Gracie R, and Ventura R, A review of extended/generalized finite element methods for material modeling, Modeling and Simulation in Materials Science and Engineering, Vol. 17, No. 4, P. 1-24 (2009)

Besson SJ, Barlaud M, and Aubert, G, Detection and tracking of moving objects using a new level set based method, Proceedings 15th International Conference on Pattern Recognition, Vol. 3, P. 1100-1105 (2000)

Boccard A, Lee WI, Springer GS, Model for determining the vent locations and the fill time of resin transfer molds, Journal of Composite Materials, Vol. 29, No. 3, P. 306-333 (1995)

Bruschke MV and Advani SG, A finite-element control volume approach to mold filling in anisotropic porous-media, Polymer Composites, Vol. 11, No. 6, P. 398-405 (1990)

Cai Z, Analysis of mold filling in RTM process, Journal of Composite Materials, Vol. 26, No.9, P. 1310-1338 (1992)

Cairns DS and Rossell SM, Fluid flow modeling of Resin Transfer Molding for composite material wind turbine blade structures, Sandia National Laboratories (2004)

Cairns DS, McKittrick LR, Combs DS, Mandell JF, Rabern DA, and VanLuchene RD, Design/manufacturing synthesis of a composite blade for the AOC 15/50 wind turbine, 18th ASME Wind Energy Symposium, P. 58-65 (1999)

Chang CJ, Hsieh JW, Chen YS, and Hu WF, Tracking multiple moving boundary objects using a level set method, International Journal of Pattern Recognition and Artificial Intelligence, Vol. 18, No. 2, P. 101-125 (2004)

Chessa J and Belytschko T, An extended finite element method and level sets for axisymmetric two-phase flow with surface tension, International Journal for Numerical Methods in Engineering, Vol. 58, No. 13, P. 2041-2064 (2003)

Chessa J and Belytschko T, An extended finite element method for two-phase fluids, Journal of Applied Mechanics, Vol. 70, No. 1, P. 10-17 (2003)

Chessa J, Smolinski P, and Belyschko T, The extended finite element method (XFEM) for solidification problems, International journal for numerical methods in engineering, Vol. 53, No. 8, P. 1959-1977 (2002)

Chung SW and Kim SJ, Parallel computation of a damage localization problem using parallel multifrontal solver, Computational Mechanics, Vol. 33, No. 1, P. 42-51 (2003)

Danisman M, Tuncol G, Kaynar A, and Sozer ME, Monitoring of resin flow in the resin transfer molding (RTM) process using point-voltage sensors, Composite Science and Technology, Vol. 67, No. 3-4, P. 367-379 (2007)

Dong C, A modified rule of mixture for the vacuum-assisted resin transfer moulding process simulation, Composite Science and Technology, Vol. 68, No. 9 P. 2125-2133 (2008)

Estacio KC and Mangiavacchi N, Simplified model for mould filling simulations using CVFEM and unstructured meshes, Numerical Methods in Biomedical Engineering, Vol. 23, No. 5, P. 345-361 (2007)

Phelan FR., Simulation of injection process in resin transfer molding, Polymer Composites, Vol. 18, No. 4, P. 460-476 (1997)

Gantois R, Cantarel A, Dusserre G, J.-N. Felices, and F. Schmidt, Numerical simulation of resin transfer molding using BEM and level set method, International Journal of Material Forming, Vol. 3, Suppl 1, P. 635-638 (2010)

Gerstenberger A and Wall WA, An eXtended Finite Element Method/Lagrange multiplier based approach for fluid?structure interaction, Computer Methods in Applied Mechanics and Engineering, Vol. 197, No. 19-20, P. 1699-1714 (2008)

Hirt CW and Nichols BD, Volume of fluid (VOF) method for the dynamics of free boundaries, Journal of Computational Physics, Vol. 39, No. 1, P. 201-225 (1981)

Hsiao KT and Advani SG, Flow sensing and control strategies to address race-tracking disturbances in resin transfer molding. Part I: design and algorithm development, Vol. 35, No. 10, P. 1149-1159 (2004)

Huang R, Sukumar N, and Pr?vost JH, Modeling quasi-static crack growth with the extended finite element method Part II: Numerical applications, International Journal of Solids and Structures, Vol. 40, No. 26, P. 7539-7552 (2003)

Ji H and Dolbow JE, On strategies for enforcing interfacial constraints and evaluating jump conditions with the extended finite element method, International Journal for Numerical Methods in Engineering, Vol.61, No. 14, P. 2508-2535 (2004)

Ji H, Chopp D, and Dolbow JE, A hybrid extended finite element/level set method for modeling phase transformations, International Journal for Numerical Methods in Engineering, Vol. 54, No. 8, P. 1209-1233 (2002)

Jiang S, Yang L, Shazly Alsoliby, Guofa Zhou, PCG solver and its computational complexity for implicit control-volume finite-element method of RTM mold filling simulation, Composites Science and Technology, Vol. 67, No. 16-17, P. 3316-3322 (2007)

Jiang S, Zhang C, and Wang B, Optimum arrangement of gate and vent locations for RTM process design using a mesh distance-based approach, Composite Part A: Applied Science and Manufacturing, Vol. 33, No. 4, P. 471-481 (2002)

Jung Y, Han WS, Vautrin A, Kim SJ, RTM process simulation by using XFEM and Levelset method, 18th International Conference on Composite Materials, Aug 21-26 2011, ICC Jeju, Seogipo Special Self-Governing Province, Korea.

Jung Y, Kim SJ, Han WS, Improvement of computational efficiency by localization of XFEM with level set method for mold filling problem in RTM process, International Journal of Numerical Method Engineering, Submitted.

Jung Y, Kim SJ, Han WS, Numerical simulation of RTM process using the extended finite element method combined with the level set method, Journal of Reinforced Plastics and Composites, Vol. 32, No. 5, P. 308-317 (2013)

Kang MK and Lee WI, A flow-front refinement technique for the numerical simulation of the resin-transfer molding process. Composites Science and Technology, Vol. 59, No. 11, P.1663-1674 (1999)

Kang MK, Jung JJ, and Lee WI, Analysis of resin transfer moulding process with controlled multiple gates resin injection. Composites Part A: applied science and manufacturing, Vol. 31, No. 5, P. 407-422 (2000)

Kendall KN, Rudd CD, Owen MJ, and V. Middleton, Characterization of the resin transfer moulding process, Composites Manufacturing, Vol. 3, No. 4, P. 235-249 (1992)

Khoei AR, Shamloo A, and Azami AR, Extended finite element method in plasticity forming of powder compaction with contact friction, International Journal of Solids and Structures, Vol. 43, No. 18-19, P. 5421-5448 (2006)

Kim JH, Lee CS and Kim SJ, High-performance domainwise parallel direct solver for large-scale structural analysis, AIAA Journal, Vol.43, No 3, P. 662-670 (2005)

Kim MS and Lee WI, A new VOF-based numerical scheme for the simulation of fluid flow with free surface. Part I: New free surface-tracking algorithm and its verification, International Journal for Numerical Methods in Fluids, Vol. 42, No. 7, P. 765-790 (2003)

Kim SJ, Performance Validation of Parallel Finite Element Structural Analysis Code, IPSAP and Its Pre-Post Processor, DIAMOND, International Conference on Computational & Experimental Engineering and Sciences(ICCES'10), LAS VEGAS(USA), 28 March - 1 April, P. 507-507, (2010)

Lee LJ, Young WB, and Lin RJ, Mold filling and cure modeling of RTM and SRIM processes, Composite Structures, Vol. 27 No. 1-2, P. 109-120 (1994)

Lin CL, Lee H, Lee T, and Weber LJ, A level set characteristic Galerkin finite element method for free surface flows, International Journal for Numerical Methods in Fluids, Vol. 49, No. 5, P. 521-547 (2005)

Lin M, Hahn HT, and Huh H, A finite element simulation of resin transfer molding based on partial nodal saturation and implicit time integration, Composite Part A: Applied Science and Manufacturing, Vol. 29, No. 5-6, P. 541-550 (1998)

Lin R, Lee LJ, and Liou M., Non-isothermal mold filling and curing simulation in thin cavities with preplaced fiber mats, International Polymer Processing, Vol. 4. No.4, P. 356-369 (1991)

Liu B, Bickerton S, and Advani SG, Modeling and simulation of resin transfer moulding (RTM)?gate control, venting and dry spot prediction, Composite Part A: Applied Science and Manufacturing, Vol. 27, No. 2, P. 89-163 (1996)

Liu XL, Isothermal flow simulation of liquid composite molding. Composites Part A: applied science and manufacturing, Vol. 31, No. 12, P. 1295-1302 (2000).

Malladi R, Sethian JA, and Vemuri BC, Shape modeling with front propagation: a level set approach, IEEE Transactions on Pattern Analysis and Machine Intelligence, Vol. 17, No. 2, P. 158-175 (1995)

Mathur R, Fink B, and Advani SG, Use of genetic algorithms to optimize gate and vent locations for the resin transfer molding process, Polymer Composites, Vol. 20, No. 2, P. 167-178 (1999)

McKittrick LR, Analysis of a composite blade design for the AOC 15/50 wind turbine using a finite element model, Sandia National Laboratories (2001)

Moes N and Belytschko T, Extended finite element method for cohesive crack growth, Engineering Fracture Mechanics, Vol. 69, No. 7, P. 813-833 (2002)

Moes N, Cloirec M, Cartraud P, and Remacle JF, A computational approach to handle complex microstructure geometries, and Engineering, Vol. 192, No. 28-30, P. 3163-3177 (2003)

Mohammadi S, Extended finite element method for fracture analysis of structures, Blackwell Publish Ltd. (2008)

Morren G, Bossuyt S, and Hugo S, 2D permeability tensor identification of fibrous reinforcements for RTM using an inverse method, Composites Part A: Applied Science and Manufacturing, Vol.39, No. 9 (2008)

Mousavi SE and Sukumar N, Generalized Gaussian quadrature rules for discontinuities and crack singularities in the extended finite element method, Computer Methods in Applied Mechanics and Engineering, Vol. 199, No. 49-52, P. 3237-3249 (2010)

Pacquaut G, Bruchon J, Moulin1N, and Drapier S, Combining a level-set method and a mixed stabilized P1/P1 formulation for coupling Stokes?Darcy flows, International Journal for Numerical Methods in Fluids, Vol. 69, No. 2, P. 459-480 (2012)

Park CH, Lee WI, Han WS, and Vautrin A, Simultaneous optimization of composite structures considering mechanical performance and manufacturing cost, Composite Structures, Vol. 65, No. 1, P. 117-127 (2004)

Park CH, Lee WI, Han WS, and Vautrin A, Weight minimization of composite laminated plates with multiple constraints, Composites Science and Technology, Vol. 63, No.7, P.1015-1026 (2003)

Peng D, Merriman B, Stanley Osher, Hongkai Zhao, and Myungjoo Kang, A PDE-based fast local level set method, Journal of Computational Physics, Vol. 155, No. 2, P.410-438 (1999)

Peter DM and Spelt, A level-set approach for simulations of flows with multiple moving contact lines with hysteresis, Journal of Computational Physics, Vol. 207, No. 2, P. 389-404 (2005)

Rouison D, Sain M, and Couturier M, Resin transfer molding of hemp fiber composites: optimization of the process and mechanical properties of the materials, Composite Science and Technology, Vol. 66, No. 7-8, P. 895-906 (2006)

Sethian JA, Level set methods and fast marching methods 2nd edition, Cambridge University Press (1999)

Shojaei A and Ghaffarian SR, Modeling and simulation approaches in the resin transfer molding process: A review, Polymer Composites, Vol. 24, No. 4, P. 525-544 (2003)

Shojaei A, Ghaffarian SR and Karimian SMH, Numerical analysis of controlled injection strategies in resin transfer molding, Journal of Composite Materials, Vol. 37, No. 11, P. 1011-1035 (2003)

Shojaei A, Ghaffarian SR, and Karimian SMH, Numerical simulation of three-dimensional mold filling process in resin transfer molding using quasi-steady state and partial saturation formulations, Composites Science and Technology, Vol. 62, No. 6, P. 861-879 (2002)

Smolianski A, Finite element level set operator splitting (FELSOS) approach for computing two-fluid unsteady flows with free moving interfaces, International Journal for Numerical Methods in Fluids, Vol 48, No. 3, P. 231-269 (2005)

Soukane S and Trochu F, Application of the level set method to the simulation of resin transfer molding, Composites Science and Technology, Vol. 66, No. 7-8, P. 1067-1080 (2006)

Subbiah S, Trafford DL, and Guceri SI, Non-isothermal flow of polymers into two-dimensional, thin cavity molds: a numerical grid generation approach, International Journal of Heat and Mass Transfer, Vol. 32, No. 3, P. 415-434 (1989)

Sukumar N, Chopp DL, Moos N, and Belytschko T, Modeling holes and inclusions by level sets in the extended finite-element method, Computer Methods in Applied Mechanics and Engineering, Vol. 190, No. 46-47, P. 6183-6200 (2001)

Sukumar N, Moes N, Moran B, and Belytschko T, Extended finite element method for three-dimensional crack modeling, International Journal for Numerical Methods in Engineering, Vol. 48, No. 11, P. 1549-1570 (2000)

Tan H and Pillai KM, Numerical simulation of reactive flow in liquid composite molding using flux-corrected transport (FCT) based finite element/control volume (FE/CV) method, International Journal of Heat and Mass Transfer, Vol. 53, No. 9-10, P. 2256-2271 (2010)

Trochu F and Gauvin R, Limitations of a boundary-fitted finite difference method for the simulation of the resin transfer molding process, Journal of Reinforced Plastics and Composites, Vol. 11, No. 7, P. 772-786 (1992)

Trochu F, Gauvin R, and Gao DM, Numerical-Analysis of the Resin Transfer Molding Process by the Finite-Element Method. Advances in Polymer Technology, Vol. 12, No. 4, P. 329-342 (1993)

Trochu F, Ruiz E, Achim V, and Soukane S, Advanced numerical simulation of liquid composite molding for process analysis and optimization, Composites Part A: applied science and manufacturing, Vol. 37, No. 6, P. 890-902 (2006)

Ventura G, On the elimination of quadrature sub-cells for discontinuous functions in the extended finite-element method, International Journal for Numerical Methods in Engineering, Vol. 66, No. 5, P. 761-791 (2006)

Young WB, Development of a helicopter landing gear prototype using resin infusion molding, Journal of Reinforced Plastics and Composites, Vol. 28, No. 7, P. 833-839 (2009)

Young WB, Gate location optimization in liquid composite molding using genetic algorithms, Journal of Composite Materials, Vol. 20, No. 2, P. 1098-1113 (1999)

Young WB, Rupel K, Han K, Lee LJ, and Liou MJ, Analysis of resin injection molding in molds with preplaced fiber mats. Ⅱ: Numerical Simulation and Experiments of Mold Filling, Polymer Composites, Vol. 12, No.1, P. 30-38 (1991)

Zhao HK, Chan T, Merriman B, and Osher S, A variational level set approach to multiphase motion, Journal of Computational Physics, Vol. 127, P. 179-195 (1996)

Zheng LL and Zhang H, An adaptive level set method for moving boundary problems: application to droplet spreading and solidification, Numerical Heat Transfer, Part B, Vol. 37, No. 4, P. 437-454 (2000)

Zienkiewicz OC and Taylor RL, The finite element method volume 3: Fluid dynamics, Butterworth Heinemann, 5th edition (2000)

Appendix A.

Multi-frontal solver of IPSAP & Diamond/RTM

1. IPSAP

IPSAP (Internet Parallel Structural Analysis Program) is large scale, high performance structural analysis software developed by Aerospace Structures Laboratory. IPSAP is divided into two types of solution package, IPSAP/Standard and IPSAP/Explicit. IPSAP/Standard is able to solve linear static analysis, thermal conduction analysis, and vibration analysis of structures, and IPSAP/Explicit has ability to solve time-dependent structural problem such as crash, metal forming, and penetration phenomena.

IPSAP/Standard has 3 type solution modules, 2 linear solution methods and 1 eigensolution method. Linear solver in IPSAP/Standard contains both serial/parallel version of Multifrontal method and hybrid domain decomposition iterative method, and eigensolver is block-Lanczos method. Multifrontal solver is

the best direct solution method in terms of requirements of computations, memory, and parallel efficiency. It is extremely efficient in the both serial and parallel machines. Hybrid domain decomposition method is based on FETI-DP method which uses multifrontal method to computational efficiency. Last, block-Lanczos eigensolver was developed for multiple eigenvalues/eigenvectors of large scale problems. IPSAP/Standard is published in Windows(x86, x64, serial and parallel), Linux(x86, x64, serial and parallel), Mac OS(G4, G5, serial) version.

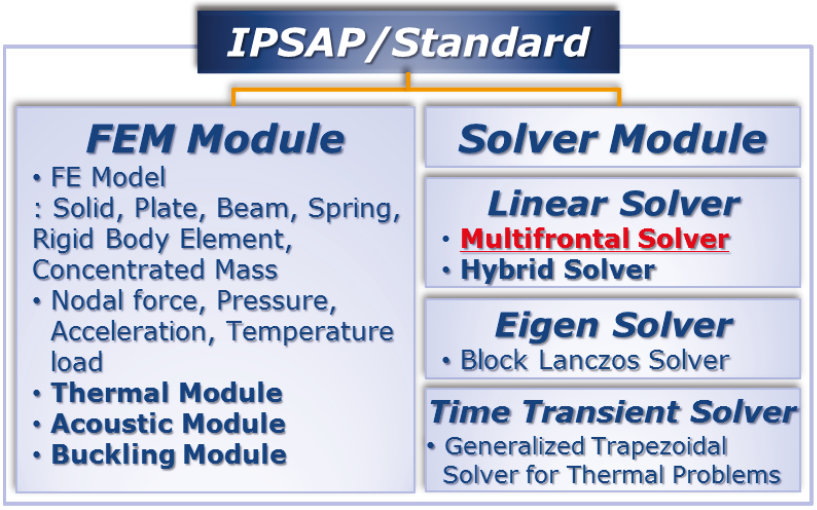

Figure A.1. Main feature of IPSAP.

2. Multi-Frontal Solver

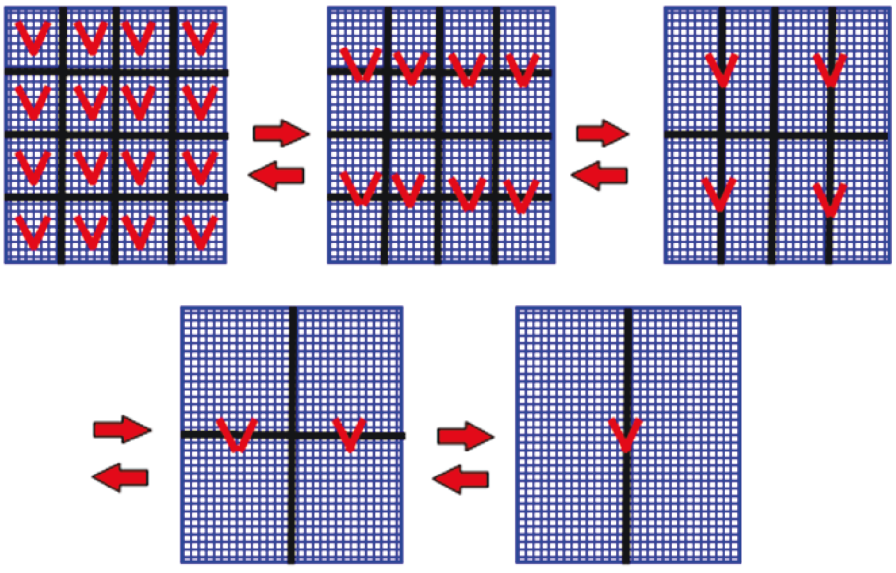

(a) Factorization of Multi-frontal solver

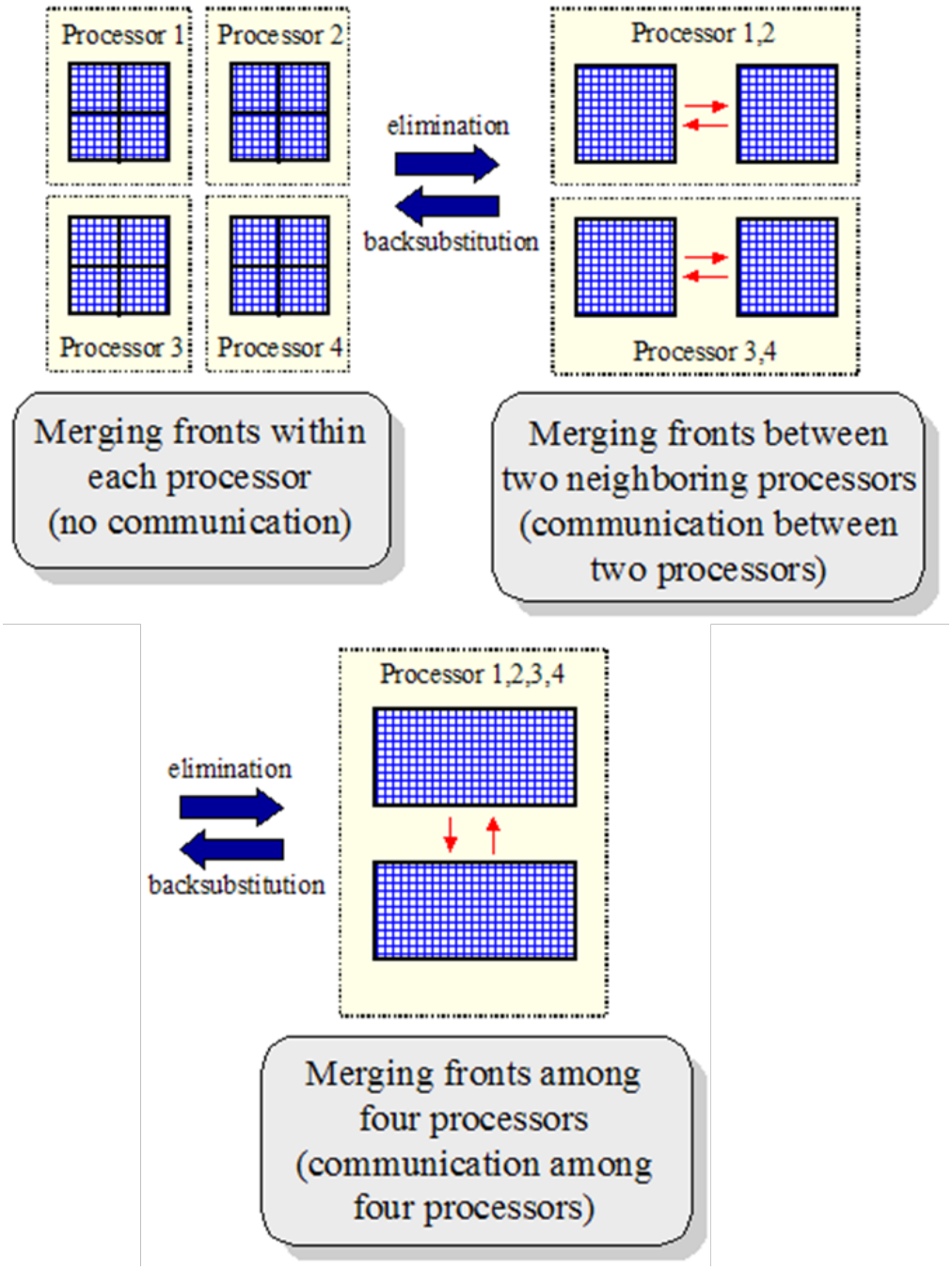

(b) Parallel extend-add operation

Figure A.2. Multi-frontal solver of IPSAP.

Multifrontal method was proposed to minimize requirements of memory and computation for finite element methods. Multifrontal solver in IPSAP is optimized

for finite element problems, direct version of domain decomposition methods. Thus, the solver doesn't need to assemble global stiffness matrix, whereas other direct solvers require assembling global stiffness matrix. IPSAP lies on distributed memory parallelism. To implement in parallel computing, PLASC was developed to handle flexible block size of matrix on distributed memory. The general introduction of parallel computing is included in Appendix C.

The figure A.2 illustrates the factorization of MFS and parallel extend-add operation on distributed memory, respectively.

3. Diamond/RTM

The present method for numerical simulation of the RTM process is implanted in Diamond, developed by Aerospace Structures Laboratory in Seoul National University. It is integrated general finite element program for structural analysis in sequential or parallel computing environment. The convenient functions of Diamond are used to generate geometry and mesh of models for RTM process simulations. In Diamond, the special functions for modeling the RTM process are embedded.

The boundary conditions are possible to set by filling the entry in the diagram as the figure A.3. The entry for the boundary conditions is the information about injection gates and vents. The locations of injection gates and vents are entered by clicking on the corresponding nodes with the mouse.

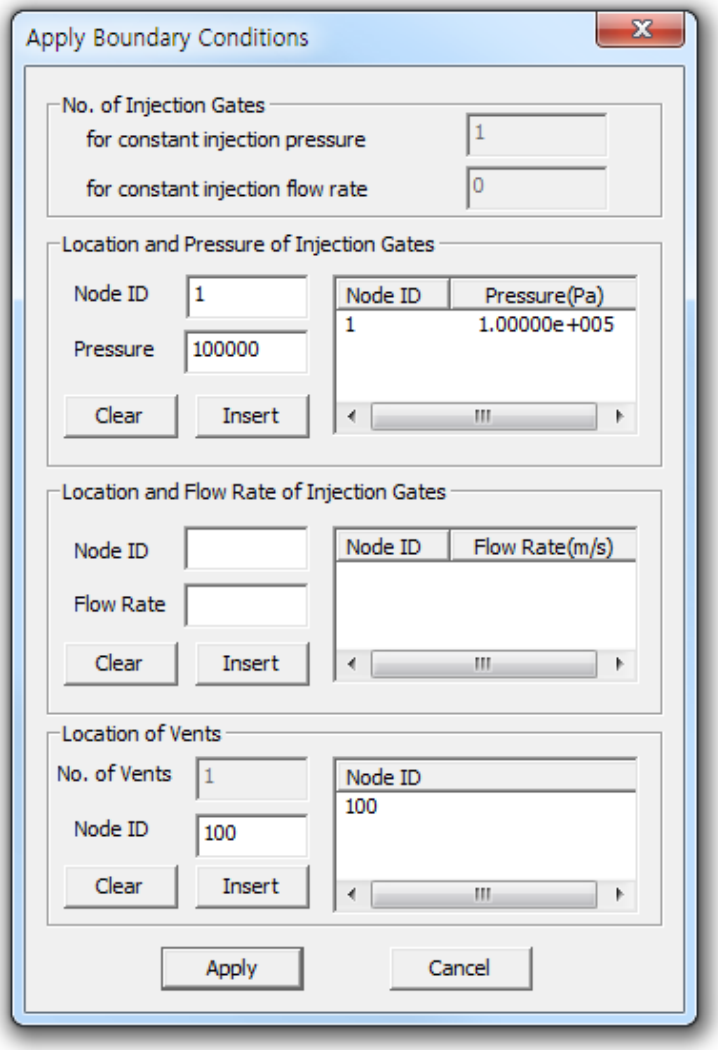

Figure A.3. Setting boundary conditions
(Injection gates & vents).

The figure A.4 is the diagram for input of material properties such as permeability, viscosity, and porosity. If the model is composed by multiple permeability values, it is possible to input them as changing the ID number.

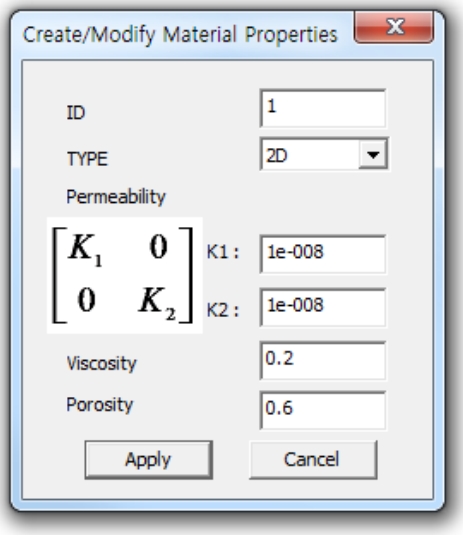

Figure A.4. Input of material properties.

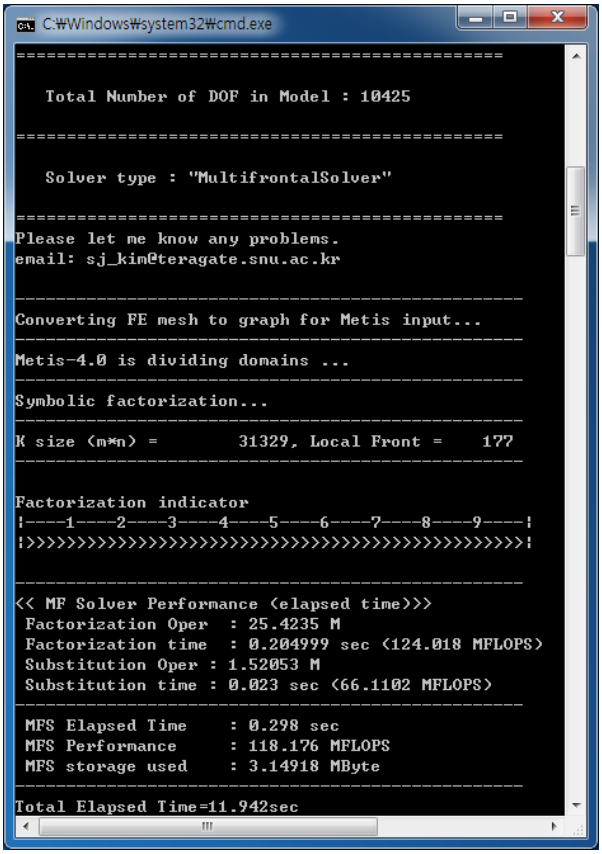

Figure A.5. Computation information of model.

After finishing the modeling, the computation is launched. The window in the figure A.5 appears to give the computation information of the model during the calculation.

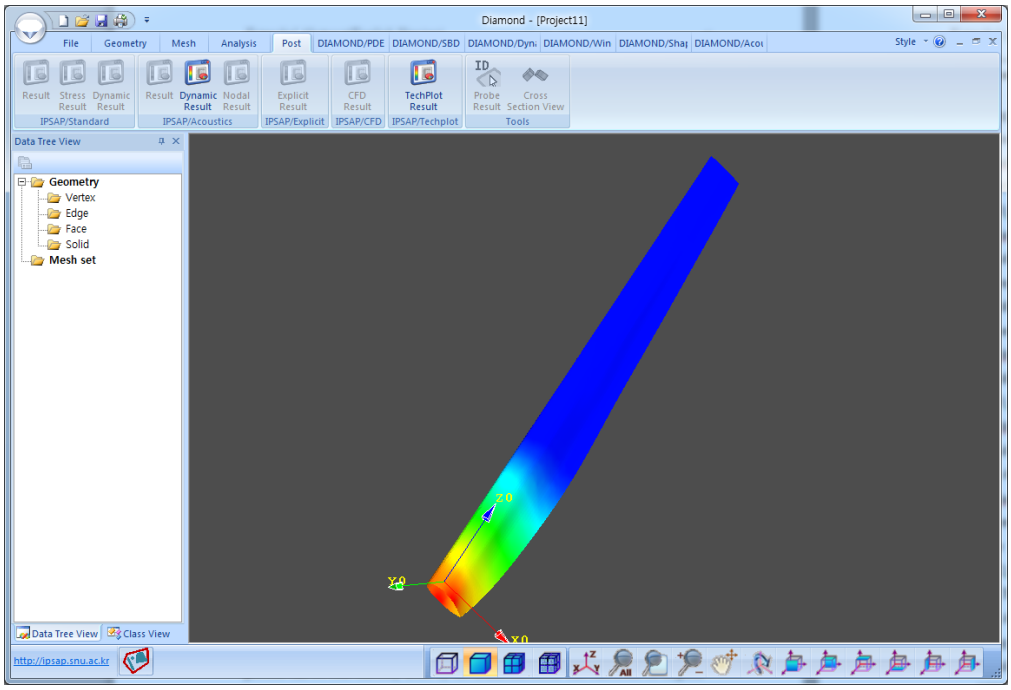

Figure A.6. Drawing a contour plot of the analysis result in Diamond.

The analysis result is able to check by using the post-processing part of Diamond. The figure 5.20 shows to draw the pressure contour of a omposite blade model.

Appendix B.

Key-points of cross-sections for the composite wind turbine blade model

The composite wind turbine blade model is drawn by 10 cross-sections. The key-points of the 10 cross-sections are given in the table B. The cross-section number is started from the root end.

Table B. Key-points of 10 cross-sections for the composite wind turbine blade model.

Cross Section	x(m)	y(m)	z(m)
1	0.0000	0.3000	0.0000
1	0.1677	0.4264	0.0000
1	0.2258	0.4353	0.0000
1	0.4498	0.4176	0.0000
1	0.5501	0.3564	0.0000
1	0.3411	0.2251	0.0000
1	0.2258	0.1917	0.0000

1	0.1954	0.1871	0.0000
1	0.1354	0.1803	0.0000
2	0.0000	0.3000	0.3983
2	0.1317	0.3991	0.3983
2	0.1982	0.4130	0.3983
2	0.2264	0.4177	0.3983
2	0.3178	0.4180	0.3983
2	0.4989	0.4057	0.3983
2	0.6477	0.3514	0.3983
2	0.5429	0.3143	0.3983
2	0.3142	0.2244	0.3983
2	0.2264	0.1971	0.3983
2	0.1954	0.1905	0.3983
2	0.1305	0.1849	0.3983
3	0.0000	0.3000	1.0633
3	0.1281	0.3882	1.0633
3	0.1960	0.4050	1.0633
3	0.2265	0.4091	1.0633
3	0.3279	0.4112	1.0633
3	0.5989	0.3858	1.0633
3	0.3266	0.2411	1.0633
3	0.2254	0.2035	1.0633
3	0.1953	0.1978	1.0633
3	0.1271	0.1942	1.0633
3	0.7214	0.3516	1.0633
3	0.5907	0.3267	1.0633
4	0.0000	0.3000	1.7363
4	0.1273	0.3803	1.7363
4	0.2272	0.3997	1.7363
4	0.3212	0.4033	1.7363

4	0.5552	0.3858	1.7363
4	0.7493	0.3517	1.7363
4	0.6221	0.3391	1.7363
4	0.3177	0.2374	1.7363
4	0.2272	0.2065	1.7363
4	0.1962	0.1992	1.7363
4	0.1263	0.2031	1.7363
5	0.0000	0.3000	2.4103
5	1.2230	0.3690	2.4103
5	0.1892	0.3837	2.4103
5	0.3215	0.3902	2.4103
5	0.5281	0.3701	2.4103
5	0.7173	0.3417	2.4103
5	0.5254	0.3206	2.4103
5	0.3228	0.2531	2.4103
5	0.2204	0.2209	2.4103
5	0.1897	0.2158	2.4103
5	0.1230	0.2217	2.4103
6	0.0000	0.3000	3.0439
6	0.1162	0.3605	3.0439
6	0.1855	0.3745	3.0439
6	0.2151	0.3779	3.0439
6	0.3047	0.3801	3.0439
6	0.4685	0.3593	3.0439
6	0.6579	0.3304	3.0439
6	0.5530	0.3233	3.0439
6	0.3035	0.2504	3.0439
6	0.2144	0.2309	3.0439
6	0.1851	0.2273	3.0439
6	0.1145	0.2387	3.0439

7	0.0000	0.3000	3.7351
7	0.1097	0.3537	3.7351
7	0.1800	0.3645	3.7351
7	0.2098	0.3680	3.7351
7	0.3141	0.3664	3.7351
7	0.4576	0.3418	3.7351
7	0.6071	0.3213	3.7351
7	0.4946	0.3099	3.7351
7	0.3128	0.2578	3.7351
7	0.2078	0.2404	3.7351
7	0.1773	0.2421	3.7351
7	0.1078	0.2542	3.7351
8	0.0000	0.3000	4.4263
8	0.1035	0.3458	4.4263
8	0.1707	0.3564	4.4263
8	0.2017	0.3598	4.4263
8	0.3074	0.3579	4.4263
8	0.4464	0.3328	4.4263
8	0.5537	0.3134	4.4263
8	0.4725	0.3056	4.4263
8	0.3060	0.2660	4.4263
8	0.2013	0.2514	4.4263
8	0.1697	0.2542	4.4263
8	0.1037	0.2640	4.4263
9	0.0000	0.3000	5.0923
9	0.0918	0.3399	5.0923
9	0.1659	0.3477	5.0923
9	0.1959	0.3503	5.0923
9	0.2991	0.3471	5.0923
9	0.3931	0.3263	5.0923

9	0.5004	0.3059	5.0923
9	0.3904	0.2927	5.0923
9	0.2960	0.2737	5.0923
9	0.1954	0.2619	5.0923
9	0.1648	0.2637	5.0923
9	0.0910	0.2715	5.0923
10	0.0000	0.3000	5.7573
10	0.0899	0.3345	5.7573
10	0.1583	0.3412	5.7573
10	0.1899	0.3414	5.7573
10	0.2921	0.3354	5.7573
10	0.3643	0.3198	5.7573
10	0.4445	0.3046	5.7573
10	0.3741	0.2983	5.7573
10	0.2915	0.2847	5.7573
10	0.1893	0.2758	5.7573
10	0.1584	0.2746	5.7573
10	0.0892	0.2768	5.7573

Appendix C.

Introduction to Parallel Computing

1. Serial vs. Parallel

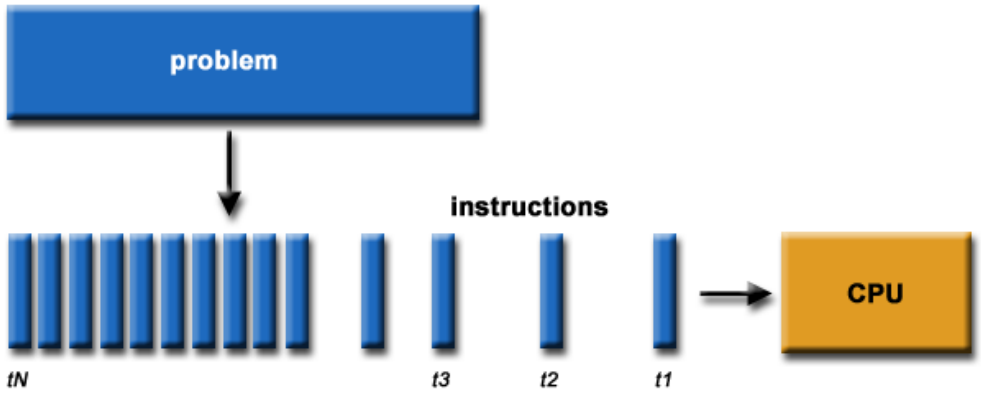

Figure C.1. Description of serial computing.

Serial computing is to use a single CPU (processor) to complete a single task, as shown in the figure C.1. The methods to improve the performance of serial computing are to optimize the program or improve the hardware (Moore's law). On the other hand, as shown in the figure C.2, parallel computing is to use the multiple CPUs to reduce the time needed to complete a single task.

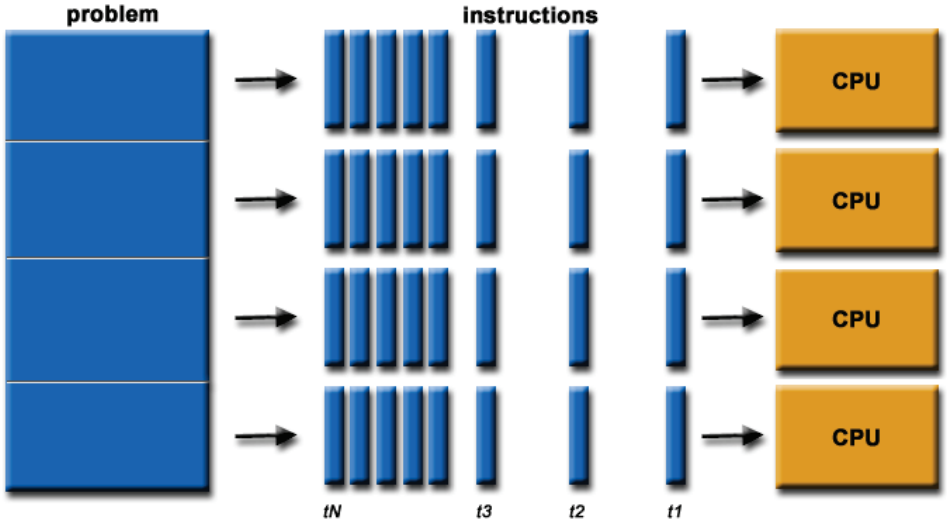

Figure C.2. Description of parallel computing.

2. Classification of computer architectures

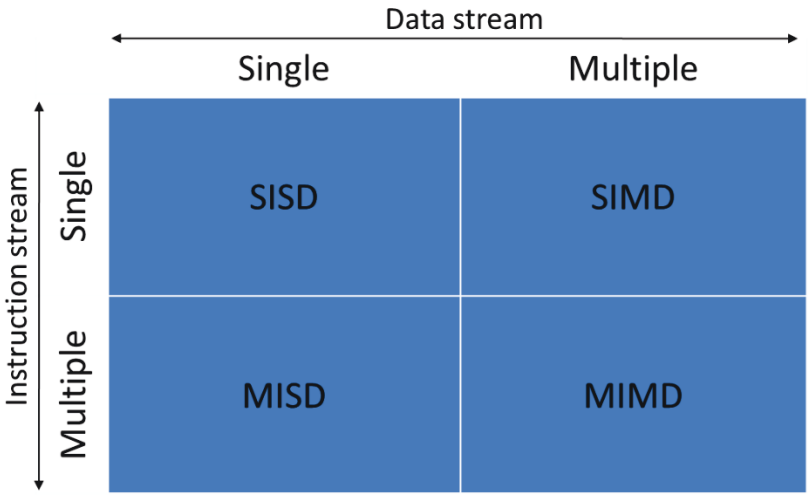

Figure C.3. Classification by Flynn's taxonomy.

The Flynn's taxonomy classifies the computer architectures to four divisions: SISD, SIMD, MISD, and MIMD. The classification is described in the figure C.3.

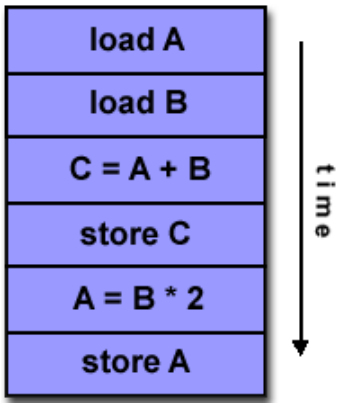

Figure C.4. Operation in SISD.

SISD is an acronym of a Single Instruction stream and a Single Data stream. A serial computer is included in this division. As shown in the figure C.4, only one instruction stream and on data stream are executed.

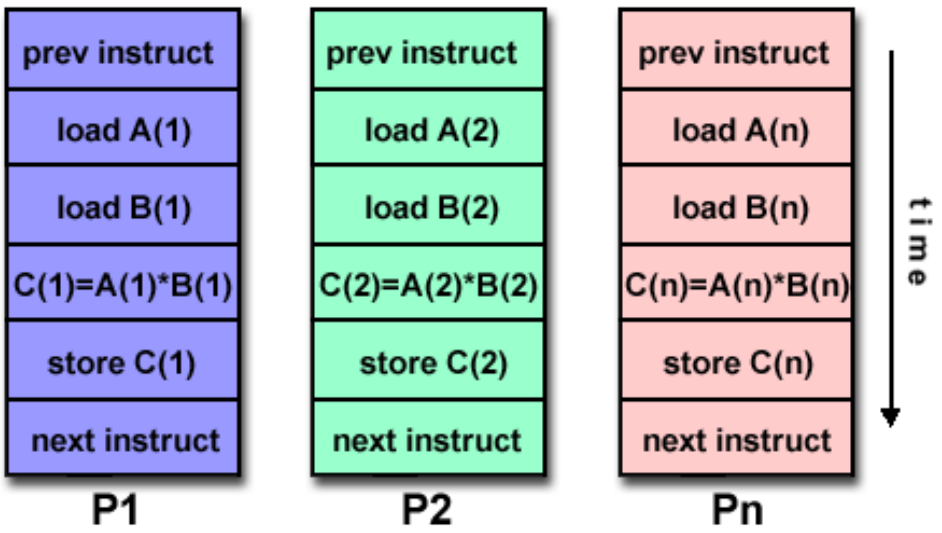

Figure C.5. Operation in SIMD.

SIMD is an acronym of a Single Instruction stream but Multiple Data streams. All processing units execute the same instruction. And, each processing unit can

operate on a different data element as the figure C.5. The early supercomputers such as Thinking Machines CM-1 and CM-2 are included in this division.

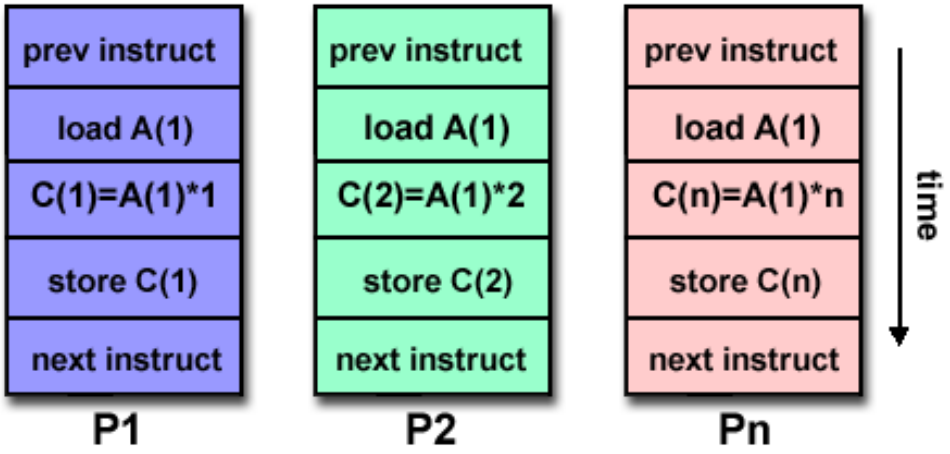

Figure C.6. Operation in MISD.

MISD is an acronym of Multiple Instruction streams and a Single Data stream as the figure C.6. In MISD computers, various instructions operate with the same data. Few actual examples of this class of parallel computer have existed.

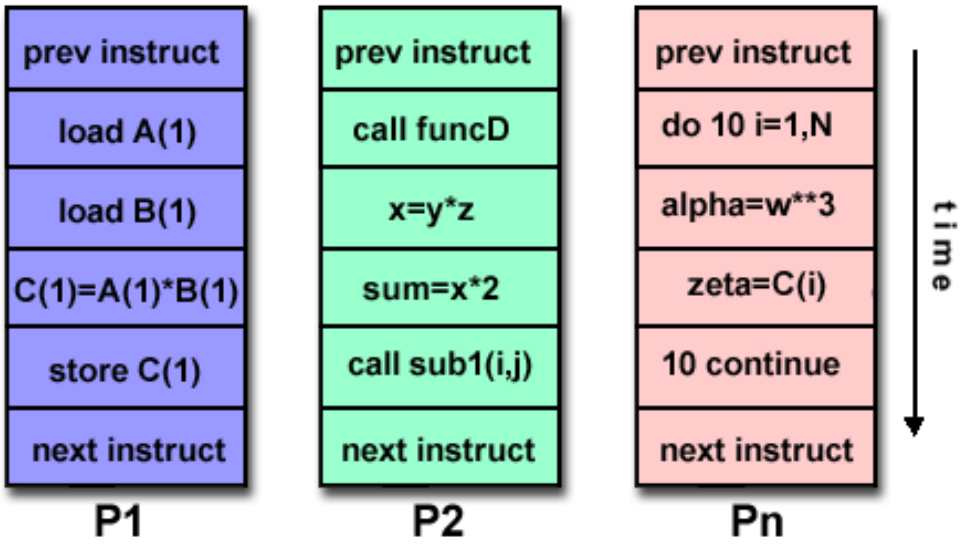

Figure C.7. Operation of MIMD.

MIMD is an acronym of Multiple Instruction streams and Multiple Data streams. The operation of MIMD is described in the figure C.7. The most common type of parallel computers is included in this division. Every processor executes a different instruction stream with a different data stream.

3. Parallel computer memory architectures

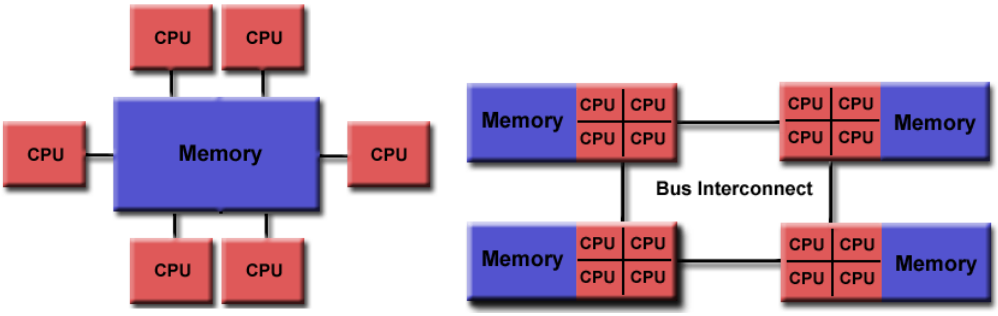

(a) UMA (b) NUMA

Figure C.8. Architecture of shared memory.

The memory architectures of parallel computer are classified to shared, distributed, and hybrid distributed-shared. In shared memory system, there are Uniform Memory Access (UMA) and Non-uniform Memory Access (NUMA). The architectures of UMA and NUMA is described in the figure C.8. Advantage of shared memory is that the data access of CPUs is fast due to the closeness between the memory and the CPUs. And, disadvantage of it is the expensive cost to increase the size of the memory and the number of CPUs.

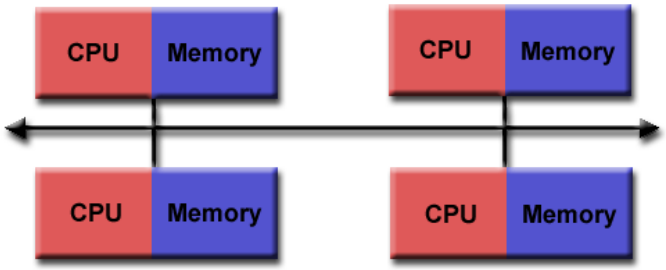

Figure C.9. Distributed memory.

The figure C.9 shows the architecture of distributed memory. In this case, each processor has its own local memory. The advantage is the inexpensive cost to increase the number of processors and the size of memory. In addition, each processor can rapidly access to its own memory. The disadvantage is that the data communication between CPUs is slower than the shared memory.

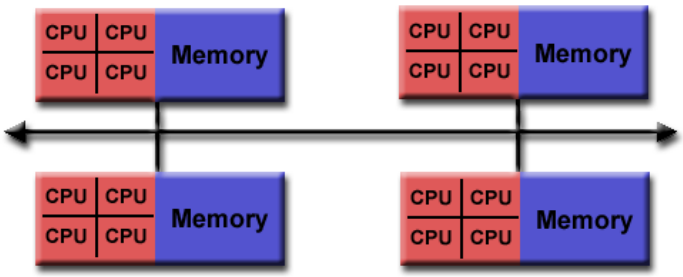

Figure C.10. Hybrid distributed-shared memory.

The last architecture is hybrid distributed-shared memory as shown in the figure C.10. The largest and fastest computers in the world today employ both shared and distributed memory architectures (cluster machines with multi-core CPUs).

4. Parallel programming

The speedup of a program using multiple processors in parallel computing is limited by the sequential fraction of the program. The speedup is calculated by Amdahl's law:

$$\text{Speedup} = \frac{1}{1 - P + \frac{P}{N}}, \qquad \text{(C.1)}$$

where P is parallel portion, N number of processors.

Application Programming Interfaces (API) of Parallelization are MPI and OpenMP. MPI is an acronym of Message Passing Interface. It is functions to specify message-passing for the parallel programming in Fortran or C. OpenMP is API for parallel programming on the shared memory environment.

Une analyse efficace du procédé RTM à l'aide de la méthode XFEM

Résumé en français

1. Introduction

Le procédé RTM (*Resin Transfer Molding*) est un des procédés de fabrication des structures composites les plus largement utilisés dans l'industrie de transport, par exemple, l'automobile, la construction navale, l'aéronautique et l'espace. Pour la fabrication des structures composites par le procédé RTM, il est indispensable de simuler l'écoulement de la résine dans le moule en vue de prédire les lignes de soudure et d'éviter la formation de poches d'air, qui pourraient être l'origine des défauts critiques dans la structure. Un des points importants est, lors de la simulation de l'écoulement de la résine, d'assurer une approximation correcte de la position du front d'écoulement à chaque instant pendant le processus de remplissage du moule. En outre, il est nécessaire de paralléliser le calcul afin de pouvoir traiter des problèmes de taille industrielle dans un temps de calcul acceptable.

L'écoulement de la résine dans le moule représente un problème d'interface mobile à travers la préforme placée *a priori* dans le moule. Les méthodes numériques utilisées pour la simulation de l'écoulement de la résine peuvent être regroupées en deux groupes : maillage mobile et maillage fixe. L'approche avec le maillage fixe est plus largement utilisé car celle du maillage mobile nécessite un calcul relativement plus cher et complexe [1-8].

Les méthodes numériques les plus souvent exploitées pendant les deux dernières décennies sont la méthode d'éléments finis avec contrôle de volume (CVFEM, *Control Volume Finite Element Method*) et les éléments finis non conformes. La méthode CVFEM a été la plus fréquemment développée pour la simulation du procédé RTM jusqu'au début des années 2000 [1-12], car la méthode CVFEM pouvait satisfaire efficacement la conservation de masse de la résine entre des éléments voisins par rapport à celle des éléments finis classique [2]. En revanche, la construction des volumes de contrôle dans le domaine de calcul entier pouvait mettre le calcul complexe [3, 5]. Trochu *et al* a proposé d'appliquer les éléments finis non conformes à la simulation du procédé RTM [5]. Puisque les éléments

finis non conformes calculent la pression aux interfaces des éléments adjacents, la vitesse de l'écoulement à la frontière des éléments peut être obtenue sans aucun traitement supplémentaire, de laquelle le taux de remplissage du moule est dérivé. Cependant, le taux de remplissage n'est pas une valeur nodale, mais celle de l'élément [5]. C'est pourquoi ces méthodes ne pouvaient pas donner une approximation propre du champ de pression dans les éléments intersectés par le front d'écoulement de la résine à cause de la discontinuité du gradient de pression près du front d'écoulement. Ce point est très important dans le cas des problèmes industriels ayant des formes géométriques complexes.

La méthode d'éléments finis étendue (XFEM, *eXtended Finite Element Method*) est largement utilisée pour traiter de divers problèmes de discontinuité tels que la rupture ou les problèmes d'interface [13-19]. Cesse *et al* a appliqué la méthode XFEM aux problèmes d'écoulement immiscible biphasé qui ont une discontinuité sur le gradient de pression à l'interface entre deux fluides [14]. Cette méthode a été retenue dans cette étude en vue d'augmenter la précision numérique du champ de gradient de pression (champ de vitesses) près du front d'écoulement.

Quant à l'approche avec le maillage fixe, la méthode VOF (*Volume Of Fluid*) est une des méthodes les plus représentatives pour tracer les interfaces mobiles [20, 21]. Cette méthode a été couramment utilisée pour la simulation du procédé RTM [1-9]. Cependant, puisque l'interface mobile est définie par le volume de fluide fractionnel dans l'élément ou le volume de contrôle suivant la méthode utilisée, il pouvait être imprécis pour les cas où on trace des mouvements complexes du front d'écoulement de la résine [22-25]. La méthode Level set est une des plus représentatives pour capturer les interfaces mobiles [26]. Cette méthode est souvent utilisée pour la simulation du procédé RTM car elle prédit intuitivement la position du front d'écoulement et est très efficace pour les fronts d'écoulement multiples dus à la forme géométrique complexe du moule ou à plusieurs points d'injection [24, 25]. Dans cette étude, une méthode de type Level set est retenue pour calculer le front d'écoulement de la résine.

Dans cette étude, les fonctions de forme enrichies de la XFEM décrivant le champ de pression sont définies par les valeurs Level set suivant [14]. Puisque la XFEM met le système d'équilibre symétrique et défini positif, une méthode de résolution en parallèle classique, comme la méthode multi-frontale, peut être utilisée afin de réduire le temps de calcul. La méthode Level set est composée de deux étapes. La première est de déplacer le front découlement, et la seconde est la réinitialisation pour maintenir la fonction Level set près de la fonction de distance avec signe. Une méthode de Galerkin à caractère implicite est utilisée pour stabiliser les oscillations numériques dues au terme convectif dans les équations d'équilibre [22]. Le champ de pression est divisé en deux régions : normale et enrichie. La zone enrichie est définie seulement près du front d'écoulement de la résine afin de réduire la taille du système d'équilibre à résoudre. Puisque la zone enrichie n'est définie que près du front d'écoulement de la résine, la taille du système d'équilibre est légèrement augmentée. Le solveur multi-frontal en parallèle proposé par ISAP [31] est retenu pour résoudre le système d'équilibre discrétisé. La localisation avec la méthode XFEM et la méthode Level set sert à augmenter l'efficacité de calcul.

La méthode développée est validée à travers quelques exemples en 2D en comparaison avec les résultats analytiques ou expérimentaux trouvés dans la littérature [32-35]. Quelques exemples de plaque 3D sont traités pour simuler l'effet du bord et la formation de macro-vides [36]. En outre, un programme intégrant la méthode présentée a été développé avec un outil d'interface graphique convivial pour les pré- et post-traitements de la simulation.

2. Modèles mathématiques

Pour la simulation du procédé RTM, l'écoulement de la résine dans le moule est modélisé avec les hypothèses suivantes : l'écoulement de la résine est considéré comme incompressible et iso-thermique. Par conséquent, la loi de conservation de masse est donnée :

$$\nabla \cdot \mathbf{u} = 0 \qquad (1)$$

où **u** est la vitesse de résine. Et, l'équation d'équilibre d'inertie est donnée :

$$\rho \, \mathrm{D}\mathbf{u}/\mathrm{D}t = -\nabla p - (\mu/\mathbf{K})\mathbf{u} \qquad (2)$$

où ρ est la masse volumique, t le temps, p la pression de la résine, **K** le tenseur de perméabilité, et μ la viscosité de la résine.

Avec l'hypothèse iso-thermique, la viscosité de la résine peut être constante durant le remplissage du moule. La perméabilité de la préforme dans le moule peut être constante due à l'hypothèse dans laquelle la préforme est considérée comme uniforme et indéformable pendant le remplissage du moule. Si l'écoulement de la résine est suffisamment lent, l'effet d'inertie peut être négligé et l'écoulement de la résine peut être considéré comme une succession d'états stationnaires de l'écoulement. Par conséquent, après l'obtention du champ de pression et de la vitesse du fluide dans le moule, le front d'écoulement de la résine est déplacé pour le pas de temps suivant S.G. Advani et al. [27]. L'équation de Darcy dans l'écoulement stationnaire est dérivée de l'équation (2) comme :

$$\mathbf{u} = -(\mathbf{K}/\mu)\nabla p \qquad (3)$$

En mettant l'équation (3) dans l'équation (1), l'équation d'équilibre pour le champ de pression devient :

$$\nabla \cdot (-(\mathbf{K}/\mu)\nabla p) = 0 \qquad (4)$$

Les conditions frontières sont données :

$$\begin{aligned} p_{in} &= \text{Pression à l'injection} && \text{aux points d'injection} \\ p_{vent} &= \text{Pression à } la\ fuite && \text{aux points de fuite} \\ \partial p/\partial n &= 0 && \text{aux parois du moules} \end{aligned} \qquad (5)$$

Le transport du front d'écoulement pour le pas de temps suivant s'effectue par la méthode Level set. Le détail de cette méthode est expliqué dans le chapitre suivant.

3. Méthodes numériques

3.1. Méthode Level Set

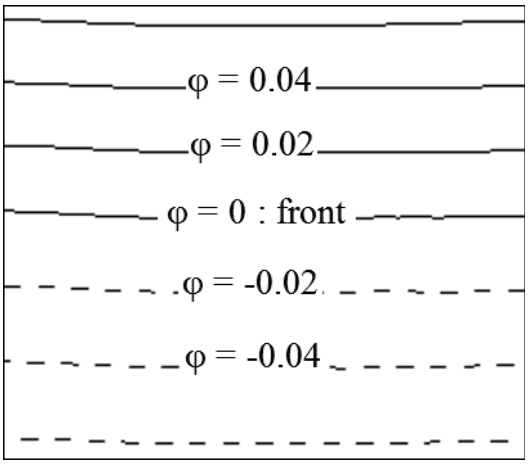

Figure 1 : les valeurs Level set composes de la région remplie, du front, et de la région non remplie.

La méthode Level set est utilisée pour le transport du front d'écoulement de la résine. La valeur Level set signifie la distance avec signe du front d'écoulement, comme illustré dans la figure 1. Au front d'écoulement, la valeur Level set est égale à 0. La région replie par la résine a une valeur positive, et la région pas encore remplie est négative. Le transport de l'écoulement de la résine est décrit par l'équation de transport suivante avec la fonction Level set.

$$\partial\varphi/\partial t + \mathbf{u} \cdot \nabla\varphi = 0 \qquad (6)$$

L'équation (6) permet de trouver la position du front d'écoulement à chaque pas de temps, mais mas les autres régions. C'est pourquoi une procédure de réinitialisation est indispensable afin de remettre les valeurs Level set à leur condition initiale, définie par :

$$\|\nabla\varphi\| = 1 \qquad (7)$$

Nous avons utilisé la méthode de réinitialisation proposée par [23] :

$$\partial\varphi/\partial t + sign(d_0)(\|\nabla d\| - 1) = 0,$$
$$d(\boldsymbol{x}, 0) = d_0(\boldsymbol{x}) = \varphi(\boldsymbol{x}, t) \quad (8)$$

où d est la fonction de distance avec signe du front, τ le temps fictif pour la procédure de réinitialisation, et $sign(d_0)$ le signe de la valeur initiale d_0. En plus, la fonction $sign(d_0)$ est définie par :

$$sign(d) = d/\sqrt{d^2 + h^2} \quad (9)$$

où h est la taille de maillage. La fonction Level set est réinitialisée pour la condition initiale en résolvant l'équation (8). La procédure de réinitialisation s'effectue à chaque pas de temps.

3.2. Méthode d'éléments finis étendue (XFEM)

La pression dans le moule est obtenue par la méthode XFEM. L'avantage principal de cette méthode est d'obtenir le champ de pression d'une manière précise sans remailler sur la zone du front d'écoulement.

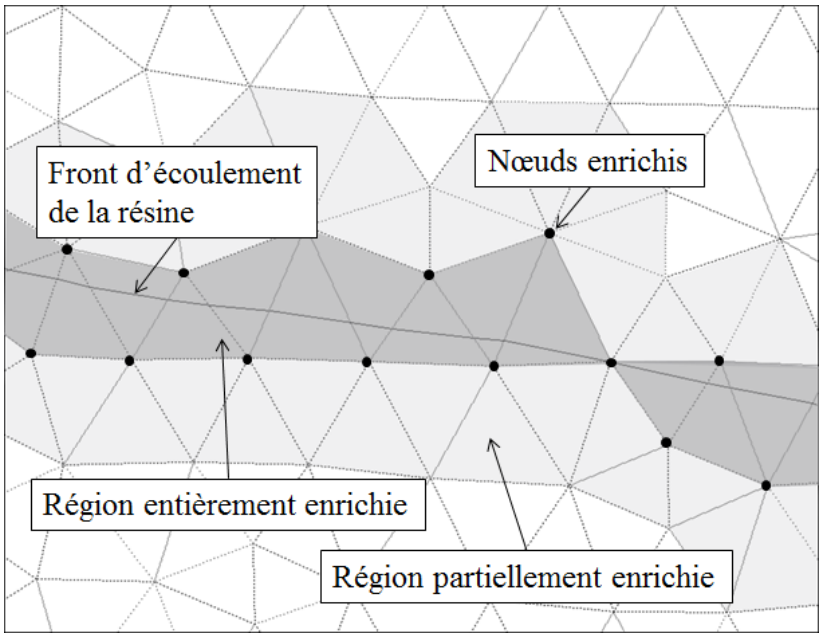

Figure 2 : la définition des nœuds enrichis et le type de régions.

Le domaine de calcul est divisé en deux régions : normale et enrichie. La région enrichie est discrétisée par des éléments ayant des nœuds enrichis. Ces nœuds sont ajoutés aux éléments intersectés par le front d'écoulement (Figure 2). La région normale est discrétisée par des éléments sans aucun nœud enrichi.

L'enrichissement signifie que les degrés de liberté (ddl) additionnels sont ajoutés dans un élément fini classique. La fonction de forme pour cet enrichissement est définie par :

$$p^h = \sum_{I \in n} N_I p_I + \sum_{J \in n_e} N_J^e a_J \qquad (10)$$

où p^h est la fonction de la pression, p_I la valeur de la pression au nœud I, a_J le paramètre nodal additionnel au nœud enrichi J, N_I la fonction de forme, N_J^e la fonction de forme enrichie, n le nombre de nœuds, et n_e le nombre de nœuds enrichis. La fonction de forme enrichie est construite comme :

$$N_J^e = N_J\left(|\varphi| - |\varphi_J|\right) \qquad (11)$$

où φ_J est la valeur Level set du nœud enrichi J. La discontinuité au front d'écoulement peut être représentée par les fonctions composées des fonctions et valeurs Level set. Comme exemple, les fonctions de forme enrichies d'un élément unidimensionnel sont montrées dans la figure 3. Le caractère significatif des fonctions de forme enrichies est que la position du front d'écoulement est prise en compte dans les fonctions de forme enrichies. Il est important de noter que les valeurs des fonctions de forme enrichies doivent être égales à 0 aux nœuds.

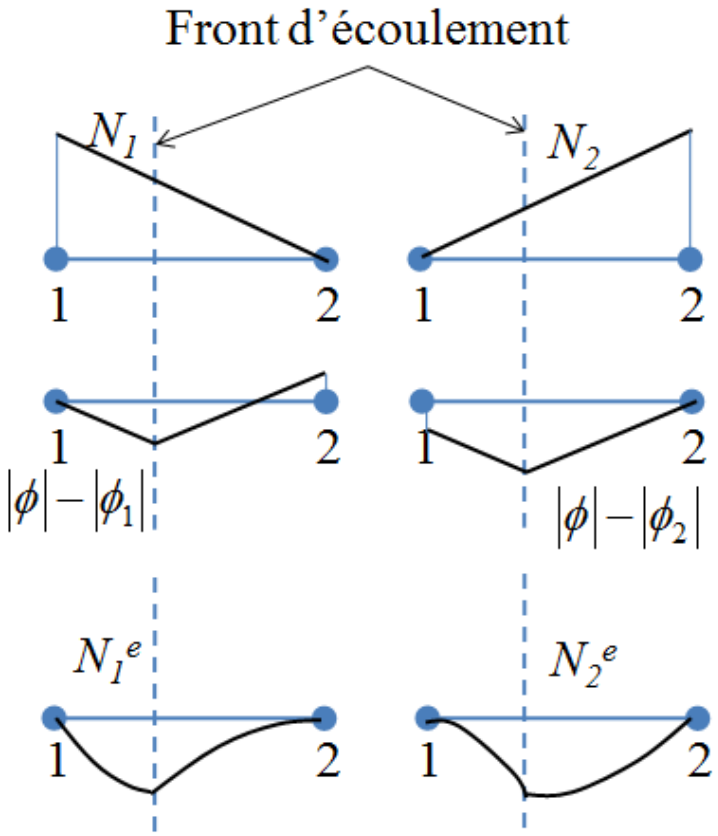

Figure 3 : les fonctions de forme enrichies d'un élément linéaire unidirectionnel.

Le gradient de pression au front d'écoulement doit être calculé précisément. Le gradient de la fonction de pression approximative dans la région enrichie s'obtient :

$$\nabla p^h = \sum_{I \in n} p_I \nabla N_I + \sum_{J \in n_e} a_J \left[\nabla N_J \left(|\varphi| - |\varphi_J|\right) + N_J sign(\varphi) \nabla \varphi\right] \qquad (12)$$

Le saut de la fonction de pression approximative à travers le front de la résine est défini par :

$$[\![\nabla p^h]\!] = 2 \sum_{J \in n_e} N_J a_J \nabla \varphi \quad \text{on the resin front} \qquad (13)$$

Il y a deux types d'enrichissement comme illustré dans la figure 2 : enrichissement complet ou partiel. L'enrichissement complet concerne les éléments n'ayant que des nœuds enrichis. L'enrichissement partiel concernent ceux ayant des nœuds enrichis et normaux. Cet enrichissement partiel est nécessaire pour maintenir la continuité du champ de pression.

4. Formulations numériques

4.1. Transport du front d'écoulement

Une méthode de Galerkin implicite est utilisée pour stabiliser le phénomène d'oscillations numériques lors de la résolution de l'équation (6) [22]. Le terme dérivé par rapport au temps est discrétisé par [28] :

$$\varphi^{n+1} - \varphi^n = -\Delta t[\mathbf{u} \cdot \nabla\varphi]_n + \Delta t^2/2 \left[\nabla \cdot \left((\mathbf{u}\otimes\mathbf{u}) \cdot \nabla\varphi\right)\right]_{n+1} \qquad (14)$$

où Δt est le pas de temps. Pour la discrétisation des termes différentiels spatiaux de l'équation (14), la méthode de Galerkin standard est utilisée :

$$\int_\Omega (\varphi^{n+1} - \varphi^n) w dV = -\Delta t \int_\Omega (\mathbf{u} \cdot \nabla\varphi^n) w dV - \Delta t^2/2 \int_\Omega \left((\mathbf{u}\otimes\mathbf{u}) \cdot \nabla\varphi^{n+1}\right) \cdot \nabla w dV \qquad (15)$$

où w est la fonction de pondération et Ω l'espace complet dans le moule. La vitesse $\mathbf{u}$ pour le transport du front d'écoulement est calculée par l'équation (3). La viscosité de la résine est définie par :

$$\mu = H(\varphi)\mu_r + (1 - H(\varphi))\mu_a \qquad (16)$$

où μ_r est la viscosité de la résine et μ_a celle de l'air, et $H(\varphi)$ la fonction Level set. $H(\varphi)$ est défini par :

$$H(\varphi) = \begin{cases} 1 & if\ \ \varphi < -h \\ \frac{1}{2}(1 - \varphi/h) & if\ \ |\varphi| \le h \\ 0 & if\ \ \varphi > h \end{cases} \tag{17}$$

L'équation de réinitialisation est aussi discrétisée par les équations (14) et (15).

$$\int_\Omega (d^{n+1} - d^n) w dV = -\Delta\tau \int_\Omega sign(d_0)|\nabla d^n| w dV - \Delta\tau^2/2 \int_\Omega \nabla d^{n+1} \cdot \nabla w dV + \Delta\tau \int_\Omega sign(d_0)\mathrm{w dV} \tag{18}$$

où $\Delta\tau$ est le pas de temps dans la procédure de réinitialisation.

4.2. Champ de pression

L'équation (4) est résolue par la méthode XFEM [14]. Suivant la méthode d'éléments finis standard, la forme faible de l'équation (4) s'écrit par :

$$\int_\Omega \big(\nabla \cdot (-\mathbf{K}/\mu\, \nabla p)\big) w dV = 0 \tag{19}$$

où *w* est une fonction de pondération. En appliquant le théorème de Green-Gauss, l'équation (19) devient :

$$\int_\Omega \nabla w \cdot (-\mathbf{K}/\mu\, \nabla p) dV - \int_{\partial\Omega} w(-\mathbf{K}/\mu\, \nabla p) \cdot \mathbf{n} dS = 0 \tag{20}$$

où **n** est le vecteur normal sortant. Par la méthode XFEM, la pression et les fonctions de pondération sont discrétisées comme l'équation (12).

Les éléments interceptés par le front d'écoulement sont divisés en deux parties : région remplie et celle non remplie. Ces deux régions sont séparément intégrées car la dérivée de la fonction de pression est légèrement discontinue au front d'écoulement [29, 30]. La viscosité de la résine des sous-domaines, entrecoupés par le front d'écoulement, est définie par :

$$\mu = \mu_r/2\,(1 - sign(\varphi)) + \mu_a/2\,(1 + sign(\varphi)) \qquad (21)$$

4.3. Procédures de calcul

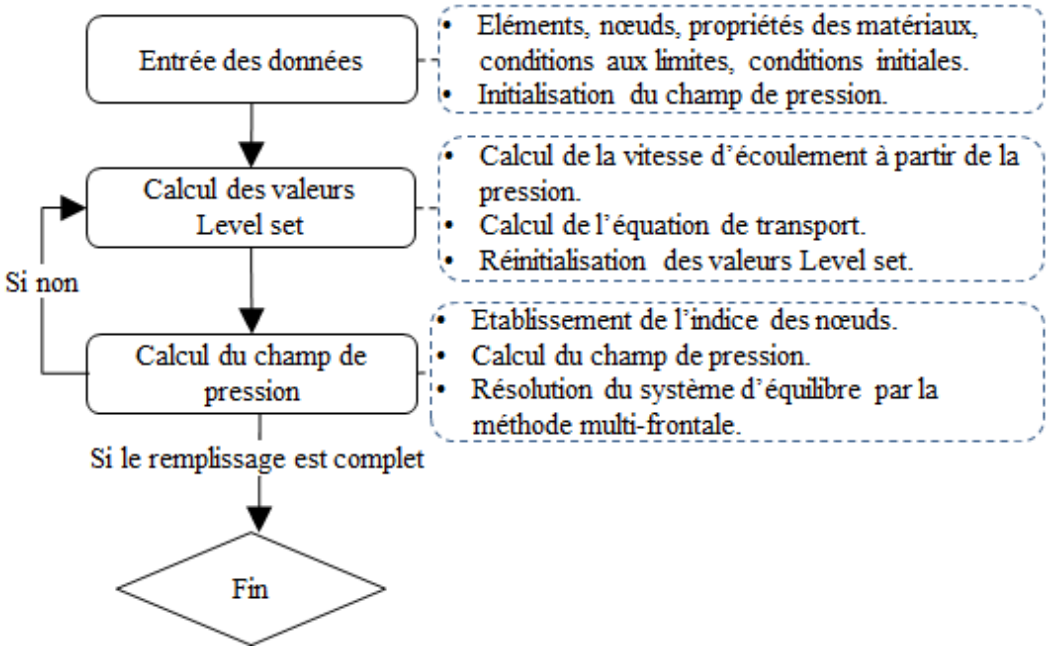

Figure 4 : Schéma global du calcul.

La figure 4 montre le schéma du calcul global. La première étape consiste à lire les données d'entrée, comme l'information sur le maillage, les propriétés des matériaux et les conditions frontières, et à initialiser le champ de pression et les valeurs Level set. A l'étape 2, la viscosité du fluide est calculée du champ de pression par l'équation (3), et l'équation (6) est servie pour transporter le front d'écoulement. L'équation (8) pour la réinitialisation des valeurs Level set se résout à chaque pas de temps. Dans la région complètement enrichie, les valeurs Level set sont calculées à chaque nœud élément par élément. A l'étape 3, après avoir scanné les valeurs Level set nodales de chaque élément, l'indice des nœuds est remise à 1 pour les nœuds enrichis et à 0 pour les normaux. Les étapes 2 et 3 sont répétées jusqu'au remplissage complet du moule. Le solveur basé sur la méthode multi-frontale proposé par IPSAP [31] est utilisé pour la résolution du système d'équilibre discrétisé.

5. Amélioration de l'efficacité de calcul par localisation

La localisation pour la méthode XFEM couplée avec la méthode Level set permet d'améliorer l'efficacité de calcul en minimisant le nombre de calcul [37]. La localisation signifie la définition d'une région en bande près du front d'écoulement de la résine. La simulation de l'écoulement de la résine dans le moule peut être traduite par la description du mouvement du front d'écoulement de la résine. Par conséquent, les valeurs Level set exceptées la région près du front d'écoulement sont insignifiantes. C'est pourquoi il est possible d'augmenter l'efficacité de calcul si le domaine est raisonnablement réduit pour obtenir seulement les valeurs Level set sans aucune influence sur les résultats. En général, la plupart du temps de calcul est consommé par la résolution du système d'équilibre du problème. C'est pourquoi si plus petite est la taille du système (nombre de DDL), le temps de calcul peut certainement être plus réduit. Même si une procédure complémentaire est nécessaire pour localiser le domaine de calcul, le temps de calcul total devait être réduit d'une manière importante car le temps de localisation est relativement très court. Dans ce chapitre, un algorithme de localisation pour la méthode XFEM couplée avec la méthode Level set est présenté. En outre, l'efficacité de calcul par localisation est prouvée à travers quelques exemples.

5.1. Localisation pour la méthode XFEM couplée avec la méthode Level Set

Cet algorithme, utilisé pour la localisation avec la méthode Level set, s'est basé sur l'algorithme proposé par Peng et al. [23]. Nous avons modifié cet algorithme en vue de l'appliquer à la méthode de Galerkin implicite.

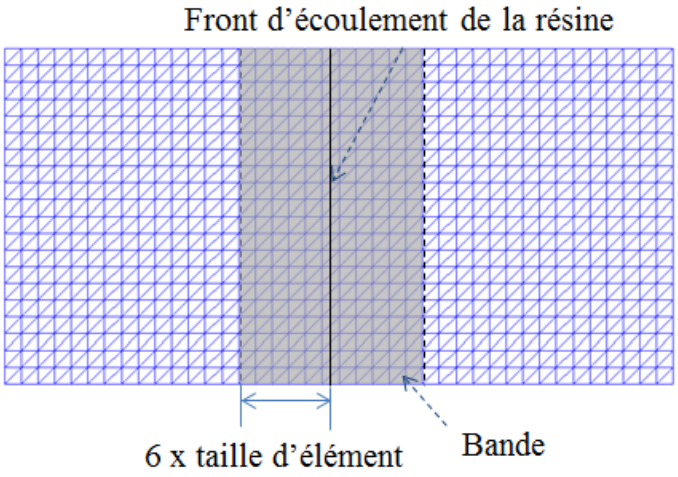

Figure 5 : Domain de calcul pour la localisation avec la méthode Level set.

Une région près du front d'écoulement est prise pour la localisation avec la méthode Level set comme présenté en couleur grise dans la figure 5. La bande est redéfinie à chaque pas de calcul suivant la position du front d'écoulement. La demi-largeur de bande est six fois de la taille d'élément [23]. Les valeurs Level set des nœuds ne sont mises à jour que dans la bande à chaque pas de calcul.

Pour la localisation avec la méthode Level set, une fonction seuil est nécessaire en vue d'éviter des oscillations numériques aux frontières de la bande. Cette fonction est définie par :

$$c(\varphi) = \begin{cases} 1 & if\ |\varphi| \le \beta \\ (|\varphi| - \gamma)^2(2|\varphi| + \gamma - 3\beta)/(\gamma - \beta)^3 & if\ \beta < |\varphi| \le \gamma \\ 0 & if\ |\varphi| > \gamma \end{cases} \qquad (22)$$

où φ est la valeur Level set, γ la demi-largeur de la bande (six fois de la taille d'élément), $\beta = \gamma / 2$ [23]. En appliquant la fonction seuil à l'équation différentielle pour calculer les valeurs Level set, l'équation d'équilibre est modifiée comme :

$$\frac{\partial \varphi}{\partial t} + c(\varphi)\mathbf{u} \cdot \nabla\varphi = 0 \qquad (23)$$

La localisation avec la méthode XFEM est désormais appliquée pour réduire le nombre de calcul sur la pression. Comme mentionné avant, la pression dans le moule sert à calculer la vitesse de l'écoulement. Avec la localisation avec la méthode Level set, la pression hors domaine de calcul en bande n'est pas prise dans le calcul avec la méthode Level set. Cet algorithme permet d'obtenir la pression dans le domaine de calcul en bande et d'éviter des calculs inutiles.

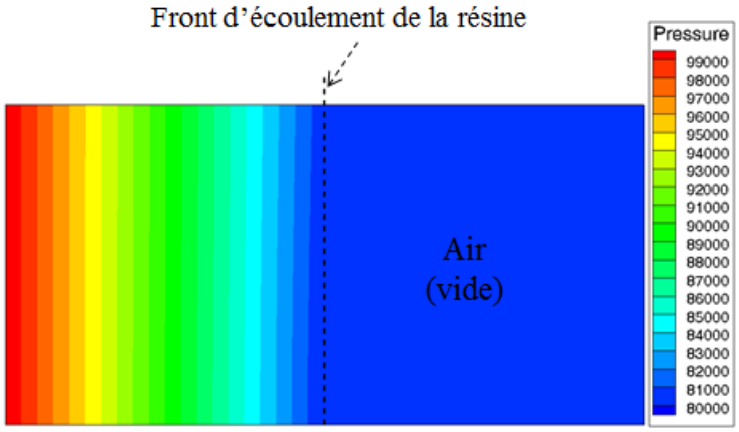

Figure 6. Pression dans le moule d'une plaque en écoulement laminaire.

Comme illustré dans la figure 6, la pression de l'air dans le moule est très peu changée par rapport à la pression de la résine. Par conséquent, nous proposons de définir le domaine de calcul comme montré dans la figure 7. Le domaine de calcul inclue la région remplie par la résine et une petite bande contenant de l'air (ou vide). La demi-largeur de cette petite bande est définie par six fois de la taille de l'élément, car elle doit être la même que celle utilisée pour la localisation de la méthode Level set.

Le point clef de la localisation de la méthode XFEM est comment appliquer les conditions aux limites, car les valeurs initiales sont prises en comptes pour le calcul de la méthode Level set, mais pas les conditions aux limites. Cependant, la pression doit être obtenue en tenant compte les conditions aux limites. Or, le front d'écoulement change à chaque pas de calcul. Par conséquent, nous imposons la

pression du point de fuite à la frontière de la bande de l'air, car la variation de la pression dans l'air est quasiment négligeable.

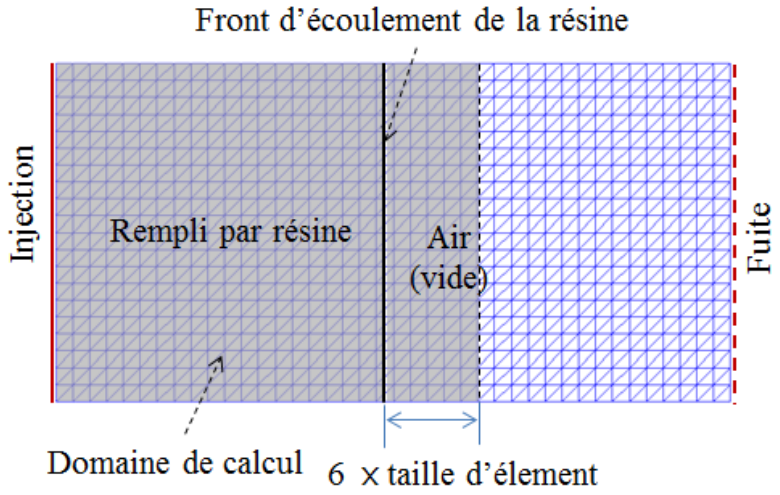

Figure 7 : Domaine de calcul pour la localisation de la méthode XFEM.

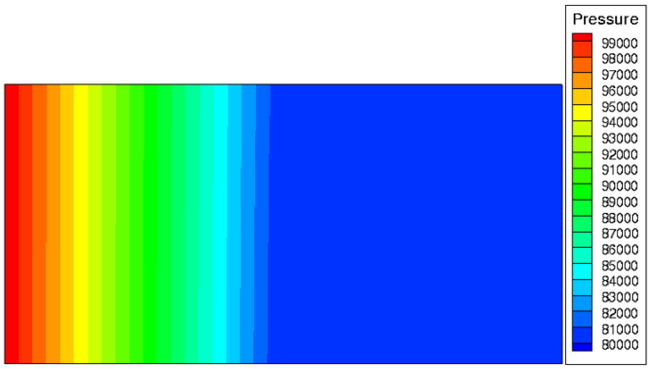

Figure 8 : Pression obtenue par la localisation de la méthode XFEM.

Dans la figure 8, la distribution de la pression est obtenue par la localisation de la méthode XFEM. La répartition est comparable à celle obtenue sans localisation (voir la figure 6).

5.2. Efficacité de la localisation

Nous prenons l'exemple de l'écoulement laminaire dans une plaque rectangulaire (Figure 9). Pour montrer l'efficacité de l'algorithme de localisation, nous

comparons le temps de calcul sur les trois cas suivants : sans localisation, la localisation uniquement avec la méthode Level set, et la localisation avec la méthode XFEM et la méthode Level set. La configuration de l'ordinateur utilisé dans cette comparaison est Intel (R) Core(TM) i7 CPU 950 (3,07 GHz, Quad-core). Le système d'opération est Windows 7 Professional K pour 64 bits.

Nb. des nœuds	Temps de calcul			Réduction du temps de calcul
	Sans localisation	Avec localisation		
861	37,5 secs.	Level set	29,0 secs.	22,7 %
		XFEM + Level set	24,1 secs.	35,7 %
2556	211,4 secs.	Level set	154,0 secs.	27,2 %
		XFEM + Level set	118,0 secs.	44,2 %
7381	1236,8 secs.	Level set	742,5 secs.	40,0 %
		XFEM + Level set	561,1 secs.	54,6 %

Tableau 1 : Temps de calcul de l'écoulement laminaire d'une plaque rectangulaire.

Le temps de calcul de l'exemple d'une plaque rectangulaire en écoulement laminaire est montré dans le tableau 1. Le temps de calcul a été mesuré à partir d'après la lecture des données jusqu'avant l'écriture des résultats lorsque le moule est complètement rempli. Nous avons déjà une réduction de temps de calcul significative seulement avec la localisation avec la méthode Level set. En outre, si la localisation est faite non seulement avec la méthode Level set mais aussi avec la méthode XFEM, la réduction du temps de calcul s'amplifie d'une manière importante.

Plus grand est le nombre des nœuds, plus important est le rapport de la réduction du temps de calcul. En plus, le nombre des opérations de la méthode Level set est plus grand que celui du calcul de la pression. C'est pourquoi la réduction du temps de calcul par la localisation avec la méthode Level set est plus importante que celle avec la méthode XFEM. De toute façon, il est évident que la localisation avec les deux méthodes maximise le calcul. Ceci représente un intérêt important

d'utiliser cette méthode pour des cas industriels qui nécessitent un temps de calcul très important.

6. Validation

Quelques exemples sont traités pour valider ces méthodes en comparaison avec les résultats analytiques ou expérimentaux trouvés dans la littérature [32-35]. Tout d'abord, deux exemples en écoulement 2D simple de type laminaire ou radial sont pris pour comparer nos résultats avec la solution analytique. Ensuite, un exemple de plaque avec une géométrie complexe est retenu pour comparer nos résultats avec les résultats expérimentaux publiés par A. Shojaei et al. [34]. Enfin, un exemple 3D de type boitier est pris pour montrer les effets du bord et la formation de macro-vides [36].

6.1. Exemples d'écoulement simple

Deux exemples d'écoulement de type laminaire ou radial simple sont traités pour valider les présentes méthodes avec les solutions analytiques. Le temps de remplissage total obtenu par nos méthodes est comparé avec celui analytique proposé par Z. Cai [32].

6.1.1. Ecoulement laminaire dans une plaque rectangulaire

La figure 9 présente un exemple d'écoulement laminaire dans une plaque rectangulaire ayant une largeur constante. La longueur, la largeur et l'épaisseur sont respectivement égales à 1 m, 0,5 m et 1 mm. La résine est injectée à travers le côté gauche de la plaque, comme indiqué par la ligne continue. Et la résine sort de la plaque par le côté droit (ligne pointillée). Un élément de plaque triangulaire bi-linaire est utilisé et le nombre total des nœuds et des éléments est égal à 861 et 1600 respectivement.

Les propriétés des matériaux et les conditions aux limites du modèle sont : viscosité de la résine = 0,1 Pa·s, perméabilité de la préforme (isotrope et

homogène) = 10^{-9} m^2, porosité = 0,5, pression d'injection = 20 KPa, pression de fuite = 0. Le temps de remplissage du moule analytique est donné par :

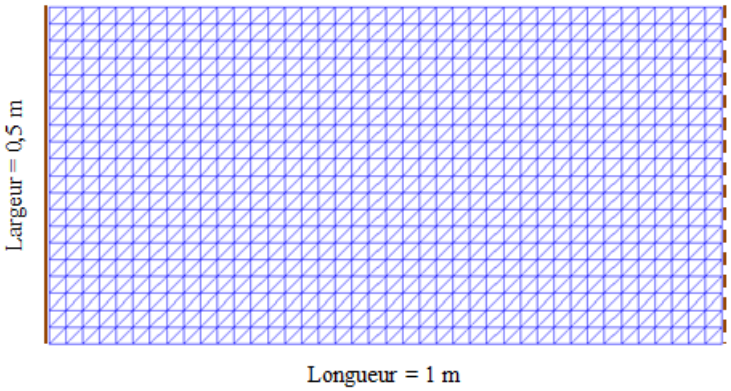

Figure 9. Géométrie et maillage de la plaque rectangulaire.

$$t_{filling} = L^2 \mu \Phi / 2KP \quad (24)$$

où L est la position du front d'écoulement dans la direction de la longueur. μ, Φ, K, et P sont la viscosité, la porosité, la perméabilité et la pression respectivement. Le temps de remplissage du moule analytique est égal à 1250 secondes, et notre méthode donne 1268.42 secondes. La différence entre les deux est inférieure à 1,5 %. En comparaison avec la solution numérique (3 % de différence) proposée par S. Soukane et al. [24], qui ont traité le même exemple, notre méthode est plus précise.

6.1.2. Ecoulement radial en 2D dans un disque circulaire

La figure 10 représente un exemple d'écoulement radial dans un disque mince circulaire. Grâce aux conditions axisymétriques, un quart de disque est modélisé. Le rayon et l'épaisseur du disque sont respectivement égaux à 1 m et 1 mm. La résine est injectée à travers un trou situé au centre, dont le rayon est égal à 0,2 m. La ligne pointillée au bord du disque représente la position de la fuite. Les valeurs de la viscosité de la résine, de la perméabilité de la préforme, de la porosité et la pression d'injection sont les mêmes que dans l'exemple précédent.

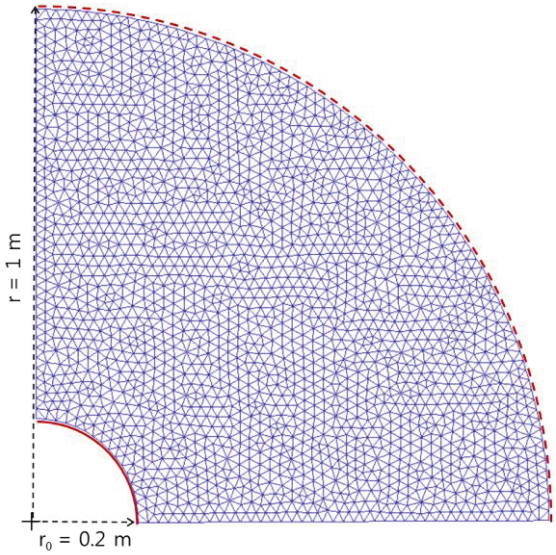

Figure 10. Géométrie et maillage de l'exemple d'écoulement radial.

Le temps de remplissage du moule analytique est donnée par :

$$t_{filling} = \mu\phi r_0^2/4KP(r/r_0)^2\,[2\ln r/r_0 + (r_0/r)^2 - 1] \qquad (25)$$

où r est le rayon du disque et r_0 le rayon du trou. Le temps de remplissage analytique est égal à 1411 secondes, et notre méthode donne 1436 secondes. La différence entre les deux résultats est égale à 1,8 %. Notre méthode est très efficace en comparaison avec M. Lin et al. [33], qui donne 4 % de différence par rapport à la solution analytique.

6.2. Plaque 2D en géométrie complexe

Une plaque 2D en géométrie complexe est retenue (Figure 11) pour comparer nos résultats numériques avec ceux expérimentaux proposés par A. Shojaei et al. [34], afin de montrer l'écoulement de la résine influencé par la complexité géométrique de la structure. La dimension dans chaque direction est égale à 0,4 m, et l'épaisseur de la plaque égale à 4,5 mm. Le point d'injection est placé au centre comme montré par le point rouge. Le diamètre du point d'injection est égal à 4 mm. Les points de fuite sont placés aux coins comme marqué par trois points

bleus. Tous les bords du moule sont enveloppés par silicone pour empêcher l'effet de bord. La plaque discrétisée a 2204 nœuds et 4111 éléments triangulaires. L'huile de moteur SAE 40 est utilisée comme résine. Sa viscosité est égale à 0,3 Pa·s à la température ambiante (25 °C). La perméabilité et la porosité de la préforme sont égales à $6{,}83 \times 10^{-9}$ m^2 and 0,81, respectivement. La pression d'injection est mise à 35 KPa. Et la pression de fuite et la pression initiale dans le moule sont mises à zéro.

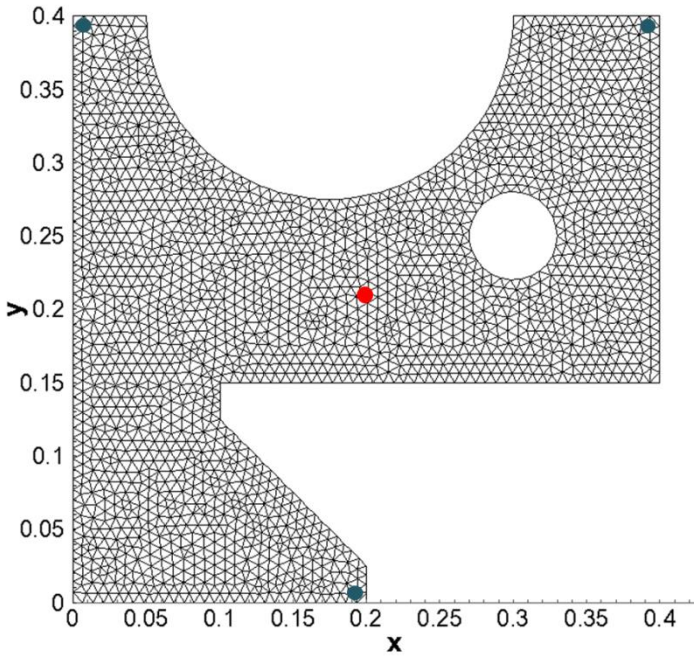

Figure 11. Géométrie et maillage de la plaque en 2D avec une géométrie complexe.

Le temps de remplissage total obtenu par notre méthode est égal à 123 seconds. Celui de [34] est de 117 seconds en expérimental et de 126 seconds en numérique. La différence entre le résultat expérimental et le nôtre est égale à 4,3 %. En comparaison avec la solution numérique de [34] dont la différence s'étend à 7,7 %, notre résultat est plus proche au résultat expérimental.

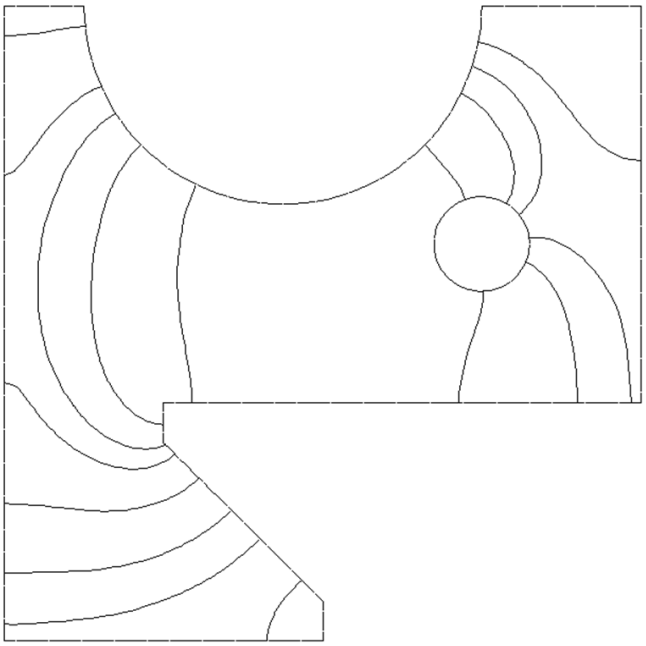

Figure 12 : Résultats obtenus par notre méthode sur la plaque 2D avec une géométrie complexe : le front d'écoulement tracé à tous les 15 seconds.

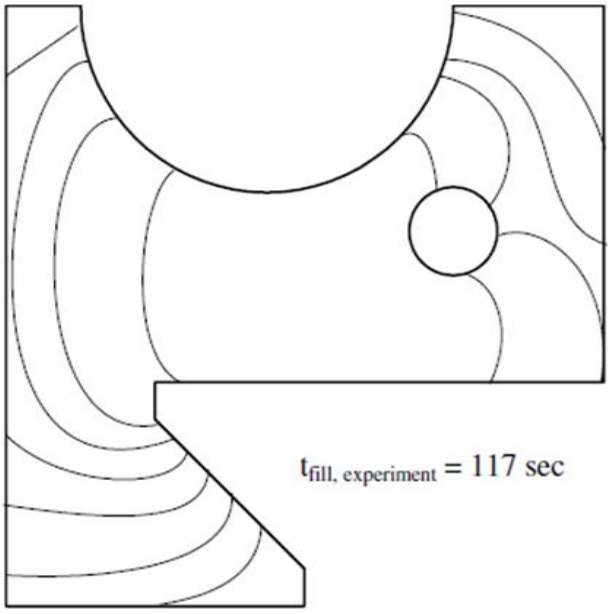

Figure 13 : Résultats publiés par A. Shojaei et al. [34] sur la plaque 2D avec une géométrie complexe : le front d'écoulement tracé à tous les 15 seconds.

La figure 12 montre la localisation du front d'écoulement durant le remplissage obtenu par la présente méthode, en comparaison avec celle expérimentale de [34] (Figure 13). La position du front d'écoulement est tracée à tous les 15 seconds.

6.3. Plaque mince 3D en forme complexe

Une plaque mince 3D en forme complexe est retenue pour montrer l'effet du bord et la formation de macro-vides dans le moule. La simulation numérique sur ces phénomènes peut être indispensable pour bien définir les variables de conception du procédé, comme les positions des points d'injection ou de fuite et leurs nombres.

Dans la figure 14, le trait continu et celui discontinu représentent respectivement la position des points d'injection et de fuite. La propriété des matériaux et les conditions aux limites sont : viscosité de la résine = 0,03 Pa·s, perméabilité de la préforme (isotrope et homogène) = $6{,}21 \times 10^{-11}$ m^2, porosité = 0,4, pression d'injection = 0,3 MPa, pression de fuite = 0 MPa.

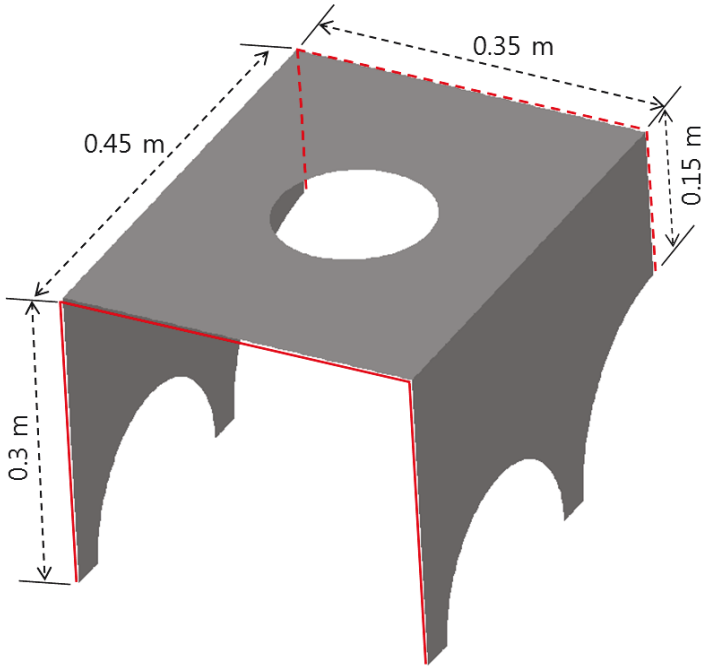

Figure 14 : Plaque mince 3D en forme complexe.

6.3.1. Effet du bord

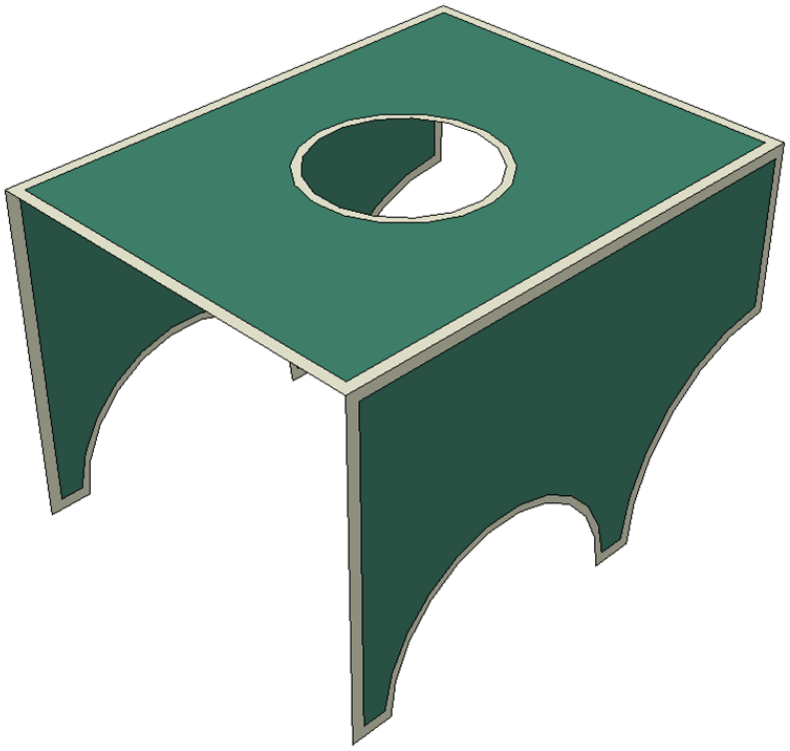

Figure 15 : Deux zones avec perméabilités différentes pour l'effet du bord.

Afin de modéliser l'effet du bord, une bande étroite au bord, dont la largeur constante est égale à 10 mm, a une haute perméabilité, égale à $6{,}21 \times 10^{-10}$ m^2. Le modèle d'éléments finis a 3684 nœuds et 7027 éléments triangulaires à 3 nœuds. La figure 16 montre le front d'écoulement de la résine obtenu par notre méthode à tous les 5 seconds. Le front d'écoulement près du bord a une courbure inverse due à l'effet du bord, et les gradients et la fusion des fronts d'écoulement autour du trou au centre sont bien représentés par notre méthode.

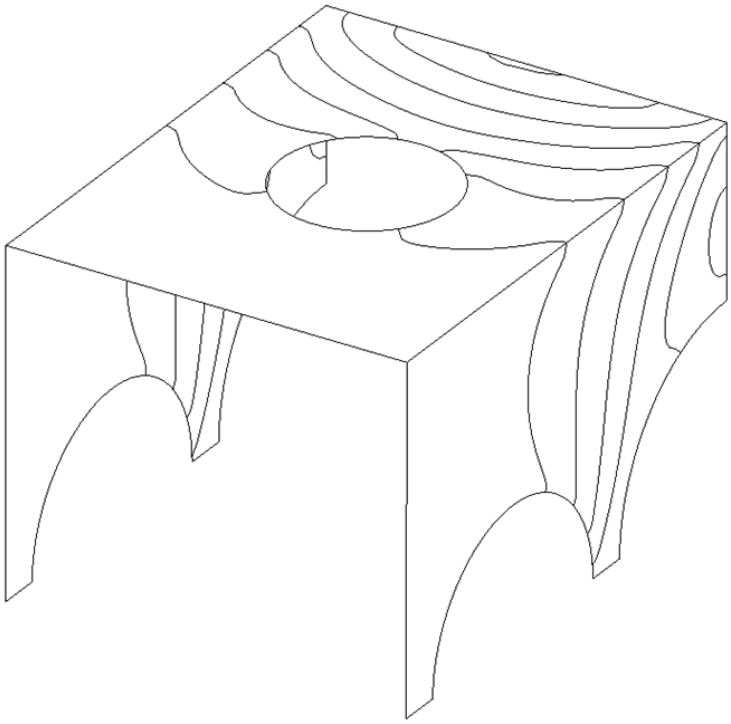

Figure 16 : Résultats du modèle avec l'effet du bord. Les fronts d'écoulement tracés à tous les 5 seconds.

6.3.2. Formation de macro-vides

En vue de montrer la formation de macro-vides durant le remplissage du moule, le trou au centre de la plaque supérieure est enlevé et l'effet du bord n'est pas tenu en compte, c'est-à-dire que la perméabilité de la bande étroite aux bords est désormais identique à celle de l'intérieur. Et les autres dimensions géométriques et les points d'injection et de fuite sont maintenus. Le modèle éléments finis est composé de 3812 nœuds et de 7328 éléments triangulaires à 3 nœuds. La figure 17 montre la position du front d'écoulement à tous les 5 minutes. Nous constatons que deux macro-vides sont formés aux coins des pieds, comme marqué par la couleur foncée. Ce résultat montre bien que notre méthode peut représenter la formation de macro-vides.

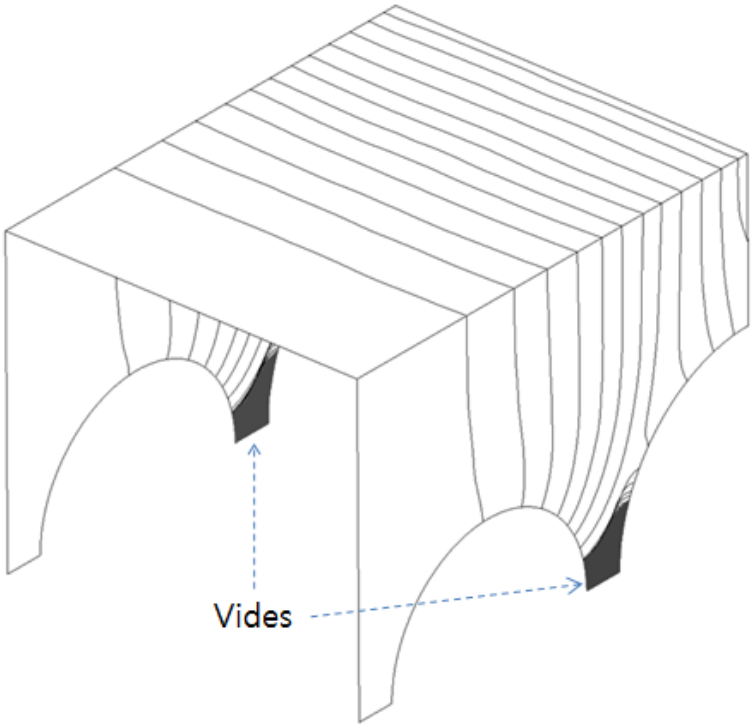

Figure 17 : Position du front d'écoulement de la résine à tous les 5 seconds et formation de macro-vides comme marqué en noir aux coins des pieds.

Ces macro-vides peuvent être évités en ajoutant des points de fuite. La figure 18 montre le front d'écoulement à tous les 5 seconds sans macro-vide, après avoir ajouté deux points de fuite, comme marqué par le trait continu. Cet exemple illustre bien l'importance de la simulation numérique lors de la conception de procédé de fabrication.

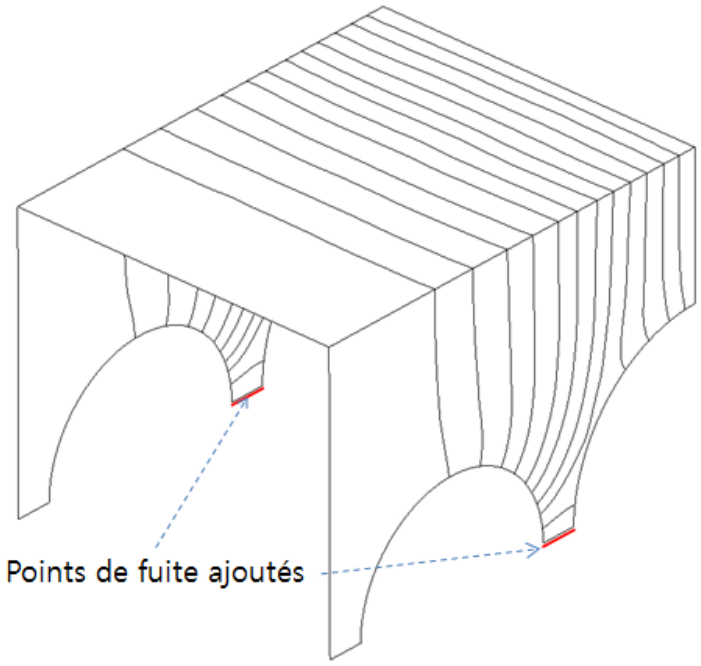

Figure 18 : Position du front d'écoulement de la résine à tous les 5 seconds après avoir ajouté deux points de fuite.

Conclusions

Dans ce travail, le procédé RTM a été simulé à l'aide de la méthode XFEM couplée avec la méthode Level set, en vue de tracer plus précisément le front d'écoulement de la résine durant le remplissage du moule. L'avantage le plus important de cette démarche est de décrire le gradient de la pression malgré la présence de sa discontinuité au front d'écoulement. Les fonctions de forme enrichies sont définies par la fonction Level set et elles reflètent la répartition de la pression suivant la position du front d'écoulement. En outre, la taille du système d'équilibre est légèrement augmentée car l'enrichissement est seulement appliqué près du front d'écoulement. La position du front d'écoulement-est déterminée par la résolution de l'équation de transport décrite avec la fonction Level set. Les équations de transport du front découlement et la réinitialisation des valeurs Level set sont résolues à l'aide d'une méthode de Galerkin implicite. Ces méthodes sont validées à travers quelques exemples en comparaison avec des

résultats analytiques ou expérimentaux trouvés dans la littérature. Les différences entre nos résultats numériques et les solutions analytiques sont très petites.

En outre, la localisation avec la méthode XFEM et la méthode Level set est faite pour augmenter l'efficacité de calcul. La localisation avec la méthode XFEM est totalement originale comme application à la simulation du procédé RTM, ce qui permet de réduire le temps de calcul d'une manière significative.

La séparation et la fusion du front d'écoulement de la résine sont bien simulées sur l'exemple d'une plaque avec des formes de bords complexes. L'analyse sur une plaque mince avec une géométrie complexe montre que la présente méthode peut décrire l'effet du bord et la formation des vides macros.

Dans cette étude, nous avons prouvé que la méthode XFEM est bénéfique pour simuler l'écoulement de la résine du procédé RTM. Les méthodes proposées dans ce travail permettent une simulation plus précise et efficace. Dans la future, une optimisation sur le procédé RTM peut être envisageable à l'aide de ces méthodes très efficaces et précises pour des problèmes de géométrie complexe. Ces méthodes sont limitées au remplissage du moule avant la cuisson. Il reste encore de tenir compte du transfert de la chaleur dans le moule et de la réaction thermique durant la cuisson comme perspectives.

Références

[1] Kang MK, Jung JJ, Lee WI. Analysis of resin transfer moulding process with controlled multiple gates resin injection. Compos Part A. 2000;31(5):407-422.

[2] Bruschke MV, Advani SG. A Finite-Element Control Volume Approach to Mold Filling in Anisotropic Porous-Media. Polym Composite. 1990;11(6):398-405.

[3] Shojaei A, Ghaffarian SR. Modeling and simulation approaches in the resin transfer molding process: A review. Polym Composite. 2003;24(4):525-544.

[4] Young WB, Rupel K, Han K, Lee LJ, Liou MJ. Analysis of Resin Injection-Molding in Molds with Preplaced Fiber Mats .2. Numerical-Simulation and Experiments of Mold Filling. Polym Composite. 1991;12(1):30-38.

[5] Trochu F, Gauvin R, Gao DM. Numerical-Analysis of the Resin Transfer Molding Process by the Finite-Element Method. Adv Polym Tech. 1993;12(4):329-342.

[6] Trochu F, Ruiz E, Achim V, Soukane S. Advanced numerical simulation of liquid composite molding for process analysis and optimization. Compos Part A. 2006;37(6):890-902.

[7] Shojaei A, Ghaffarian SR, Karimian SMH. Numerical simulation of three-dimensional mold filling process in resin transfer molding using quasi-steady state and partial saturation formulations. Compos Sci Technol. 2002;62(6):861-879.

[8] Liu XL. Isothermal flow simulation of liquid composite molding. Compos Part A. 2000;31(12):1295-1302.

[9] Kang MK, Lee WI. A flow-front refinement technique for the numerical simulation of the resin-transfer molding process. Compos Sci Technol. 1999;59(11):1663-1674.

[10] Dong CS. A modified rule of mixture for the vacuum-assisted resin transfer moulding process simulation. Compos Sci Technol. 2008;68(9):2125-2133.

[11] Phelan FR. Simulation of the injection process in resin transfer molding. Polym Composite. 1997;18(4):460-476.

[12] Jiang SF, Yang L, Alsoliby SL, Zhou GF. PCG solver and its computational complexity for implicit control-volume finite-element method of RTM mold filling simulation. Compos Sci Technol. 2007;67(15-16):3316-3322.

[13] Chessa J, Smolinski P, Belytschko T. The extended finite element method (XFEM) for solidification problems. Int J Numer Meth Eng. 2002;53(8):1959-1977.

[14] Chessa J, Belytschko T. An extended finite element method for two-phase fluids. J Appl Mech-T ASME. 2003;70(1):10-17.

[15] Chessa J, Belytschko T. An enriched finite element method and level sets for axisymmetric two-phase flow with surface tension. Int J Numer Meth Eng. 2003;58(13):2041-2064.

[16] Belytschko T, Gracie R, Ventura G. A review of extended/generalized finite element methods for material modeling. Model Simul Mater Sc. 2009;17(4).

[17] Ji H, Chopp D, Dolbow JE. A hybrid extended finite element/level set method for modeling phase transformations. Int J Numer Meth Eng. 2002;54(8):1209-1233.

[18] Ji H, Dolbow JE. On strategies for enforcing interfacial constraints and evaluating jump conditions with the extended finite element method. Int J Numer Meth Eng. 2004;61(14):2508-2535.

[19] Zhuang Z, Cheng BB. Development of X-FEM methodology and study on mixed-mode crack propagation. Acta Mech Sinica-Prc. 2011;27(3):406-415.

[20] Hirt CW, Nichols BD. Volume of Fluid (Vof) Method for the Dynamics of Free Boundaries. J Comput Phys. 1981;39(1):201-225.

[21] Kim MS, Lee WI. A new VOF-based numerical scheme for the simulation of fluid flow with free surface. Part I: New free surface-tracking algorithm and its verification. Int J Numer Meth Fl. 2003;42(7):765-790.

[22] Lin CL, Lee H, Lee T, Weber LJ. A level set characteristic Galerkin finite element method for free surface flows. Int J Numer Meth Fl. 2005;49(5):521-547.

[23] Peng DP, Merriman B, Osher S, Zhao HK, Kang MJ. A PDE-based fast local level set method. J Comput Phys. 1999;155(2):410-438.

[24] Soukane S, Trochu F. Application of the level set method to the simulation of resin transfer molding. Compos Sci Technol. 2006;66(7-8):1067-1080.

[25] Gantois R, Cantarel A, Dusserre G, Felices JN, Schmidt F. Numerical Simulation of Resin Transfer Molding using BEM and Level Set Method. Int J Mater Form. 2010;3(1):635-638.

[26] Sethian JA. Level set methods and fast marching methods, 2nd edition. Cambridge University Press; 1999.

[27] Advani SG, Sozer EM. Process modeling in composites manufacturing. Marcel Dekker, Inc.; 2003.

[28] Zienkiewicz OC, Taylor RL. The finite element method volume 3: fluid dynamics, 5th edition. Butterworth Heinemann; 2000.

[29] Ventura G. On the elimination of quadrature subcells for discontinuous functions in the eXtended Finite-Element Method. Int J Numer Meth Eng. 2006;66(5):761-795.

[30] Mousavi SE, Sukumar N. Generalized Gaussian quadrature rules for discontinuities and crack singularities in the extended finite element method. Comput Method Appl M. 2010;199(49-52):3237-3249.

[31] Kim JH, Lee CS, Kim SJ. High-performance domainwise parallel direct solver for large-scale structural analysis. AIAA J. 2005;43(3):662-670.

[32] Cai Z. Simplified Mold Filling Simulation in Resin Transfer Molding. J Compos Mater. 1992;26(17):2606-2630.

[33] Lin M, Hahn HT, Huh H. A finite element simulation of resin transfer molding based on partial nodal saturation and implicit time integration. Compos Part A. 1998;29(5-6):541-550.

[34] Shojaei A, Ghaffarian SR, Karimian SMH. Numerical simulation of three-dimensional mold filling process in resin transfer molding using quasi-steady state and partial saturation formulations. Compos Sci Technol. 2002;62(6):861-879.

[35] Jung Y, Han WS, Vautrin A, Kim SJ, RTM process simulation by using XFEM and Levelset method. 18th Int C on Compos Mat. Aug 21-26 2011, ICC Jeju, Seogipo Special Self-Governing Province, Korea.

[36] Jung Y, Kim SJ, Han WS, Numerical simulation of RTM process using the extended finite element method combined with the level set method. J of Reinforced Plastics and Compos. 2013;32(5):308-317.

[37] Jung Y, Kim SJ, Han WS, Improvement of computational efficiency by localization of XFEM and level set method for mold filling problem in RTM process, Int J Numer Meth Eng., Submitted.

확장 유한요소법을 적용한 Resin Transfer Molding 기법의 효율적 수치해석

한글 요약문

제 1 장. 소개

Resin Transfer Molding (RTM) 공정은 자동차, 선박, 항공 등의 산업분야에서 많이 이용되는 복학재 구조물 제작을 위한 대표적인 공정 중 하나이다. 공기 구멍의 생성 등과 같이 생산 과정에서 발생 할 수 있는 구조적 결함을 예방하고 효율적 제작 공정의 설계 위해서, 금형 안의 수지 유동을 시뮬레이션 하는 것은 중요하다. 수지 유동을 시뮬레이션 하는 것에서 가장 중요한 점은 금형을 충진하는 동안 수지 유동의 전면부를 수치적으로 정밀하게 근사하는 것이다. 그리고 합당한 계산 시간 내에 복잡한 문제를 다루기 위해서 계산의 병렬화 하는 것도 필요하다.

금형 안 수지의 유동은 수지가 미리 자리 잡은 섬유 예비성형체 통과하는 유동 문제임으로 대표적인 이동 경계 문제이다. 이동 경계 문제를 풀기 위한 수치기법은 크게 이동 그리고 고정 격자 기법으로 분류 된다. 그런데 이동 격자 기법은 상대적으로 계산이 어렵고 계산량이 많기 때문에 고정 격자 기법이 더 많이 이용된다 [1-8].

RTM 공정 시뮬레이션에 많이 이용하는 대표적은 수치기법은 검사체적 유한요소법과 비순응 유한요소법이다. 검사체적 유한요소법은 2000 년대 초반까지 가장 자주 이용되는 기법 이였다 [1-12]. 왜냐하면 일반

유한요소법과 달리 검사체적 유한요소법은 두개의 요소가 접합하는 부분에서 수지의 질량 보존을 효과적으로 만족 시킬 수 있기 때문이다 [2]. 그러나 전체 요소 위에 검사 체적을 다시 정의 하는 것이 때로는 계산을 복잡하게 만든다 [3, 5]. Trochu 등은 비순응 유한요소법을 RTM 공정 시뮬레이션에 이용했다 [5]. 이 기법을 이용하면 요소의 경계면 중앙에서 압력을 계산하기 때문에 어떤 추가적 처리없이 요소 경계면에서의 유동비를 구할 수 있다. 그러나 이 기법은 충진 지수가 요소의 값으로 계산된다. 그리고 위의 두 기법은 유동 전면부가 요소를 통과하는 경우 발생하는 압력 구배의 비연속성에 대해서 고려하지 않고 있다. 그러므로 이 두 기법은 복잡한 모양의 문제를 계산할 때 수지 유동의 전면부를 사실적으로 근사하는 것에 한계가 있다.

확장유한요소법은 균열과 같은 다양한 불연속적 문제에 적용된다 [13-19]. Chessa 와 Belyschko 는 이상 비혼합 유동 문제에서 경계면의 비연속적 압력구배 계산하기 위해 확장유한요소법을 이용했다 [14]. 본 연구에서도 유동 전면부에서 압력 계산의 정확도를 높이기 위해 확장유한요소법을 이용한다.

고정 격자 기법에서 경계면을 트랙하는 방법의 대표는 Volume of Fluid (VOF)기법이다 [20,21]. VOF 기법은 RTM 공정 시뮬레이션에 많이 적용되었다 [1-9]. 그러나 이 기법은 요소내의 경계면의 위치를 정확히

파악하는 것에 한계가 있다 [22-25]. Level set 법은 대표적인 이동경계면 캡쳐 기법이다 [26]. 다수의 주입구로 복잡한 형상의 구조물의 제작에서는 유동 전면부의 모양이 아주 복잡한데 Level set 법은 이러한 복잡한 전면부를 매우 효율적으로 예측할 수 있기 때문에 최근 RTM 공정 시뮬레이션에 많이 사용된다 [24,25]. 본 연구에서는 Level set 법이 수지 전면부 위치를 계산할 때 적용된다.

본 논문에서 확장형상함수가 Level set 값을 이용하여 정의된다 [14]. 그리고 확장유한요소법으로 구성되는 평형계는 대칭 정치행렬이기 때문에 효율적 계산을 위해서 다중 프론탈 기법이 이용된다. Level set 법을 이용한 계산은 유동전면부를 이송하는 부분과 레벨셋 합수를 재초기화하는 부분으로 나누어 진다. 두 계산 모두 내연적 특성 Galerkin 유한요소법을 적용하여 수치해의 진동을 안정시킨다 [22]. 확장유한요소법에 의한 확장은 단지 유동 전면부만 적용되므로 평형계의 크기는 아주 적게 증가한다. 이산화된 평형계는 IPSAP [31]의 병렬 다중 프론트 기법을 적용해 계산한다. 마지막으로 본 연구에서는 계산 효율 증가를 위한 확장유한요소법과 레벨셋 기법의 국소화 기법에 대해 설명하고 그 효율성을 입증한다.

본 연구는 이차원과 삼차원 예제를 계산한 결과를 이론치 혹은 실험치 비교하여 검증된다 [32-35]. 이와 더불어 삼차원 평판 예제를 이용하여

Race-tracking 효과와 기공 형성을 시뮬레이션 한다 [36]. 그리고 제안한 알고리즘은 시뮬레이션의 전/후처리를 위한 그래픽 사용자 인터페이스 툴로서 실현된다.

제 2 장. 수학적 모델

금형 내의 수지 유동은 몇 가지 가정과 함께 단순화된다. 먼저, 유동은 비압축성이고 등온상태라고 가정한다. 그러므로 질량보존식은 다음과 같이 주어진다:

$$\nabla \cdot \mathbf{u} = 0 \tag{1}$$

여기서 **u** 는 유체의 속도이다. 그리고, 다공성 매질의 통과하는 유체의 운동량평형식은:

$$\rho \, \mathrm{D}\mathbf{u}/\mathrm{D}t = -\nabla p - (\mu/\mathbf{K})\mathbf{u} \tag{2}$$

이고, **ρ** 는 밀도, t 는 시간, p 는 유체압력, **K** 는 투과성**,** μ 는 유체 점성이다.

수지 점성은 등온상태라는 가정 때문에 충진 과정 동안 일정하다. 섬유 예비성형물은 균일한 비변형상태로 가정하기 때문에 충진 하는 동안 그 투과성은 일정하다. 수지 유동이 충분히 느리다면 관성의 영향은 미미하므로, 이때 수지의 유동은 정상상태가 연속되는 것으로 고려할 수 있다. 그러므로, 전체적인 계산 흐름은 정상상태에서 압력장을 매

시간 간격마다 계산한 후, 다음 시간으로 유동 전면부를 이송시킨다 [27]. 정상상태에서 Darcy 의 식은 다음과 같이 유도된다:

$$\mathbf{u} = -(\mathbf{K}/\mu)\nabla p \tag{3}$$

식 (3)을 식 (1)에 대입하면, 압력장을 구하기 위한 지배방적식이 유도된다:

$$\nabla \cdot (-(\mathbf{K}/\mu)\nabla p) = 0 \tag{4}$$

경계조건은 다음과 같이 주어진다:

$$\begin{aligned} p_{in} &= \text{주입압력} \quad && \text{주입구에서} \\ p_{vent} &= \text{배출 압력} && \text{배출구에서} \\ \partial p/\partial n &= 0 && \text{금형 벽에서} \end{aligned} \tag{5}$$

매 시간간격마다 유동 전면부의 이송은 Level set 기법을 이용하여 계산한다. 자세한 사항은 다음 장에서 설명된다.

제 3 장. 수치기법

제 1 절. Level set 기법

그림 1 에 나타나듯이 Level set 값은 유동 전면으로부터의 부호 거리 값이다. 그래서 Level set 값이 전면에서는 0 이고, 빈 공간에서는 음수, 수지가 찬 부분에서는 양수이다.

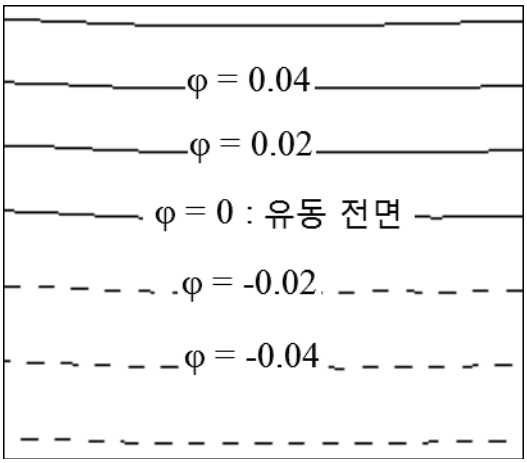

그림 1. 각 구역에서의 Level set 값

수지 전면부의 이송은 아래 식에 의해 지배된다:

$$\partial\varphi/\partial t + \mathbf{u}\cdot\nabla\varphi = 0 \tag{6}$$

식 (6)으로는 단지 전면의 이송만 가능하므로 전면 이외 지역의 Level set 값은 재초기화 과정을 통해 다음의 조건을 만족하도록 계산해 주어야 한다:

$$\|\nabla\varphi\| = 1 \tag{7}$$

Level set 의 재초기화를 위해 Peng 등이 제안한 다음과 같은 식을 이용한다 [23]:

$$\begin{aligned}&\partial\varphi/\partial t + sign(d_0)(\|\nabla d\| - 1) = 0,\\ &d(\boldsymbol{x},0) = d_0(\boldsymbol{x}) = \varphi(\boldsymbol{x},t)\end{aligned} \tag{8}$$

여기서, d 는전면으로부터의 부호 거리 값이고, τ는 재초기화 과정에서의 가상 시간이다. 그리고, $sign(d_0)$은 초기값 d_0 의 부호이다. 이 $sign(d)$ 함수는 다음과 같이 정의된다:

$$sign(d) = d/\sqrt{d^2 + h^2} \tag{9}$$

여기서 h 는 요소 크기이다. 재초기화 과정은 매 시간간격마다 실행된다.

제 2 절. 확장 유한 요소 법

확장유한요소법은 유동 전면이 위치한 지역의 압력장을 정밀하게 구하기 위해 사용된다.

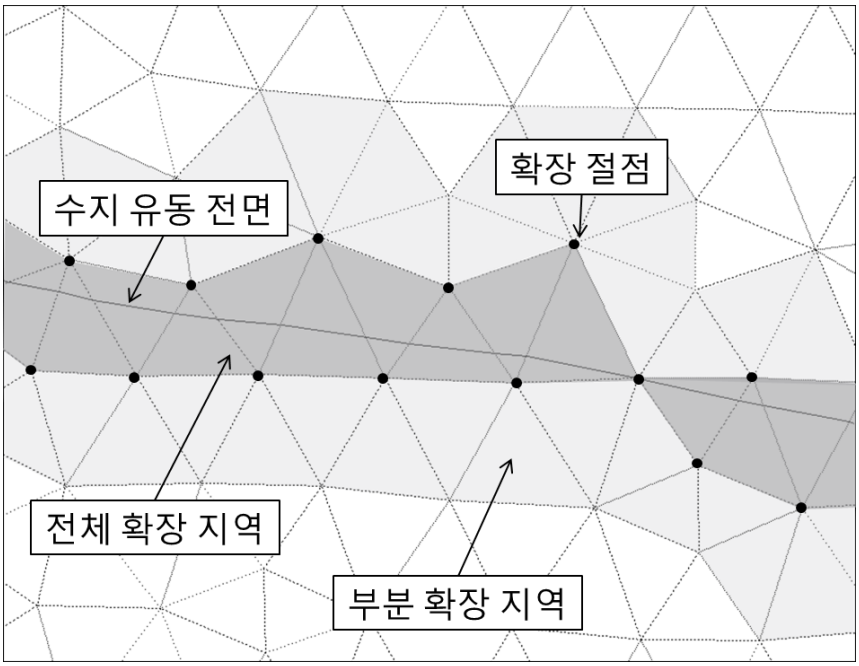

그림 2. 확장 절점과 지역 분류의 정의.

계산 영역은 일반과 확장 지역으로 나누어 진다. 확장 지역은 그림 2 에서 볼 수 있듯이 전면부가 지나가는 요소를 구성하는 절점이 포함되어 있는 곳이다. 확장이란 추가적으로 DOF 를 더하는 것을 의미하므로 압력의 근사는 아래의 식과 같이 정의된다:

$$p^h = \sum_{I \in n} N_I p_I + \sum_{J \in n_e} N_J^e a_J \tag{10}$$

여기서, p^h 는 압력 함수, p_I 절점 I 에서 압력, a_J 는 확장 절점 J 에서 추가 절점 변수, N_I 는 일반형상함수, N_J^e 는 확장형상함수, n 은 절점의 개수, n_e 확장 절점의 개수 이다. 그 확장형상함수는 다음과 같이 정의된다:

$$N_J^e = N_J\left(|\varphi| - |\varphi_J|\right) \tag{11}$$

여기서, φ_J 는 확장절점 J 의 Level set 값이다. 확장 형상 함수에 대해 쉽게 설명하기 위해 그림 3 에서는 1 차원 선형요소의 확장 형상 함수의 생성 과정을 그래프로 보여준다. 확장형상함수의 중요한 특징은 요소 내의 전면부의 위치가 반영이 되어 있다는 것이다. 그리고 절점에서 확정형상 함수의 값이 0 인 것이 특징이다.

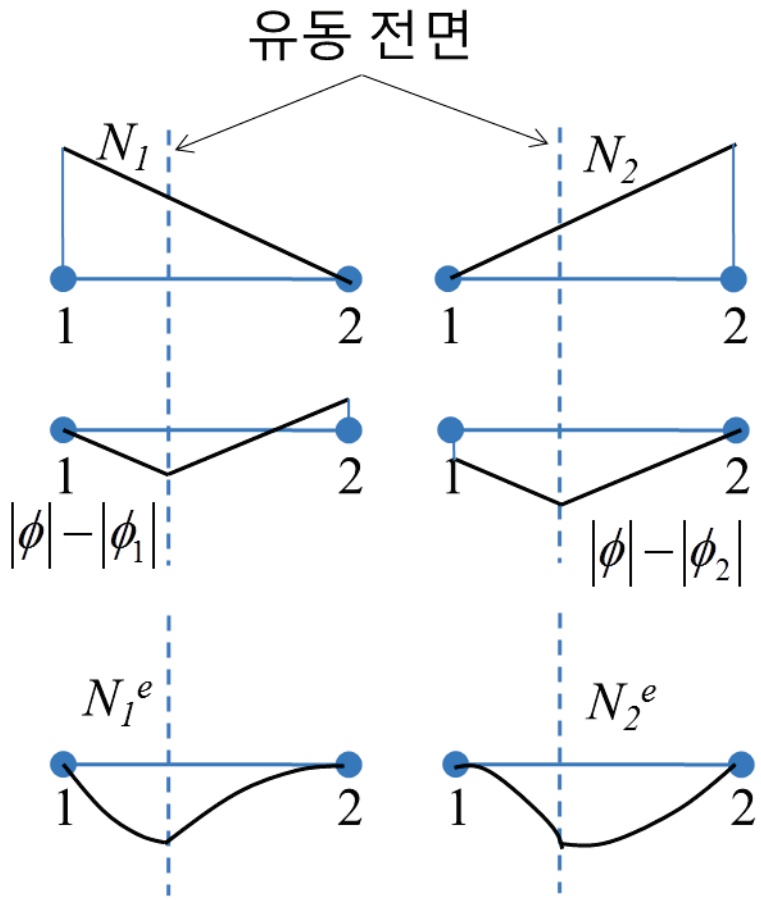

그림 3. 1 차원 선형 요소의 확장 형상 함수.

한편, 확장 유한 요소 법에 의해 근사 된 유동 전면에서 압력 구배는 다음과 같이 계산 될 수 있다:

$$\nabla p^h = \sum_{I \in n} p_I \nabla N_I + \sum_{J \in n_e} a_J \left[\nabla N_J \left(|\varphi| - |\varphi_J| \right) + N_J sign(\varphi) \nabla \varphi \right] \tag{12}$$

그 근사 된 압력 함수에서 점프 조건은 아래와 같다:

$$[\![\nabla p^h]\!] = 2 \sum_{J \in n_e} N_J a_J \nabla \varphi \quad \text{on the resin front} \tag{13}$$

그림 2 에서 볼 수 있듯이, 확장 지역은 두 가지 유형으로 분류된다 (전체 혹은 부분 확장 지역). 여기서 전체 확장 지역은 확장 절점으로만 구성되어 있고 부분 확장 지역은 일반 그리고 확장 절점으로 이루어진다. 부분 확장 지역은 확장과 일반 지역 사이의 압력 장을 연속적으로 유지하기 위해 필요하다.

제 4 장. 수식화

제 1 절. 유동 전면부의 이송

식 (6)은 외연적 특성 Galerkin 유한 요소 법을 적용하여 계산한다 [22]. 시간에 대한 미분항은 외연적 특성 기법에 의해 이산화 된다 [28]:

$$\varphi^{n+1} - \varphi^n = -\Delta t[\mathbf{u} \cdot \nabla\varphi]_n + \Delta t^2/2\left[\nabla \cdot \left((\mathbf{u}\otimes\mathbf{u}) \cdot \nabla\varphi\right)\right]_{n+1} \tag{14}$$

여기서 Δt 는 시간간격이다. 공간에 대한 미분항의 이산화에는 Galerkin 유한 요소 법을 적용한다:

$$\begin{aligned}\int_\Omega (\varphi^{n+1} - \varphi^n) w dV = -\Delta t \int_\Omega (\mathbf{u} \cdot \nabla\varphi^n) w dV \\ - \Delta t^2/2 \int_\Omega \left((\mathbf{u}\otimes\mathbf{u}) \cdot \nabla\varphi^{n+1}\right) \cdot \nabla w dV\end{aligned} \tag{15}$$

여기서 w 는 가중함수이고 Ω 는 전체 계산 영역이다. 전면 이송 속도 $\mathbf{u}$ 은 식 (3)을 이용하여 계산한다. 그리고 점성은 다음과 같이 정의한다:

$$\mu = H(\varphi)\mu_r + (1 - H(\varphi))\mu_a \tag{16}$$

여기서, μ_γ는 수지 점성, μ_α는 공기 점성, φ 는 Level set 값이다. $H(\varphi)$는 아래와 같이 정의된다:

$$H(\varphi) = \begin{cases} 1 & if\ \ \varphi < -h \\ \frac{1}{2}(1 - \varphi/h) & if\ \ |\varphi| \le h \\ 0 & if\ \ \varphi > h \end{cases} \tag{17}$$

재초기화를 위한 식 또한 식 (14)와 (15)의 과정을 따라 이산화 된다:

$$\int_\Omega (d^{n+1} - d^n) w dV = -\Delta\tau \int_\Omega sign(d_0)|\nabla d^n| w dV - \Delta\tau^2/2 \int_\Omega \nabla d^{n+1} \cdot \nabla w dV + \Delta\tau \int_\Omega sign(d_0)\mathrm{wdV} \tag{18}$$

제 2 절. 압력장

유한 요소 법에 따라 식 (4)의 약형은 다음과 같다:

$$\int_\Omega \left(\nabla \cdot (-\mathbf{K}/\mu\, \nabla p)\right) w dV = 0 \tag{19}$$

Green-Gauss 이론을 적용하면 식 (19)는 아래와 같이 된다:

$$\int_\Omega \nabla w \cdot (-\mathbf{K}/\mu\, \nabla p) dV - \int_{\partial\Omega} w(-\mathbf{K}/\mu\, \nabla p) \cdot \mathbf{n} dS = 0 \tag{20}$$

여기서 **n** 은 법선 벡터이다. 확장 유한 요소 법을 적용하여 압력과 가중 함수는 식 (12)와 같이 이산화된다. 한편, 확장 지역에서 점성은 아래와 같이 정의 된다:

$$\mu = \mu_r/2\,(1 - sign(\varphi)) + \mu_a/2\,(1 + sign(\varphi)) \qquad (21)$$

제 3 절. 계산 과정

그림 4 는 전체 계산 과정을 보여준다. 첫째 단계에서는 요소정보, 물성, 경계조건 등의 입력 데이터를 읽어 들인다. 그리고 압력과 Level set 값을 초기화한다. 둘째 단계에서는 식(3)을 이용해 속도를 계산한 후 식(6)을 계산해 유동 전면부를 이송하고 식 (8)을 이용한 재초기화를 진행한다. 셋째 단계에서는 절점의 Level set 값을 읽어서 일반과 확장 절점을 분류한다. Level set 값을 이용한 절점의 분류는 확장 지역을 구성하는 요소의 절점에서 Level set 값이 서로 다른 부호를 가지므로 가능하다. 둘째와 셋째 단계는 금형 충진이 완료될 때까지 반복된다. IPSAP 의 다중 프론트 솔버[31]가 평형 계를 계산하는데 이용된다.

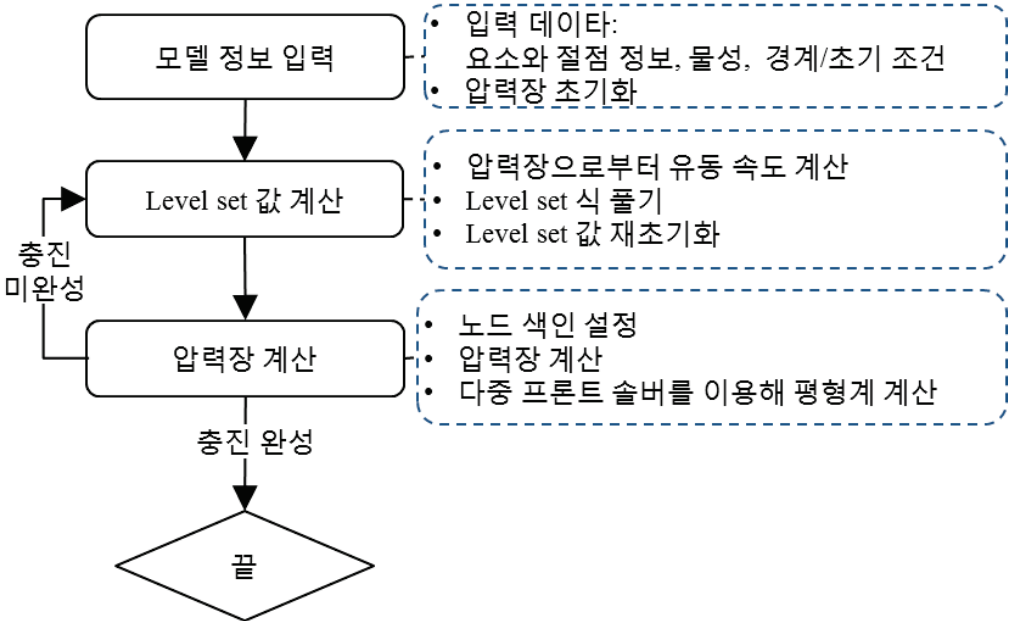

그림 4. 전체 계산 순서도

제 5 장. 기역화 기법에 의한 효율성 향상

본 연구는 확장유한요소법과 레벨셋 기법의 지역화를 통해 계산효율을 증가시킨다 [37]. 여기서 국소화는 유동 전면부 근처의 작은 지역을 계산 영역으로 할당하는 것을 의미한다. 금형 내의 수지 유동을 시뮬레이션 하는 것은 엄밀히 수지 유동 전면부의 움직임을 묘사하는 것이다. 그러므로 유동 전면부 이외 지역의 레벨셋 값은 불필요하다. 만약, 결과에 대한 영향 없이 필요한 레벨셋 값 만을 구하도록 영역이 축소시킬 수 있다면, 계산 효율은 증가할 것이다. 일반적으로 편미분방정식을 풀 때, 선형시스템을 계산하는 부분에서 가장 많은 시간이 소요된다. 그러므로 시스템 크기가 적어지면 계산시간은 확연히 줄어든다. 이번 장에서는 확장유한요소법과 레벨셋 기법의 국소화의 알고리즘을 설명하고 국소화에 의한 효율성을 몇 가지 예제를 통해 보여준다.

제 1 절. 확장유한요소법과 레벨셋 기법의 국소화

레벨셋 기법의 국소화 알고리즘은 Peng[23]등이 제안한 방법을 기초로 하고 있다. 본 연구에서는 그들의 알고리즘을 외연적 특성 Galerkin 유한요소법에 적용하기 위해 수정한다.

그림 5 는 유동 전면부 근처의 영역이 레벨셋 기법의 국소화를 위해 할당되는 것을 보여준다. 그림 5 에서 회색으로 표시된 밴드가 할당된 지역이다. 그 밴드는 유동 전면부가 움직이는 동안 매 시간 간격마다 새롭게 정의된다. 유동 전면부에서 밴드 경계까지의 거리는 요소 크기보다 6 배 길다[23]. 절점의 레벨셋 값은 매 시간 간격마다 밴드 안에서만 갱신된다.

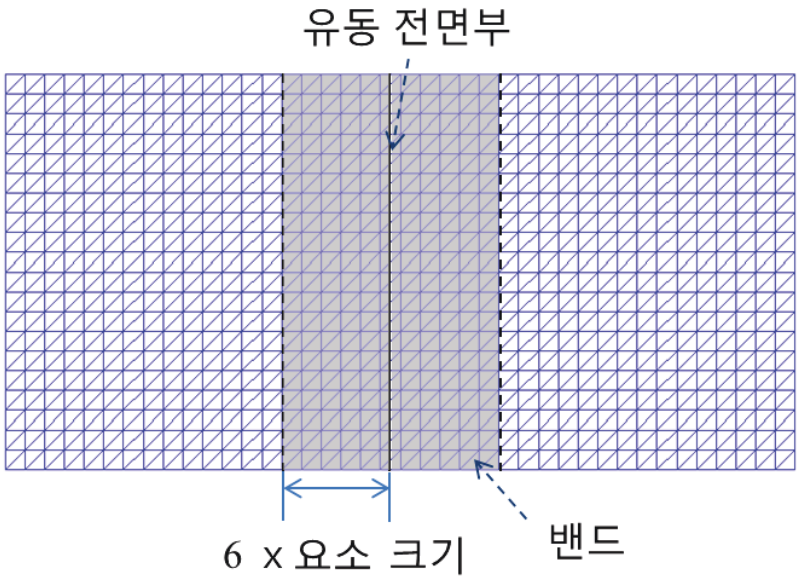

그림 5. 레벨셋의 국소화를 위해 수지 유동 전면부 근처의 계산 영역

레벨셋 기법의 국소화에는 밴드 경계에서의 수치해의 진동을 예방하기 위한 단절함수를 이용한다. 그 단절 함수는 이와 같이 정의된다.

$$c(\varphi) = \begin{cases} 1 & if\ |\varphi| \le \beta \\ (|\varphi| - \gamma)^2(2|\varphi| + \gamma - 3\beta)/(\gamma - \beta)^3 & if\ \beta < |\varphi| \le \gamma \\ 0 & if\ |\varphi| > \gamma \end{cases} \qquad (22)$$

여기서 φ 는 레벨셋 값을 의미하고 γ 와 β 는 각각 요소 크기의 6 배, 3 배수를 의미한다 [23]. 단절함수를 적용하는 경우, 레벨셋 값을 계산하기 위한 지배 방정식은 아래와 같이 변형된다.

$$\frac{\partial \varphi}{\partial t} + c(\varphi)\mathbf{u} \cdot \nabla \varphi = 0 \tag{23}$$

확장유한요소법의 국소화는 압력 계산에서 계산량을 줄이기 위해 시도된다. 앞에서 언급했듯이 레벨셋 계산에서 필요한 속도를 압력으로부터 구해낸다. 그런데 국소화로 인해 레벨셋 계산 영역이 줄어들었기 때문에 압력 계산이 필요한 영역이 줄어든다. 그래서 필요한 영역의 압력만을 계산하기 위해 확장유한요소법의 국소화를 시도한다.

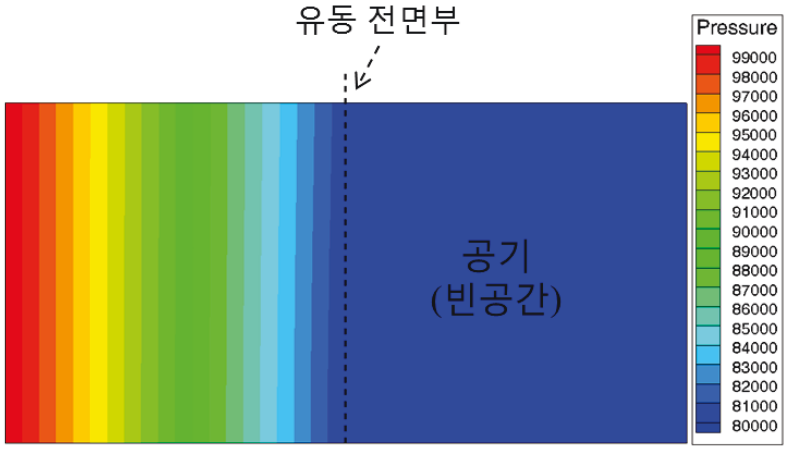

그림 6. 채널 유동 예제의 몰드 내에서 압력

그림 6 에서 볼 수 있듯이 주형 내의 압력은 수지가 찬 부분에서는 변화가 있지만 공기가 찬 부분에서는 거의 변화가 없다. 그래서 국소

영역을 그림 7 과 같이 정해준다. 즉, 수지가 찬 부분은 모두 국소 영역에 포함시키고 공기부분은 레벨셋의 국소 영역과 동일하게 요소의 6 배까지만 국소 영역에 넣어준다.

확장유한요소법의 국소화에서 중요한 것은 경계조건을 정하는 것이다. 레벨셋 계산은 초기치 문제이기 때문에 지역화 기법에서 경계조건을 정할 필요가 없었다. 하지만 압력 계산 모델은 경계조건문제이기 때문에 국소 영역에 경계조건을 설정해 줄 필요가 있다. 그래서 경계조건으로서 국소 영역 중 공기 부분에 위치한 경계 면에 공기의 압력을 넣어준다.

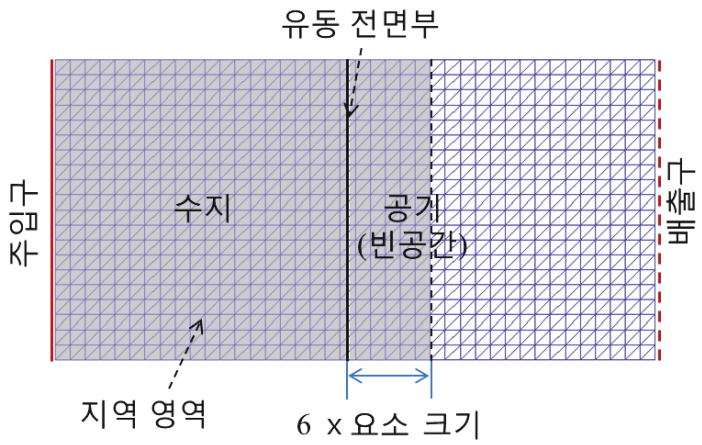

그림 7. 확장유한요소법 국소화 위한 계산 영역

그림 8 에서 압력분포는 확장유한요소법의 국소화 기법을 이용해서 계산된 것이다. 이 압력분포는 국소화 기법을 이용하지 않았을 때 계산 결과 (그림 6)와 매우 흡사하다.

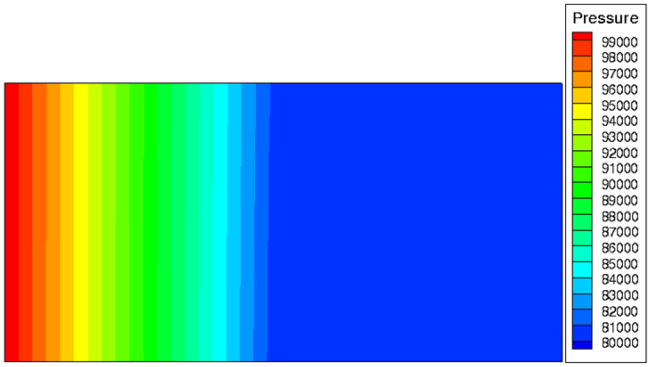

그림 8. 확장유한요소법 국소화를 이용하여 계산한 압력

제 2 절. 국소화의 효율성

국소화의 효율성을 테스트하기 위해 그림 9 의 채널 유동 모델을 이용한다. 국소화 기법으로 얼마나 시간이 단축되는 지를 테스트 하기 위해 국소화 기법을 사용하지 않은 경우, 레벨셋의 국소화만 사용하는 경우, 레벨셋과 확장유한요소법의 국소화를 같이 사용하는 경우의 계산 시간을 측정하였다. 계산에 사용된 컴퓨터의 사양은 인텔(R) 코어(TM) i7 CPU 950 (3.07 GHz, 쿼드코어)이고 사용운영체제는 윈도우 7 프로페셔널 K (64 bit) 이다.

국소화기법을 사용한 경우 계산 시간이 감소하는 양을 백분율로 나타낸 것이다. 레벨셋의 국소화만 적용한 경우에는 절점수가 다른 세가지 모델에서 각각 23%, 27%, 40%의 비율로 계산 시간이 감소하였다. 그리고 확장유한요소법과 레벨셋의 국소화를 같이 적용하였을 때는 각각 36%, 44%, 55%의 비율로 계산 시간이 감소하였다.

표 1. 채널 유동 모델의 계산 시간

절점 개수	계산 시간			감소율
	국소화 미적용	국소화 적용		
861	37.5 초	레벨셋	29.0 초	22.7 %
		확장유한요소법 + 레벨셋	24.1 초	35.7 %
2556	211.4 초	레벨셋	154.0 초	27.2 %
		확장유한요소법 + 레벨셋	118.0 초	44.2 %
7381	1236.8 초	레벨셋	742.5 초	40.0 %
		확장유한요소법 + 레벨셋	561.1 초	54.6 %

표 1 은 채널유동 모델의 계산시간 측정 결과이다. 감소율은

계산 시간의 감소율은 절점의 개수가 증가할수록 커졌다. 그 이유는 절점이 많은 모델일수록 계산량의 감소 비율이 크기 때문이다. 그리고 레벨셋의 부분의 계산양이 압력을 구하는 부분의 계산 양보다 많기 때문에 레벨셋의 국소화가 확장유한요소법의 국소화보다 계산시간의 단축에 더 큰 영향을 주었지만, 확장유한요소법의 국소화가 레벨셋의 국소화와 더불어 계산시간의 단축을 극대화 하였다고 볼 수 있다. 계산 시간 테스트를 통해 국소화 기법의 적용은 계산 효율의 증가에 크게 기여 한다는 것을 확인할 수 있었다.

제 6 장. 검증

본 연구에서는 문헌으로부터 얻은 몇 가지 예제를 계산하고 이론치 혹은 실험치와 그 결과를 비교한다 [32-35]. 먼저, 이차원 채널 혹은 방사상 유동을 계산하고 이론치와 비교한다. 다음으로 Shojaei 등 [34]이 제안한 복잡한 형상 예제를 이용하여 해석하고 그 결과를 실험치와 비교한다. 마지막에는 삼차원 평판 모델을 이용하여 Race-Tracking 효과와 기공형성을 보여준다 [36].

제 1 절. 단순 유동 모델

단순 채널 모델의 결과는 Cai[32]가 제안한 이론치를 이용해 비교한다.

1. 직사각형 평판의 이차원 채널 유동

그림 9 는 직사각형 평판의 이차원 채널 유동을 위한 예제이다. 이 예제의 길이, 넓이, 두께는 각각 1 m, 0.5 m, 1 mm 이다. 수지는 실선으로 표시된 왼쪽 면으로부터 주입되고 점선으로 표시된 오른쪽 면을 통해서 빠져나간다. 선형 삼각 평판 요소가 이용되고 전체 노드와 요소의 개수는 각각 861, 1600 개이다.

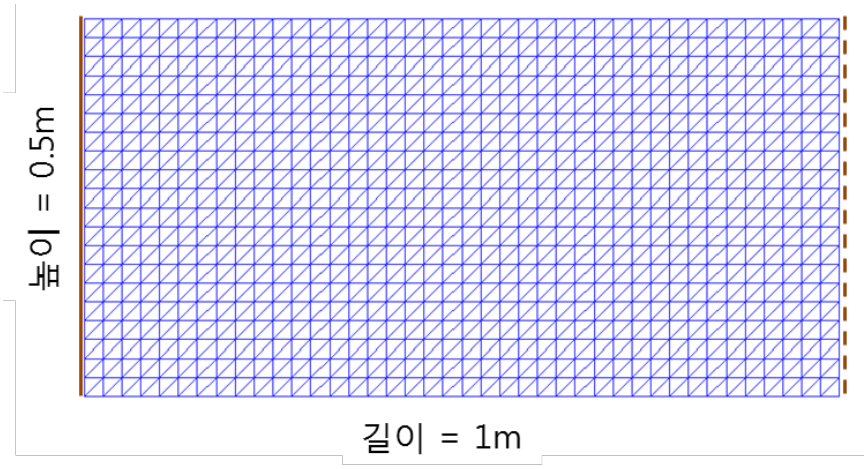

그림 9. 채널 유동을 위한 직사각 평판 의 형상과 그물망

물성과 경계조건은 다음과 같다: 수지 점성 = 0.1 Pa·s, 투과성 = 10^{-9} m^2, porosity = 0.5, 주입 압력 = 20 KPa, 배출구 압력 = 0. 채널 유동을 위한 이론적 충진 시간은 다음 식으로 계산된다:

$$t_{filling} = L^2\mu\Phi/2KP \tag{24}$$

여기서 L 은 길이 방향에서 유동 전면부의 위치이다. 그리고 μ, Φ, K, P 는 각각 점성, 공극률, 투과성, 압력을 의미한다. 이 모델의 이론적 충진 시간은 1250 초이고, 우리의 해석 결과는 1268.42 초이다. 두 결과의 차이는 1.5 %이다. 같은 예제를 계산한 Soukane 과 Trochu [24]의 수치 결과가 이론치와 3%의 차이가 나는 것과 비교할 때, 우리의 계산이 이론치와 더 비슷함을 알 수 있다.

2. 원형 디스크의 이차원 방사상 유동

그림 10 은 얇은 원형 디스크의 이차원 방사상 유동 예제이다. 이 예제의 선대칭 특징 때문에 디스트의 4 분의 1 만 모델링 되었다. 반지름과 두께는 각각 1 m 과 1 mm 이다. 수지는 원의 중심에 위치한 반지름 0.2m 의 구멍을 통해서 주입된다. 그리고 점선으로 표시된 바깥 둘레를 통해서 수지가 배출된다. 물성은 이차원 채널 유동 예제와 동일하다.

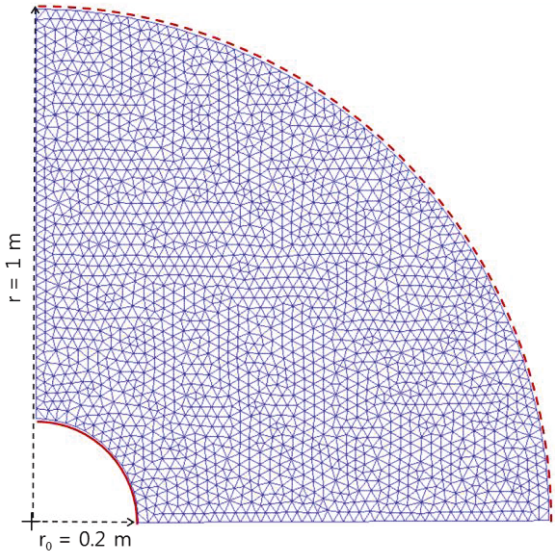

그림 10. 방사형 유동 모델의 형상과 그물망

이 예제의 이론적 주입 시간은 다음 식으로 계산된다:

$$t_{filling} = \mu\phi r_0^2/4KP(r/r_0)^2\,[2\ln r/r_0 + (r_0/r)^2 - 1] \qquad (25)$$

여기서 r 은 평판의 반지름, r_0은 주입구의 반지름이다 [32, 35]. 이론적 주입시간은 1411 초이고 우리의 해석 시간은 1436 초이다. 두 결과 사이의 차이는 1.8%이다. Lin 등 [33]의 수치해석계산에서 이론식과 비교해서 4%의 차이가 있는 것을 볼 때 우리의 프로그램이 더 효율적이다.

제 2 절. 이차원 복잡한 형상 평판

그림 11 의 이차원 복잡한 형상 평판을 이용하여 Shojaei 등[34]이 수행한 실험결과를 우리의 해석 결과와 비교한다. 복잡한 형상의 금형을 충진하는 동안 수지의 유동은 복잡한 모양으로 흘러간다. 각 방향의 길이와 두께는 각각 0.4 m 와 6.5 mm 이다. 주입구의 위치는 가운데 빨간 색 점으로 표시되어 있다. 주입구의 지름은 4 mm 이다. 배출구는 파란색으로 표시된 세 점에 위치해 있다. Shojaei 등[34]은 금형의 모든 모서리에 실리콘을 도포하여 모서리 효과를 예방했다. 그물망은 2204 개의 절점과 4111 개의 3 절점 삼각 요소로 이루어져 있다. 주입되는 SAE 40 모터 오일의 점성은 상온에서 0.3 Pa·s 이다 (25 ℃). 투과성과 공극율은 각각 6.83×10^{-9} m^2 과 0.81 이고 주입 압력은 35 KPa 이다.

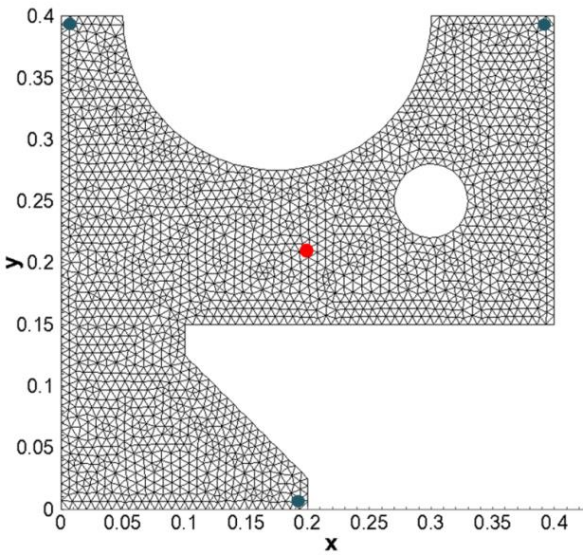

그림 11. 이차원 복잡한 모양 평판의 형상과 그물망

우리 프로그램으로 계산한 주입시간은 123 초이고 Shojaei 등[34]의 실험과 해석 결과는 각각 117 초와 126 초이다. 실험치와의 차이는 우리의 해석치는 4.3 %이고 Shojaei 등 [34]의 해석치는 7.7 %이다. 그러므로 본 연구의 해석 결과가 실험 결과와 더 비슷하다. 그림 12 은 우리의 계산결과이고 충진 동안 수지 전면부의 위치를 15 초 마다 그린 것이다. 그리고 그림 13 는 실험으로 측정된 전면부의 위치를 15 초 마다 그린 것이다.

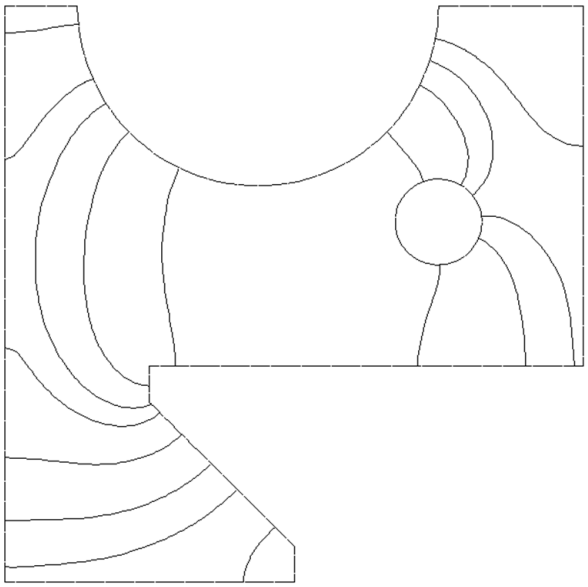

그림 12. 이차원 복잡한 형상 평판 모델의 본 연구의 해석 결과

- 유동 전면의 위치 (매 15 분)

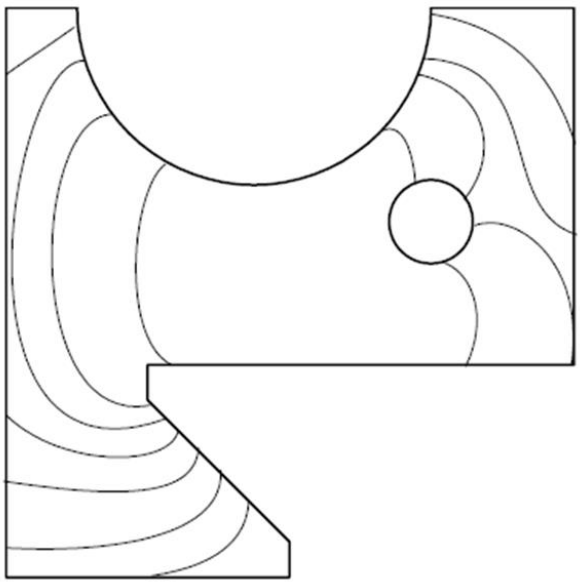

그림 13. 이차원 복잡한 형상 평판 모델의 Shojaei 등 [34]의 실험 결과

- 유동 전면의 위치 (매 15 분)

제 3 절. 삼차원의 얇고 복잡한 형상 평판

이번 절에서는 그림 14 에 묘사된 삼차원의 얇고 복잡한 형상 평판 예제를 이용하여 Race-tracking 효과와 기공 생성을 보여준다 [36]. 그림 10 에서 실선과 점선으로 표시된 부분은 각각 주입구와 배출구의 위치를 나타낸다. 본 예제의 물성과 경계조건은 다음과 같다: 수지 점성 = 0.03 Pa·s, 투과성 = 6.21 x 10^{-11} m^2, 공극률 = 0.4, 주입압력 = 0.3 MPa, 배출구 압력 = 0.

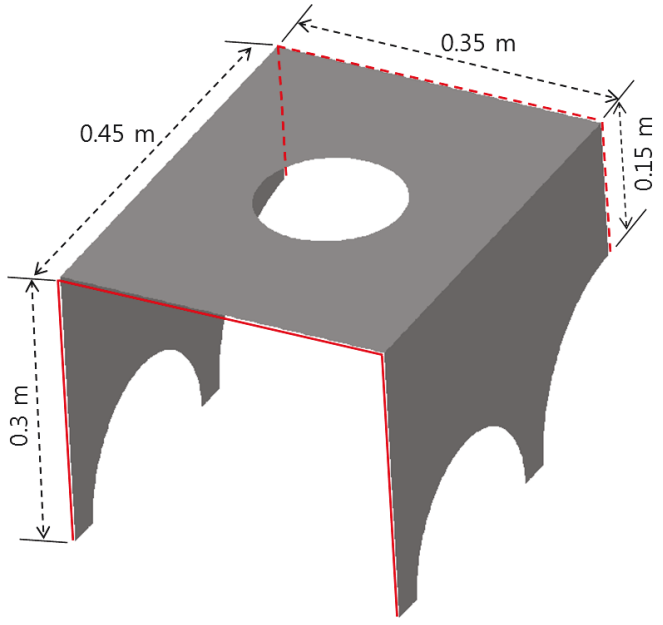

그림. 14. 삼차원의 얇고 복잡한 형상 평판

1. Race-tracking 효과

위의 예제에 Race-tracking 효과를 주기 위해서 그림 15 과 같이 모서리로부터 10mm 까지 지점의 투과성을 6.21 x 10^{-10} m^2 로 놓는다. 본 모델은 3684 개의 절점과 7027 의 삼절점 삼각 요소로 이루어져 있다.

그림 16 는 계산한 유동 전면부의 위치를 매 5 초마다 그린 것이다. 그림 16 에서 볼 수 있듯이 Race-tracking 효과 때문에 모서리 근처에서 전면부의 기울기가 달라진다. 또한 전면부가 갈라지고 합쳐지는 것도 잘 시뮬레이션 되고 있다.

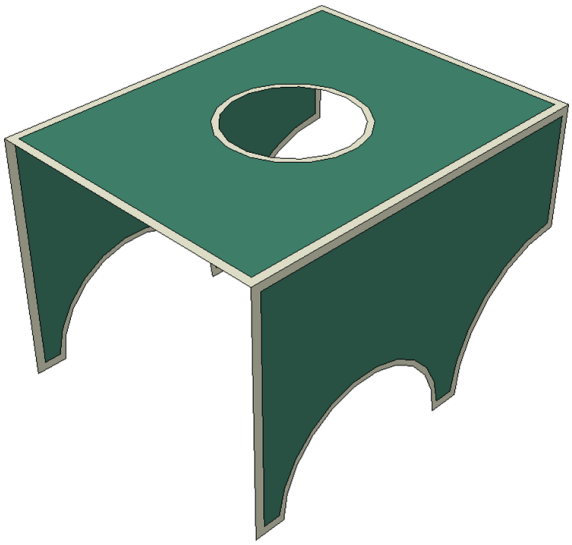

그림 15. Race-tracking 효과를 적용하기 위해 투과성이 다른 두 지역

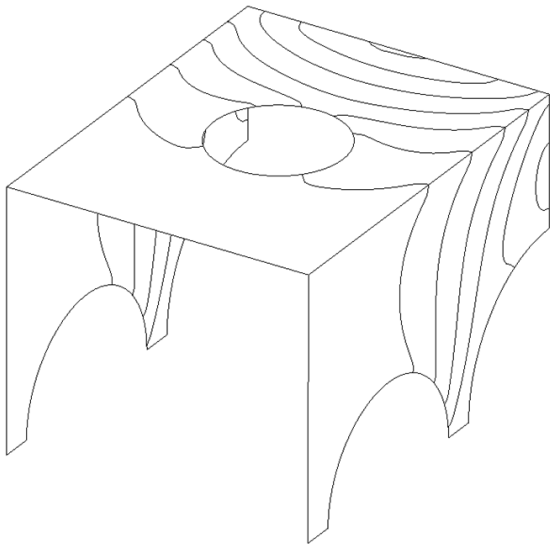

그림 16. Race-tracking 효과를 적용한 예제의 계산 결과
(매 5 초마다 전면부의 위치)

2. 기공 형성

본 계산에서는 기공이 형성되는 것을 보기 위해서 위의 모델에서 가운데에 위치한 큰 구멍을 없애고 전 구간에 동일한 투과성을 대입하였다. 형상 크기와 주입구/배출구의 위치는 위의 예제와 동일하다. 본 예제는 3812 개의 절점과 7328 개의 세절점 삼각 요소로 이루어져 있다. 그림 17 은 해석 후 얻어진 매 5 초마다 유동 전면부의 위치를 그린 것이다. 그림 17 에서 까만 부분은 기공이 형성된 부분이다. 본 프로그램이 기공 형성을 잘 포착함을 알 수 있다.

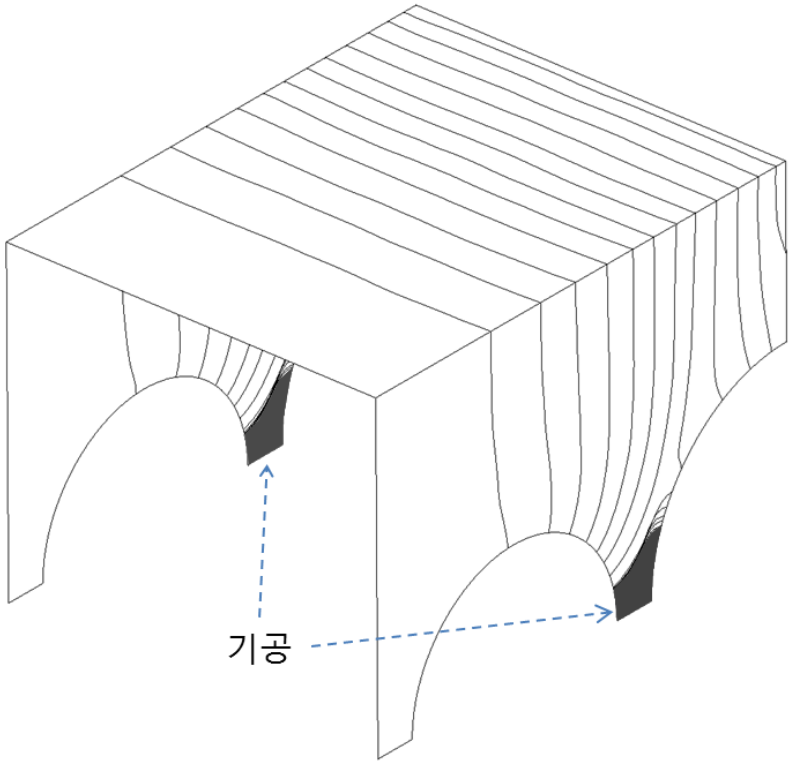

그림 17. 기공 (코너의 까만 부분) 생성 예제 해석 결과

- 5 초마다 전면부의 위치 그래프

기공의 형성은 배출구를 추가하여 예방할 수 있다. 그림 17 에서 기공이 형성된 모서리 부분에 배출구를 추가하여 계산하였고 그 결과가 그림 18 와 같이 매 5 초마다 전면부의 위치 그래프로 나타나 있다. 결과에서 볼 수 있듯이 본 예제에서는 기공이 생성되지 않고 수지가 완벽하게 잘 주입되었다. 본 예제를 통해 RTM 제작 공정 설계에서 수치해석의 역할이 중요함을 알 수 있다.

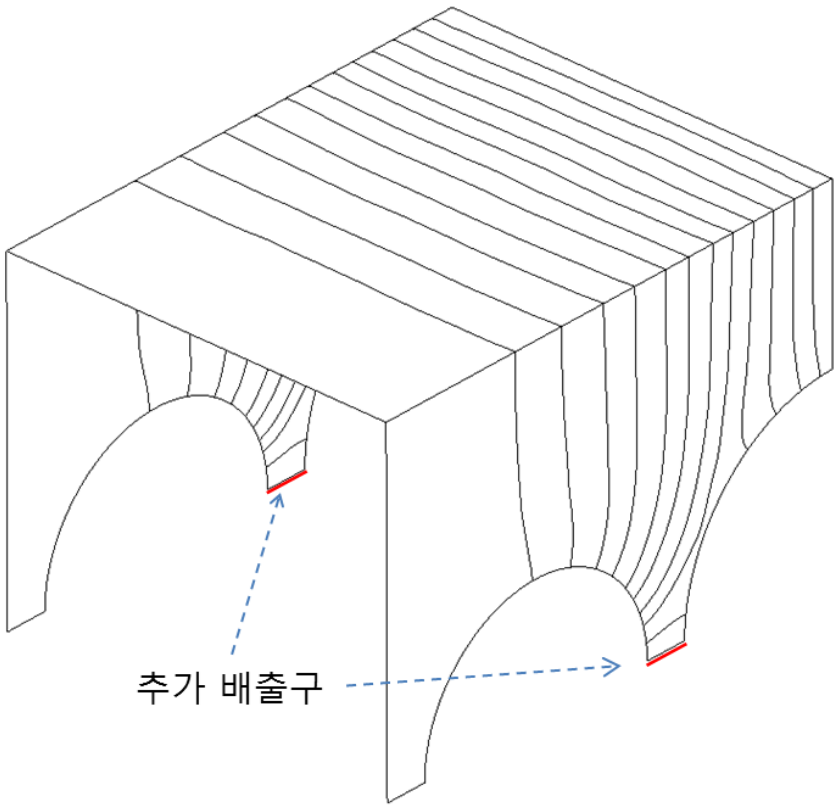

그림 18. 배출구를 추가한 예제의 계산 결과

– 매 5 초마다 전면부의 위치

제 7 장. 결론

본 연구를 에서는 RTM 공정을 좀 더 정밀하게 해석하기 위해서 레벨셋 기법과 결합된 확장유한요소법을 이용하였다. 이 기법 적용의 가장 큰 장점은 수지 전면부의 비연속적인 압력 구배를 수치해석에 반영할 수 있는 것이다. 여기서 사용되는 확장형상함수는 레벨셋 함수를 이용해서 전면부의 위치를 반영할 수 있도록 만들었다. 그리고 확장유한요소법을 적용할 경우 유동 전면부 근처의 절점만 확장영역에 포함되므로 해석에 필요한 전체적인 자유도는 아주 적게 증가하였다. 그리고 본 연구에서는 전면부의 위치를 계산하기 위해 레벨셋 함수로 이루어진 이송방정식을 이용하였다. 그 이송방정식과 레벨셋 값의 재초기화 식을 풀기 위해 내연적 특성 Galerkin 유한요소법을 적용하였다. 본 연구의 검증을 위해 해석 결과를 문헌에서 얻은 이론값과 비교하였다. 수행한 해석 결과는 이론 값과 비교했을 때 차이가 거의 없었다.

본 연구는 효율성 향상 방안으로 확장 유한 요소법과 레벨셋 기법의 국소화를 적용하였다. XFEM 의 국소화는 level set 기법의 국소화에서 힌트를 얻어 본 연구에서 처음으로 적용하였는데, 그 국소화 적용에 의해 계산 시간이 눈에 띄게 줄어듦을 확인할 수 있었다.

가장자리가 복잡한 모양의 평판 해석에서는 수지 전면부의 갈라지고 합쳐지는 현상이 잘 시뮬레이션 되었다. 그리고 얇고 복잡한 모양의 평판 해석에서는 race tracking 과 기공 형성 현상을 잘 묘사할 수 있었다.

본 연구를 통해서, 우리는 확장유한요소법이 RTM 공정에서 몰드내의 수지 유동 해석에 유용하게 쓰일 수 있는 것을 확인하였다. 본 연구에서 제안한 기법들은 해석을 더 효율적이고 정밀하게 만들어 주었다. 더 나아가, 본 연구가 RTM 공정의 설계 변수를 최적화하기 위해 사용된다면 높은 효율성과 정확성 같은 장점이 더욱 부각될 수 있을 것이라 예상된다. 그리고 본 연구에 경화 반응과 열전달 과정이 추가 된다면 그 사용 범위를 더 확장할 수 있을 것이라 생각된다.

참고문헌

[1] Kang MK, Jung JJ, Lee WI. Analysis of resin transfer moulding process with controlled multiple gates resin injection. Compos Part A. 2000;31(5):407-422.

[2] Bruschke MV, Advani SG. A Finite-Element Control Volume Approach to Mold Filling in Anisotropic Porous-Media. Polym Composite. 1990;11(6):398-405.

[3] Shojaei A, Ghaffarian SR. Modeling and simulation approaches in the resin transfer molding process: A review. Polym Composite. 2003;24(4):525-544.

[4] Young WB, Rupel K, Han K, Lee LJ, Liou MJ. Analysis of Resin Injection-Molding in Molds with Preplaced Fiber Mats .2. Numerical-Simulation and Experiments of Mold Filling. Polym Composite. 1991;12(1):30-38.

[5] Trochu F, Gauvin R, Gao DM. Numerical-Analysis of the Resin Transfer Molding Process by the Finite-Element Method. Adv Polym Tech. 1993;12(4):329-342.

[6] Trochu F, Ruiz E, Achim V, Soukane S. Advanced numerical simulation of liquid composite molding for process analysis and optimization. Compos Part A. 2006;37(6):890-902.

[7] Shojaei A, Ghaffarian SR, Karimian SMH. Numerical simulation of three-dimensional mold filling process in resin transfer molding using quasi-steady state and partial saturation formulations. Compos Sci Technol. 2002;62(6):861-879.

[8] Liu XL. Isothermal flow simulation of liquid composite molding. Compos Part A. 2000;31(12):1295-1302.

[9] Kang MK, Lee WI. A flow-front refinement technique for the numerical simulation of the resin-transfer molding process. Compos Sci Technol. 1999;59(11):1663-1674.

[10] Dong CS. A modified rule of mixture for the vacuum-assisted resin transfer moulding process simulation. Compos Sci Technol. 2008;68(9):2125-2133.

[11] Phelan FR. Simulation of the injection process in resin transfer molding. Polym Composite. 1997;18(4):460-476.

[12] Jiang SF, Yang L, Alsoliby SL, Zhou GF. PCG solver and its computational complexity for implicit control-volume finite-element method of RTM mold filling simulation. Compos Sci Technol. 2007;67(15-16):3316-3322.

[13] Chessa J, Smolinski P, Belytschko T. The extended finite element method (XFEM) for solidification problems. Int J Numer Meth Eng. 2002;53(8):1959-1977.

[14] Chessa J, Belytschko T. An extended finite element method for two-phase fluids. J Appl Mech-T ASME. 2003;70(1):10-17.

[15] Chessa J, Belytschko T. An enriched finite element method and level sets for axisymmetric two-phase flow with surface tension. Int J Numer Meth Eng. 2003;58(13):2041-2064.

[16] Belytschko T, Gracie R, Ventura G. A review of extended/generalized finite element methods for material modeling. Model Simul Mater Sc. 2009;17(4).

[17] Ji H, Chopp D, Dolbow JE. A hybrid extended finite element/level set method for modeling phase transformations. Int J Numer Meth Eng. 2002;54(8):1209-1233.

[18] Ji H, Dolbow JE. On strategies for enforcing interfacial constraints and evaluating jump conditions with the extended finite element method. Int J Numer Meth Eng. 2004;61(14):2508-2535.

[19] Zhuang Z, Cheng BB. Development of X-FEM methodology and study on mixed-mode crack propagation. Acta Mech Sinica-Prc. 2011;27(3):406-415.

[20] Hirt CW, Nichols BD. Volume of Fluid (Vof) Method for the Dynamics of Free Boundaries. J Comput Phys. 1981;39(1):201-225.

[21] Kim MS, Lee WI. A new VOF-based numerical scheme for the simulation of fluid flow with free surface. Part I: New free surface-tracking algorithm and its verification. Int J Numer Meth Fl. 2003;42(7):765-790.

[22] Lin CL, Lee H, Lee T, Weber LJ. A level set characteristic Galerkin finite element method for free surface flows. Int J Numer Meth Fl. 2005;49(5):521-547.

[23] Peng DP, Merriman B, Osher S, Zhao HK, Kang MJ. A PDE-based fast local level set method. J Comput Phys. 1999;155(2):410-438.

[24] Soukane S, Trochu F. Application of the level set method to the simulation of resin transfer molding. Compos Sci Technol. 2006;66(7-8):1067-1080.

[25] Gantois R, Cantarel A, Dusserre G, Felices JN, Schmidt F. Numerical Simulation of Resin Transfer Molding using BEM and Level Set Method. Int J Mater Form. 2010;3(1):635-638.

[26] Sethian JA. Level set methods and fast marching methods, 2nd edition. Cambridge University Press; 1999.

[27] Advani SG, Sozer EM. Process modeling in composites manufacturing. Marcel Dekker, Inc.; 2003.

[28] Zienkiewicz OC, Taylor RL. The finite element method volume 3: fluid dynamics, 5th edition. Butterworth Heinemann; 2000.

[29] Ventura G. On the elimination of quadrature subcells for discontinuous functions in the eXtended Finite-Element Method. Int J Numer Meth Eng. 2006;66(5):761-795.

[30] Mousavi SE, Sukumar N. Generalized Gaussian quadrature rules for discontinuities and crack singularities in the extended finite element method. Comput Method Appl M. 2010;199(49-52):3237-3249.

[31] Kim JH, Lee CS, Kim SJ. High-performance domainwise parallel direct solver for large-scale structural analysis. AIAA J. 2005;43(3):662-670.

[32] Cai Z. Simplified Mold Filling Simulation in Resin Transfer Molding. J Compos Mater. 1992;26(17):2606-2630.

[33] Lin M, Hahn HT, Huh H. A finite element simulation of resin transfer molding based on partial nodal saturation and implicit time integration. Compos Part A. 1998;29(5-6):541-550.

[34] Shojaei A, Ghaffarian SR, Karimian SMH. Numerical simulation of three-dimensional mold filling process in resin transfer molding using quasi-steady state and partial saturation formulations. Compos Sci Technol. 2002;62(6):861-879.

[35] Jung Y, Han WS, Vautrin A, Kim SJ, RTM process simulation by using XFEM and Levelset method. 18th Int C on Compos Mat. Aug 21-26 2011, ICC Jeju, Seogipo Special Self-Governing Province, Korea.

[36] Jung Y, Kim SJ, Han WS, Numerical simulation of RTM process using the extended finite element method combined with the level set method. J of Reinforced Plastics and Compos. 2013;32(5):308-317.

[37] Jung Y, Kim SJ, Han WS, Improvement of computational efficiency by localization of XFEM with level set method for mold filling problem in RTM process, Int J Numer Meth Eng., Submitted.

École Nationale Supérieure des Mines
de Saint-Étienne

NNT : 2013 EMSE 0701

Prénom NOM : Yeonhee JUNG

DISSERTATION TITLE

An efficient analysis of resin transfer molding process using extended finite element method

Speciality: Mechanical Engineering

Keywords: RTM Process, XFEM, Level Set Method, Numerical Analysis, Localization method.

Abstract:

Numerical simulation for Resin Transfer Molding (RTM) manufacturing process is attempted by using the eXtended Finite Element Method (XFEM) combined with the level set method. XFEM allows to obtaining a good numerical precision of the pressure near the resin flow front, where its gradient is discontinuous. The enriched shape functions of XFEM are derived by using the level set values so as to correctly describe the interpolation with the resin flow front. In addition, the level set method is used to transport the resin flow front at each time step during the mold filling. The level set values are calculated by an implicit characteristic Galerkin FEM. The multi-frontal solver of IPSAP is adopted to solve the system. This work is validated by comparing the obtained results with analytic solutions.

Moreover, a localization method of XFEM and level set method is proposed to increase the computing efficiency. The computation domain is reduced to the small region near the resin flow front. Therefore, the total computing time is strongly reduced by it. The efficiency test is made with simple channel or radial flow models.

Several application examples are analyzed to demonstrate ability of this method. A wind turbine blade is also treated as industrial application. Finally, a Graphic User Interface (GUI) tool is developed so as to make easy the pre/post-processing of the simulation.

École Nationale Supérieure des Mines
de Saint-Étienne

NNT : 2013 EMSE 0701

Prénom NOM : Yeonhee JUNG

TITRE DE LA THÈSE

Une analyse efficace du procédé RTM à l'aide de la méthode XFEM

Spécialité: Mécanique et Ingénierie

Mots clefs : Procédé RTM, XFEM, Level set, Simulation numérique, Méthode de localisation.

Résumé :

Le procédé de fabrication par RTM (Resin Transfer Molding) a été étudié numériquement à l'aide de la méthode XFEM (eXtended Finite Element Method) combinée avec la méthode Level set. La méthode XFEM permet d'obtenir une bonne précision numérique de la pression près du front d'écoulement, où son gradient est discontinu. Les fonctions de forme enrichies de la méthode XFEM sont proposées à l'aide des valeurs de Level set en vue de décrire correctement l'interpolation avec le front d'écoulement. En plus, la méthode de Level set est utilisée pour transporter le front d'écoulement à chaque pas de temps durant le remplissage du moule. Les valeurs de Level set sont calculées à l'aide d'une méthode de Galerkin implicite. Le solveur multi-frontal d'IPSAP a été utilisé pour la résolution du système. Cette étude a été validée en comparaison avec les solutions analytiques.

En outre, une méthode de localisation avec XFEM et la méthode Level set a été proposée afin d'améliorer l'efficacité de calcul. Elle permet de réduire le domaine de calcul près du front d'écoulement. Par conséquent, le temps de calcul est fortement réduit grâce à cette méthode. Un test d'efficacité a été fait avec des modèles simples en écoulement laminaire ou radial.

Quelques exemples d'application sont présentés pour illustrer la capacité de cette méthode. Une pale d'éolienne a également traitée comme application industrielle. Enfin, une interface d'utilisateur graphique a été développée en vue de fournir une facilité des pré- et post-processus.